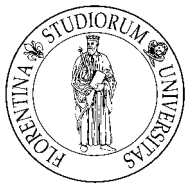

Università degli Studi di Firenze
LENS
European Laboratory for Non-Linear Spectroscopy

International Ph.D. degree in Atomic and Molecular Spectroscopy
XXVI Cicle
CHIM/02

Charge and Energy Transfer in Complex Systems

Ph.D. Candidate:
Alessandro Iagatti

Supervisor:
Prof. Paolo Foggi

External Supervisor:
Prof.ssa Loredana Latterini

Coordinator:
Prof. Francesco Saverio Pavone

A.A. 2011/2013

Charge and Energy Transfer in Complex Systems

Alla mia famiglia...

Contents

Chapter 1

Introduction

The increasing energy demand in the near future will force us to seek environmentally clean alternative energy resources. The present thesis fits in this context. Therefore, the aim of the work is to obtain pieces of information about systems capable to give photoindeced charge transfer for their application in third generation photovoltaic systems, such DSSC and solar concentrators. In addition some supramolecular systems have been investigated for excited energy transfer in order to be used as antenna system in artificial photosynthetic devices. These experiments were performed with steady-state photochemical measurements and ultrafast laser technique in order to allow a better understanding of the overall mechanisms and the optical properties of these systems.
In the last few years, the emergence of nanomaterials as new building blocks for the construction of light harvesting assemblies has opened up new pathways in the usage of renewable energy sources. This part of the work was carried out in collaboration with the research group of Prof.ssa Loredana Latterini at the University of Perugia. CdTe quantum dots were chosen and they have been synthesized in aqueous solution with soft chemical procedures and respecting green chemistry principles.
Since exciton generation and recombination dynamics in semiconductor nanocrystals are very sensitive to small variations of dimensions, shape and surface capping, we have previously characterized

the optical properties of these materials using 3-mercaptopropionic acid and 1-thioglycerol as stabilizers. The morphological and steady-state optical characterizations shown a strong influence of the stabilizers on the luminescence properties, likely due to the size distribution of the colloids and to the defects created during the synthesis process. A combined study by single photon counting and femtosecond transient absorption techniques has shown a different electronic evolution in the particles with different capping agents. Electron-hole radiative recombination occurs with nonexponential decays for both colloids, although the average decay time values (in the order of tens of nanoseconds) are different for the two samples. The ultrafast characterization is performed exciting each sample with two different wavelengths (near the band gap and at higher energy) for both samples. Transient absorption spectra show two different decaying signals associated to the bleaching of the band-gap transition band and to the excited transient absorption of the electrons in the conducting band. The signals in the time domain show a quite complex behaviour involving a rise component and a triexponential decay. The data are analysed in terms of dynamic processes considering surface trapping states, Auger recombination and electron-hole radiative recombination processes. Significant differences on the decay times were recorded on nanocrystals with different capping agents.

As a next step, we have investigated the possibility to transfer the electrons from CdTe-MPA capped quantum dots to an electron acceptor system as methiviologen (MV^{2+}). Steady-state measurements have confirmed the presence of a static interaction between the nanocrystals and MV^{2+} molecules. Ns-laser transient absorption experiments have been carried out to investigate the nature of the interactions between the nanocrystals and MV^{2+} molecules. Upon excitation of the nanocrystals at 355 nm, the transient spectra, detectable only in the presence of MV^{2+}, show the formation of transient signals due to MV^{2+} transient species. Femtosecond transient spectroscopy has shown a significative reduction of the exciton lifetime due to electron capture from MV^{2+} and a strong influence on the decay time of the trapping state and Auger recombination.

Subsequently, the investigation has been extended to a molecular

organic system (F500), a promising system to be utilized in solar concentrators. It gives intramolecular charge transfer process. When the dye is excited, the charge is transferred from the electron rich thiophenic groups to the acceptor group represented by a benzothiadiazole. We have performed a characterization study in which the solvatochromic effect was investigated as a function of the solvent polarity. Steady-state measurements have shown the presence of molecular conformers with increasing solvent polarity. Furthermore, a significant variation of the dipole moment was observed. The analysis of ultrafast transient spectra has shown a strong dependence from the different molecular conformers. Lastly, we have compared the data obtained for F500 in solution with those obtained by dispersing the molecule in a PMMA solid matrix. These measurements have shown a similar behavior with the molecules dispersed in apolar solvents.
As antenna systems for photosynthetic devices, we have investigated a BODIPY-Aminostyryl pyridinium bichromophore complex and a calix[4]arene supramolecular system. A first analysis of BODIPY bicromophore with stationary techniques using chloroform and acetonitrile as solvents, has shown a small coupling between the two dyes when these are linked togheter. However, from the emission quantum yields is evident the presence of an efficient excited energy transfer influenced by the nature of the solvents. Ultrafast transient spectroscopy measurements confirmed the efficiency of this process, characterized by a time constant of few hundreds femtoseconds. The transient spectra have also shown an important dynamical Stokes shift and a delayed transfer process due to different structural conformations of the bichromophore. Further information about energy transfer process have been achieved by inserting in *Förster* model the center-to-center separation obtained by Ab initio structural calculations.
The supramolecular calix[4]arenes assemblies were studied using Nilered as an acceptor and NDB as a donor. In order to obtain new pieces of information about the electronic evolution and energy transfer efficiency with different structure conformation of calix[4]arene, steady-state measurements and transient spectroscopic characterization have been used in solution with organic solvent at different polarities. Steady-state measurements have shown ab-

sorption spectra with profles given by the sum of the spectra of the reference compounds, while the emission data have allowed to observe a very efficient excitation energy transfer from the donor NBD to the acceptor Nilered. Transient absorption measurements have been performed on the single reference compounds and on the supramolecular structures in order to understand how the properties of the chromophores are influenced in a blocked system. Transient absorption spectra show three different decay signals affected by the different structural conformations and by the solvent polarity.

Chapter 2

Theoretical Background

2.1 Electron Transfer

Photoinduced electron transfer is one of the most important phenomena in nature and it plays a fundamental role in processes studied in biology, physics and chemistry. Understanding this process in well-defined artificial systems may lead to further insight into the primary events occurring in the biological processes responsible for a large part of the energy production on earth. Indeed electron transfer occurs in photosynthetic reaction center where the electron transfer is used to create a charge imbalance across a membrane, originating a proton pumping mechanism to produce ATP. Moreover nonradiative and radiative electron transfer also plays a key role in many processes involving isolated molecules and supermolecules, condensed phases, surfaces and interfaces, electrochemical systems and in solar cells. His presence in vital, environmental and artificials processes underscores the great importance of this phenomenon.
Light induced electron transfer is a process in which an electron is transferred from an electron donating species (D) to an electron accepting species (A). The mechanism is well summarized in Figure 2.1 where the electron transfer occurs after the excitation of one of the two components with light radiation. The charge transfer state created can evolve through different pathways. The more

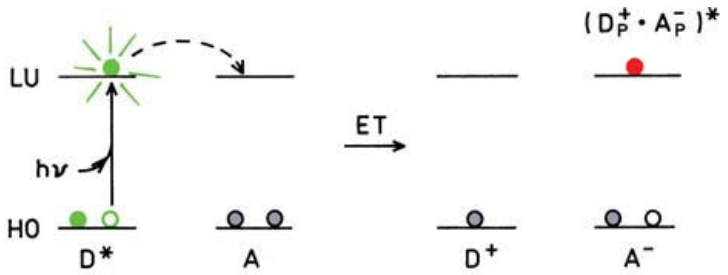

Figure 2.1: Molecular orbital schematic for photoinduced electron transfer[1]

common situation is when the excited state of a fluorophore acts as an electron acceptor, a typical example is an electron-rich moiety which can donate electrons to an acceptor[1]. Considering photovoltaic devices of third generation, the species that acts as donor is that which is excited by light radiation. A process that can follow charge separation is the charge recombination or back electron transfer leading to the initial relaxed state. This common process is often the limiting factor of the yield of an event of charge transfer.

2.1.1 Theory and Molecular Models of Electron Transfer

The results of a phothoinduced electron transfer is the formation of a cation-anion pair due to the excitation of one of the two species (donor or acceptor) with electromagnetic radiation. It follows that this process produces a fluorescence quenching of the excited species competing with the radiative and nonradiative processes, as shown in Figure 2.2, going to influence the fluorescence quantum yield and the excited state lifetime. Therefore, the electron transfer can be regarded as an extra deactivation path of the excited singlet state that can occur along with the internal conversion (IC), intersystem crossing (ISC) to the triplet manifold, and emission. However other mechanisms can be responsible for emission quenching as the energy transfer (see below), hydrogen bond, proton transfer and the heavy atom effect.

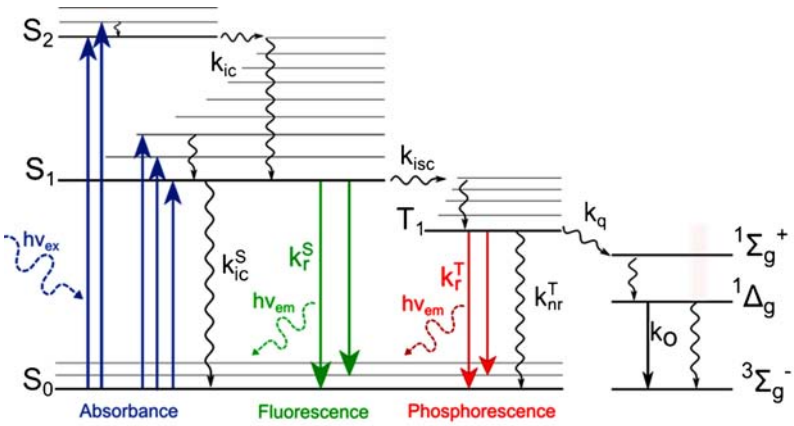

Figure 2.2: Perrin–Jablonski diagram [2]

The electron transfer depends on the redox properties of the donor acceptor couple together with the excitation energy. In polar solvents it can be said that the Gibbs free energy change for charge separation (ΔG_{CS}), is given by:

$$\Delta G_{CS} = e^{E^0(D^+/D) - E^0(A^-/A)} - \Delta E_{0,0} \tag{2.1}$$

The excitation energy ($\Delta E_{0,0}$) must be higher than the energy cost to oxidize the donor and to reduce the acceptor. For a single specie in solution, the fluorescence quantum yield and the fluorescence life time can be described using the rate constants (k) of the basic processes (fluorescence, phosphorescence, IC and ISC). But the introduction of a second chromophore group may lead to a number of other decay processes and if the charge separated state (CS) is formed out of a locally excited acceptor state the process is called hole transfer (HT):

$$D - A \xrightarrow{h\nu} D^* - A \xrightarrow{ET} D^+ - A^- \tag{2.2}$$

$$D - A \xrightarrow{h\nu} D - A^* \xrightarrow{HT} D^+ - A^- \tag{2.3}$$

In case of a strong electronic coupling between the ground state, the CS state and a locally excited state, or between the ground state and a CS state, a charge transfer absorption band can be observed.

This represents the direct excitation to the CS state. The energy level of a CS state depends strongly on the solvent polarity and it is more stabilized in polar solvents due to the very polar nature of this state.
The efficiency of the electron transfer processes depends by the rate constant of the transfer and by the rate constant of the other radiative (k_r) and nonradiative (k_{nr}) competing deactivation pathways. The lifetime constant for an excited donor molecule D^* (or acceptor A^*), is given by the inverse of the sum of the of the rates of all decay processes as shown in eq.2.4:

$$\tau_{D^*} = \frac{1}{\sum k_{decay}} = \frac{1}{k_r + k_{nr}} \tag{2.4}$$

The quantum yield of fluorescence (ϕ_r) is defined as the fraction of excited molecules that decay via fluorescence. When both ϕ_r and τ_{D^*} are known, k_r it is possible calculate:

$$\tau_{D^*} = \frac{\phi_r}{k_r} \tag{2.5}$$

The lifetime of the excited dono can be determined by time-resolved absorption spectroscopy, time-resolved fluorescence spectroscopy and time-resolved microwave conductivity.
If we consider a system with an electron acceptor species where charge transfer phenomena occur, the eq.2.4 becomes:

$$\tau_{D^*-A} = \frac{1}{k_r + k_{nr} + k_{ET}} \tag{2.6}$$

Assuming that the introduction of an acceptor does not influence the rates of the other deactivating processes, the excited donor k_{ET} can be determened:

$$k_{ET} = \frac{1}{\tau_{D^*-A}} - \frac{1}{\tau_{D^*}} \tag{2.7}$$

$$\tau_{k_{ET}} = \frac{\phi_r(D^*)}{\phi_{D^*-A}\tau_{D^*}} - \frac{1}{\tau_r(D^*)} \tag{2.8}$$

Another way to determine the value of k_{ET} is the absorption measurements of the charge transfer state by transient absorption technique.

2.1.2 A Semi-Classical Theory

A semi-classical approach has been addressed by a number of workers to include quantum effects into the classical Marcus theory [3–6].
The necessity to introduce quantum effects become clear introducing the harmonic oscillator vibrational energy levels within the potential curves. The nonadiabatic electron transfer between donor and acceptor centers is treated by the Fermi golden rule of perturbation theory, and the rate constant for the transfer process is given by eq. 2.9:

$$\begin{aligned} k_{et} &= \frac{2\pi}{\hbar} \left|\langle R \left| H \right| P \rangle\right|^2 \left|\langle r_{vib} | p_{vib} \rangle\right| 2\delta(E_R - E_P) \\ &= \frac{2\pi}{\hbar} \left|\langle R \left| H \right| P \rangle\right|^2 \left|\langle r_{vib} | p_{vib} \rangle\right| 2\rho(E_P) \\ &= \frac{2\pi}{\hbar} \left|\langle R \left| H \right| P \rangle\right|^2 (DFWC) \\ &= \frac{2\pi}{H_{RP}} (DFWC) \end{aligned} \tag{2.9}$$

where the electron transfer rate constant is given first in terms of isolated levels for the reactant and product, then in terms of density of states, $\rho(E_P)$ of the product, and finally in terms of density of states weighted Franck-Condon factor (DWFC). As regarding the other parameters, H_{RP} is the electronic matrix element that mixes the donor and acceptor states, $|r_{vib}>$ and $|p_{vib}>$ represent vibrational states of reactants and products respectively and H is the Hamiltonian for the entire system. Using the polaron model, where two electronic states coupled with a number of vibrational levels, is possible write the hamiltonian of the system as follows:

$$\begin{aligned} H =& |R><R| \left[E_R^0 + \frac{1}{2} \sum_l f_l (q_l - q_{R,l})^2 \right] + \\ & |P><P| \left[E_P^0 + \frac{1}{2} \sum_l f_l (q_l - q_{P,l})^2 \right] + \\ & (|R><P| + |P><R|) H_{RP} \end{aligned} \tag{2.10}$$

where the first term in braces is the reactants energy and the second set of braces is the same energy term for the products, E_R^0 and

E_P^0 are respectively the energy origin of the states and are characterized by the force constant f_l for the l mode, whose displacement origin is $q_{R,L}$ and $q_{P,L}$ in the reactants and products respectively. In addition to the classical solvent motion, one can specifies one coupled vibration characterized by frequency ω and equilibrium displacement Δq_e, then is possible to define the intramolecular reorganization energy for this mode as:

$$\lambda_i = \left(\frac{f}{2}\right)(\Delta q_e)^2 \tag{2.11}$$

from eq. 2.11 is possible obtain an adimensional parameter that describe the electron coupling and is called Huang-Rhys factor or electron vibrational coupling constant. This factor is represented in eq. 2.12:

$$S = \left(\frac{\lambda_i}{\hbar\omega}\right) \tag{2.12}$$

generalizing the equation of the k_{et} for diabatc electron transfer for one coupled mode in the quantum mechanical limits, is possible obtain:

$$k_{et} = \frac{2\pi}{\hbar} H_{RP}^2 \left(\frac{1}{4\pi\lambda k_B T}\right)^{\frac{1}{2}} (FC) \tag{2.13}$$

where FC is the Franck-Condon factor

$$(FC) = \sum_{\nu'} exp(-S)\frac{S^{\nu'}}{\nu'!} exp\left[-\frac{(\lambda + \nu'\hbar\omega + \Delta G^0)^2}{4\lambda k_B T}\right] \tag{2.14}$$

The term in front the FC factor is the frequency of electron transfer in the absence of barrier and contains H_{RP} and the classical density of states. The FC factor consists of the sum over all possible vibrational overlap integrals between the initial vibrational level ν and the final level. ν'. Each individual ν' represents a separate $\nu = 0 \rightarrow \nu$' reaction channel. Each separated exponential term in the sum is the population of molecules having the required energy to undergo electron transfer with energy conservation through channel $\nu = 0 \rightarrow \nu$'. The sum is dominated by those channels for

which $|\Delta G^0| \approx \lambda + \nu' \hbar\omega$, so there is a close energy match between the energy released (ΔG^0) and the sum of the reorganization energy and the initial product vibrational energy ($\nu' \hbar\omega$).
In the case of thermal excitation of the local molecular and medium highfrequency modes, theories mentioned before predicted the classical Marcus relation in the normal Marcus region. While in the inverted region, significant deviation on the parabolic energy gap dependence is expected (Figure 2.3). The inverted Marcus region

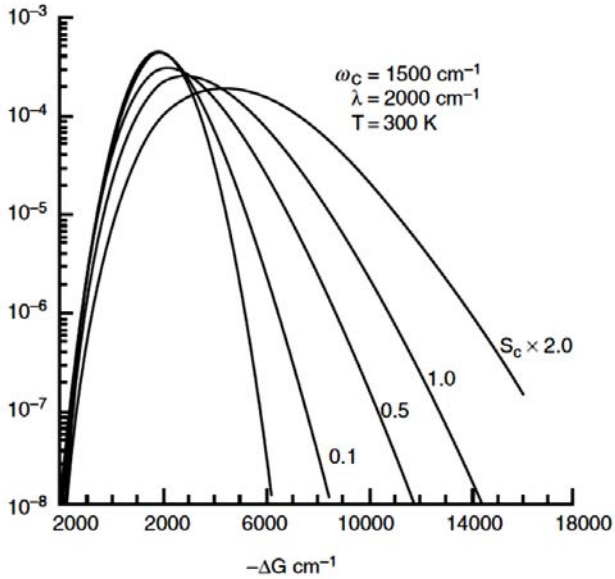

Figure 2.3: The energy gap dependence of the nuclear Franck–Condon factor, which incorporates the role of the high-frequency intramolecular modes. $S_c = \Delta/2$ is the dimensionless electron–vibration coupling, given in terms that reduce replacement (Δ) between the minimum of the nuclear potential surfaces of the initial and final electronic states[7]

cannot be experimentally observed if the stabilization of the first electron transfer product for the accounting of the high-frequency vibrational mode occurs faster than the equilibrium of the solvent polarization with the momentary charge distribution can be established. Another source of the deviation is the nonparabolic shape of the activation barrier[7].

2.2 Energy transfer

In the previous section has been discussed how the excitation can be transferred through a charge transfer from a donor to an acceptor molecule. In this section will be treated how this excitation exchange occurs by an energy transfer, always between donor and acceptor species.
The energy transfer between different states represents an important part on the photochemistry and photophysics behaviour determination of the molecules, which occurs in a variety of situations. The most important distinction should be made between radiative and non-radiative transfer but is possible differentiate the process in heterotransfer or homotransfer and if the transfer occurs by intermolecular way between two different species in solution, or by intramolecular mechanism where the donor and the acceptor is two diffrent groups prensent in the same molecule.
It is important to distinguish between radiative and non-radiative transfer. Radiative transfer corresponds to the absorption by an acceptor molecule of a photon emitted by a donor molecule, and is observed when the average distance between donor and acceptor is larger than the wavelength. Such a transfer does not require any interaction between the partners, but it depends on the spectral overlap and on the concentration. In contrast, non-radiative transfer occurs at distances less than the wavelength, without previous emission of photons, and results from short- or long-range interactions between molecules. For instance, non-radiative transfer by dipole-dipole interaction is possible at distances up to nearly 20 nm. Consequently, such a transfer provides a tool for determining distances of a few nm between chromophores. Non-radiative energy transfer can result from different interaction mechanisms. The interactions may be Coulombic and/or due to intermolecular orbital overlap. The Coulombic interactions consist of long-range dipole-dipole interactions (*Förster's* mechanism) and short-range multi-polar interactions.
Radiative and non-radiative transfers have different effects on the characteristics of fluorescence emission from the donor, which allows us to make a distinction between these two types of transfer.

2.2.1 Short-Range Exchange Mechanism

In the short-range exchange mechanism (also called Dexter-type[8]) it's necessary that donor and acceptor come in contact and have the overlap of the interaction spheres of Van Der Walls with formation of an intermediate in which the energy is still localized on the donor.
The rate constant for the exchange mechanism can be expressed by eq. 2.15:

$$k_{en}^{D} = \frac{4\pi^2}{h}(H^{en})^2 J_D \tag{2.15}$$

where the electronic term H^{en} is obtained from the electronic coupling between donor and acceptor, exponentially dependent on distance:

$$H^{en} = H^{en}(0)exp\left[-\frac{\beta^{en}}{2}(r_{AB} - r_0)\right] \tag{2.16}$$

The nuclear factor J_D is the Dexter overlap integral between the emission spectrum of the donor and the absorption spectrum of the acceptor:

$$J_D = \frac{\int F(\tilde{\nu})\epsilon(\tilde{\nu})d\tilde{\nu}}{\int F(\tilde{\nu})d\tilde{\nu} \int \epsilon(\tilde{\nu})d\tilde{\nu}} \tag{2.17}$$

The exchange interaction can be regarded as a double electron transfer process, one-electron moving from the LUMO of the excited donor to the LUMO of the acceptor, and the other from the acceptor HOMO to the donor HOMO. This important insight is illustrated in Figure 2.4, from which it is clear that the attenuation factor β^{en} for exchange energy transfer should be approximately equal to the sum of the attenuation factors for two separated electron transfer processes, i.e. β^{el} for electron transfer between the LUMO of the donor and acceptor (2.4), and β^{ht} for the electron transfer between the HOMO (superscript ht denotes for hole transfer from the donor to the acceptor). The transfer process with exchange mechanism can be seen as a particular chemical reaction between the donor and acceptor species, where is present only the energy transfer and the chemical structure of the reagents remain

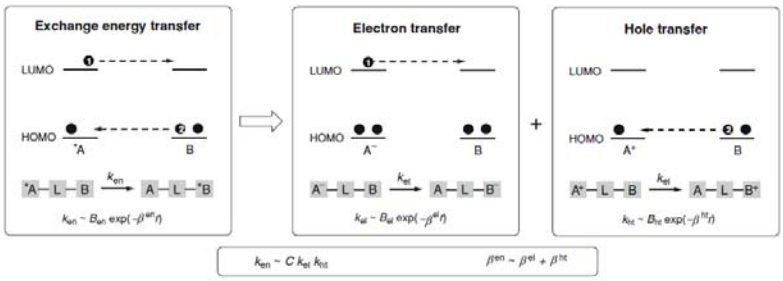

Figure 2.4: Analysis of the exchange energy transfer mechanism in terms of electron–and hole transfer processes. The relationships between the rate constants and the attenuation factors of the three processes are also shown [9]

the same. With these conditions, the transition state is caracterized by a separation between acceptor and donor similar to the sum of the collision ray and the exchange mechanism occurs within 10 Angstroms. This mechanism has in common with the classical chemical reactions the fact that the probability is different from zero only when the potential energy of the reagents and products are linked by a continuos surface that describes the potential energy trend in function of the intermolecular distance.
The exchange mechanism is based on the Wigner spin conservation rule, the spin correlation law imposes that the products must have a total spin equal to one of the values assumed by activated complex. In atoms or little molecules is necessary the presence of the spin correlation, orbital moment, parity, etc.. However in more complex molecules with lower simmetry is only required the spin correlation. This enables the exchange mechanism to be operative in many instances in which the excited states involved are spin forbidden in the usual spectroscopic sense, for example triplet-triplet energy transfer ($D^*(T_1) + A(S_0) \rightarrow D(S_0) + A^*(T_1)$) is possible only with orbitals overlap (i.e. only with a Dexter mechanism). In Figure 2.5 is shown the exchange mechanism in relation with the Wigner correlation spine rules:

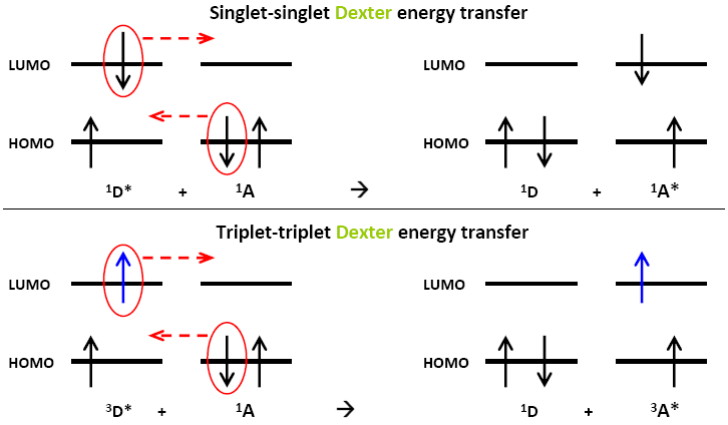

Figure 2.5: Schematic diagram for Dexter energy transfer

2.2.2 Resonant Energy Transfer Mechanism

Fluorescence Resonance Energy Transfer (FRET) was first described by *Förster*[10] (with which the process itself is now almost universally associated) in 1948, and experimentally verified by Latt et al.[11]. It is a powerful tool to measure distances between two dyes, a donor and an acceptor, in the range of 10–80 Angstrom. The excitation energy is transferred from the donor to the acceptor via an induced dipole–induced dipole interaction. The rate of energy transfer from a donor to an acceptor $k_T(r)$ is given by:

$$k_T(r) = \frac{1}{\tau_D}\left(\frac{R_0}{r}\right)^6 \tag{2.18}$$

where τ_D is the lifetime of the donor in the absence of acceptor, R_0 is the *Förster* distance, and r is the donor to acceptor distance. Hence, the rate of transfer is equal to the decay rate of the donor ($1/\tau_D$) when the donor to acceptor distance (r) is equal to the *Förster* distance (R_0), and the transfer efficiency is 50%. At this distance (r = R_0) the donor emission would be decreased to half its intensity in the absence of acceptors. The rate of resonance energy transfer depends strongly on distance, and is proportional to r^{-6}. In according with equation 2.18, if the transfer rate is much faster than the decay rate, then energy transfer will be efficient. If the

transfer rate is slower than the decay rate, then little transfer will occur during the excited-state lifetime, and the transfer will be inefficient.
The efficiency (E) of FRET process can be written as the fraction of photons absorbed by the donor which are transferred to the acceptor:

$$E = \frac{k_T(r)}{\tau_D^{-1} + k_T(r)} \tag{2.19}$$

Considering as said in equation 2.18 about the $k_T(r)$, the previous relation can be rewritten as follow:

$$E = \frac{R_0^6}{R_0^6 + r^6} \tag{2.20}$$

In agreement with this equation, plotting the efficiency as a function of the fluorophores distance (Figure 2.6), it's possible to notice how the transfer efficiency is strongly dependent on distance when r is near the *Förster* distance. However, in according with the Dexter theory about the orbitals overlapping, is not practical to use RET to measure distances outside the range of 0.5 $R_0 >$ r < 2 R_0.

The transfer efficiency can be experimentally measured using the relative fluorescence intensity of the donor, in the absence (F_D) and presence (F_{DA}) of acceptor or from the lifetimes at the same conditions (τ_{DA} and τ_D):

$$E = 1 - \frac{F_{DA}}{F_D} \tag{2.21}$$

$$E = 1 - \frac{\tau_{DA}}{\tau_D} \tag{2.22}$$

It is important to notice that resonance energy transfer is a process that does not involve emission and reabsorption of photons. The theory of energy transfer is based on the concept of a fluorophore as an oscillating dipole, which can exchange energy with another dipole with a similar resonance frequency[12].
Resonance energy transfer contains molecular information that is

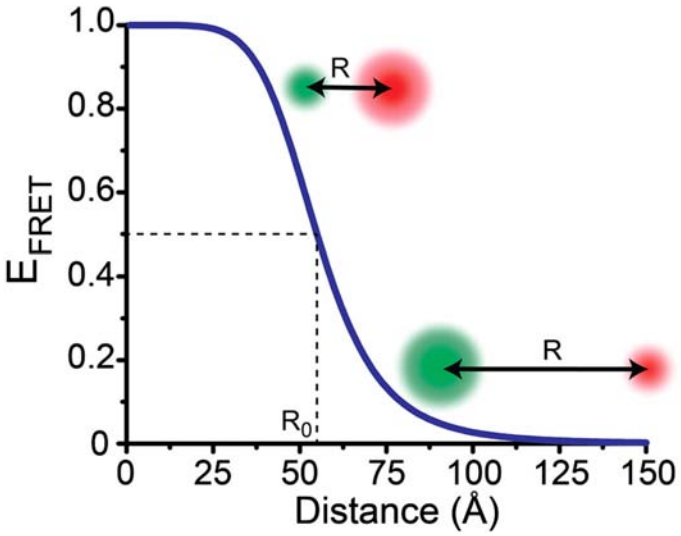

Figure 2.6: Energy transfer efficiency (E) dependence with the fluorophores distance

different from that revealed by fluorescence quenching, solvent relaxation, fluorescence anisotropy or excited-state reactions. These fluorescence phenomena depend on interactions of the fluorophore with other molecules in the surrounding solvent shell. These nearby interactions are less important for energy transfer, except for their effects on the spectral properties of the donor and acceptor. FRET is effective over much longer distances, and the intervening solvent or macromolecule has little effect on the efficiency of energy transfer, which depends primarily on the donor and acceptor distance [1]. Resonant energy transfer is best understood by considering a single donor and acceptor separated by a distance (r). The rate of transfer for a donor and acceptor separated by a distance r is describe in eq. 2.23

$$k_T(r) = \frac{\phi_D \kappa^2}{\tau_D r^6} \left(\frac{9000(ln10)}{128\pi^5 N n^4} \right) \int_0^\infty F_D(\lambda)\epsilon_A(\lambda)\lambda^4 d\lambda \qquad (2.23)$$

where ϕ_D is the quantum yield of the donor in absence of acceptor, N is de Avogadro's number and n is the refractive index of the

medium. Furtheremore the parameters into the overlap integral (Figure 2.7) represent $F_D(\lambda)$ the normalized emission spectrum of the excited donor in the wavelength range λ to $\lambda + \Delta\lambda$, ϵ_A is the extintion coefficient of the acceptor at the wavelength λ, and the factor κ^2 describe the relative orientation in space of the transition dipoles of the donor and acceptor.

The equation 2.23 can be rewritten in term of the *Förster* dis-

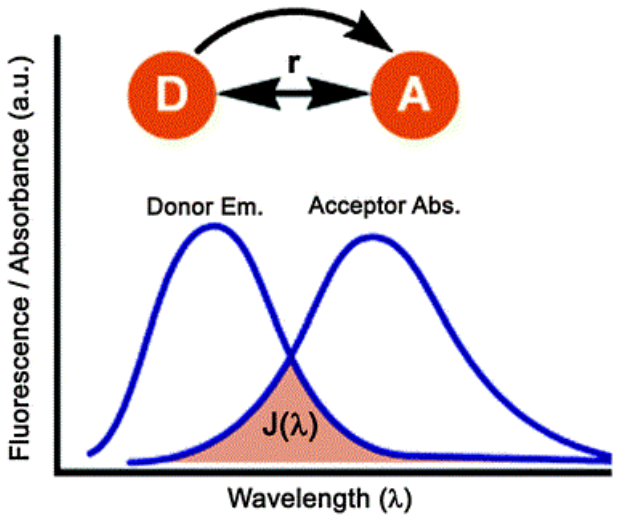

Figure 2.7: Overlap integral (J(λ)) of the donor emission spectrum with the acceptor absorption spectrum

tance (R_0), which is generally in the range 1–8 nm and describe the situation where half the donor molecules decay by energy transfer and half decay by the usual radiative and non-radiative rates.

$$R_0^6 = \frac{9000(ln10)\phi_D\kappa^2}{128\pi^5 N n^4} \int_0^\infty F_D(\lambda)\epsilon_A(\lambda)\lambda^4 d\lambda \tag{2.24}$$

This expression allows the *Förster* distance to be calculated from the spectral properties of the donor and the acceptor and the donor quantum yield.

As it is clear from equation 2.24, the *Förster* distance depends on the orientation factor (κ^2) of interacting dipoles. Since, the rate of energy transfer depends on R_0, the orientation factor also affects

the rate of energy transfer. The electric field due to the donor dipole at an acceptor dipole is given by:

$$\vec{E}_D = \frac{|m_D|}{R^3}\left\{2cos\theta_D\hat{R} + sin\theta_D\hat{\theta}_D\right\} \tag{2.25}$$

where $|m_D|$ is the time-independent dipole strength. R^3 is the distance between the point dipoles, and $\hat{R}$ is the unit vector from the dipole to the position $\vec{R}$. $theta_D$ is the angle between $\hat{m}_D$ and $\hat{R}$. $\hat{\theta}_D$ is the unit vector in the direction of the end of the $\hat{R}$ vector as it increases in the direction of $theta_D$.
The rate of energy transfer in equation 2.18 is proportional to the square of interaction energy between the donor and acceptor dipoles $\hat{m}_D$ and $\hat{m}_A$,

$$\begin{aligned} k_T(r) \propto (U_{D\to A})^2 &= \left(\vec{E}_D \cdot \vec{m}_A\right)^2 \\ &\frac{|m_D|^2 |m_A|^2}{R^6}\left\{2cos\theta_D\hat{R}\cdot\vec{m}_A + sin\theta_D\hat{\theta}_D\cdot\vec{m}_A\right\}^2 \\ &\frac{|m_D|^2 |m_A|^2}{R^6}\kappa^2 \end{aligned} \tag{2.26}$$

where the factor κ^2 is given by:

$$\kappa^2 = \left\{2cos\theta_D\hat{R}\cdot\vec{m}_A + sin\theta_D\hat{\theta}_D\cdot\vec{m}_A\right\}^2 \tag{2.27}$$

Depending upon the relative orientation of donor and acceptor the orientation factor can range from 0 to 4. Let us consider a few situations to make this point more clear. If the two dipoles have orientations in space perpendicular to each other, and if the acceptor dipole is juxtaposed next to the donor, but in the direction perpendicular to the direction of the donor dipole, then $\kappa^2 = 0$ (because $\theta_D = \frac{\pi}{2}$, so $\cos\theta_D = 0$ and $\hat{\theta}_D \cdot \vec{m}_A = 0$"). In this situation, even if the donor spectrum and acceptor spectrum overlap significantly, the transfer rate will be zero. When the transition moments are parallel, $\kappa^2 = 1$, and when they are collinear $\kappa^2 = 4$.
In the case where the donor and acceptor are free to rotate at a rate that is much faster than the deexcitation rate of the donor (isotropic dynamic averaging), the average value of κ^2 is 2/3. However this is not the only case where this is true, indeed many of

the dyes used for FRET have more than a single transition dipole, which can be excited at the same wavelengths, and since different transition dipoles of a fluorophore are usually not parallel to each other (they are often perpendicular to each other), this leads again to a κ^2 averaging value of 2/3.

Chapter 3

Spectroscopic thechniques

3.1 Transient Absorption

The advent of pulsed laser systems has allowed the development of spectroscopic analysis techniques for the direct investigation of new matter properties. Indeed the observation of intermediate conformations between reactant and product species has been a major goal since Eyring and Polanyi formulated the "transition-state theory" in the 1930's. Transient absorption spectroscopy (TAS) is an optical pump-probe timeresolved technique that makes use of ultrashort laser pulses. In general, pump-probe experiments are used to investigate the nature and the evolution of electronic excited states in chemical systems. In these experiments a shorth laser pulse excites the molecules towards allowed excited electronic states. Afterwards the evolution of the excited states is monitored by a second spectrally broad pulse, called probe pulse, that is delayed in time with respect to the pump. At this point the electron can interact with the probe pulse returning to the ground state through radiative or non-radiative paths, or absorbing the radiation and be excited in states with higher energy. The change in the sample absorbance ΔA before and after the excitation is the physical quantity that one wants to measure. A pump-probe pulse sequence allows to obtain an excited state absorption spectrum at a certain delay time. By repeating this sequence as a function of the

pump-probe delay, it is possible to obtain the dynamical evolution (kinetics) of the transient absorption signal.

3.1.1 Instrumental Apparatus

The experimental instrumentation for femtosecond time-resolved transient absorption spectroscopy has been described in detail in previous reports[13–15]. A scheme of apparatus is show in figure 3.1 Indeed, it must generate pulses short enough to ensure the proper

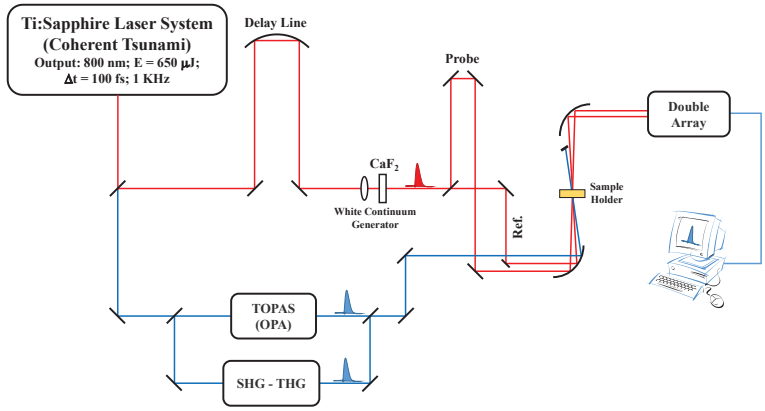

Figure 3.1: Schematical set-up of ultrafast UV/Vis transient absorption spectroscopy (TAS)

time resolution, with a high peak power in order to ensure frequency tunability through parametric amplification. The system used in the experiments of this thesis is based on a self-modelocked Ti:sapphire laser (Spectra Physics, Tsunami), pumped by an intracavity frequency doubled cw Nd:YVO laser (Spectra Physics, Millennia). The pulses (800 nm, $\approx$ 70 fs, 82 MHz) emitted by the main oscillator are stretched, amplified and recompressed by a regenerative amplifier (BMI Alpha 1000) to give amplified pulses of $\approx$ 100 fs, with an average power of $\approx$ 600 mW at 1 KHz repetition rate. The pulse train is divided into two portions of unequal intensity ($\approx$ 95/5).

The more intense one is used to produce the excitation beam. Pump beams at 400 nm and 266 nm are obtained, respectively, by second and third harmonic generation from the fundamental pulses at 800 nm by means of a BBO crystal. Additional tunability is obtained by pumping a parametric amplifier, the TOPAS (Travelling-wave Optical Parametric Amplifier of Super-fluorescence)[16,17]. The parametric amplifier generates two pulses at different frequencies, the signal and the idler, that are continuously tunable from roughly 1100 to 1600 nm and from 1600 to 2400 nm, respectively. The frequencies of signal and idler are determined by the phase-matching angle of the BBO crystal. As most electronic transitions are in the UV-vis spectral range, signal and idler can be doubled or combined with the fundamental, to obtain pump pulses from 800 up to 240 nm. The basic principles for obtaining the multiple output wavelengths required for the excitation beam are well known and fully described by Neuwahl et al.[14]. In the experimental section relative to each sample taken into account in this work, the experimental conditions are reported.
The weakest portion of light, 1-2 mW, is focused on a CaF_2 plate to produce spectrally broad ("white continuum"), i.e., containing all wavelengths between 350 and 750 nm. The exact wavelength range depends on the specifications of the white light generation. In alternative, by replacing calcium fluorite plate with sapphire, the near infrared components of the probe spectrum (approximately until 1000 nm) become accessible, to the detriment of the blue side. However, this configuration is not adopted for the measurements reported in this thesis.
The white-light continuum was further split into two parts of equal intensity by a 50/50 fused-silica-Al beam splitter. One part, acting as a probe beam, was spatially overlapped with the excitation beam in the sample, the second part crossed the sample in a different position, acting as a reference signal. The beams reach the sample with a variable delay with respect to the excitation pulse, thanks to a suitable optical delay line, while the reference travels along a shorter path and always strikes the sample before the excitation. The reference beam provides a convenient normalization function for the transient spectrum, significantly increasing the signal to noise (S/N) ratio. The delay of the probe with respect to the

pump pulse is determined by the distance traveled in the optical delay line, with a minimum step of 30 μm, corresponding to 100 fs. The three linearly polarized beams are focused on the same region of the solution by means of a parabolic mirror in a quasi-collinear geometry. The relative pump-probe polarization angle is set to 54.7 degree in order to exclude rotational contributions to the transient signal.
Sample's solution is usually inserted in a quartz cell (Hellma) with 2 mm optical path. The irradiated volume is refreshed by stirring the sample with a micro magnet inside the 2 mm cell and transient absorption spectra were recorded reducing the repetition rate from 1 KHz to 100 Hz to avoid photo-damage of the sample.
The acquisition of the transient absorption signal has been performed by a multichannel detection system. The pump and probe beams were spectrally dispersed by a Jobin-Yvon CP 140-1824 spectrometer and detected by a Hamamatsu double linear-array system. The electric signals, processed from a home made front-end circuit, were converted by a two channels analog to digital acquisition board (ADLINK DAQ-2010), and data acquisition was done in LabVIEW computer programming.

3.1.2 Measurements of Time Resolved Spectra

Transient absorption spectroscopy is commonly used to monitor the change of absorbance spectrum following the photoexcitation of molecules. The quantity of interest can be extract from the signal according to the following equation:

$$\Delta A(\lambda, \tau) = -logT(\lambda, \tau) \tag{3.1}$$

where T(λ, τ) is the photoinduced or transient transmittance. Similarly to the static transmittance, the transient one is defined as the ratio of the intensity of the probe beam recorded with [I(λ, τ)] and without [$I_0(\lambda, \tau)$] the pump pulse and can be calculated by:

$$T(\lambda, \tau) = \frac{I(\lambda, \tau)}{I_r(\lambda)} \cdot \frac{I_r(\lambda)}{I_0(\lambda)} \tag{3.2}$$

The intensity of the probe is always normalized with respect by the intensity Ir (λ) of the reference beam, that always interacts with the

sample before the excitation process. The last factor is the ratio between the intensities of the two beams without the excitation pulse, i.e. the "baseline".
The probe and reference beams are dispersed in wavelength after the dispersion element and a multichannel detection is achieved, so that the intensity profile of the probe $I_p(\lambda)$ and of the reference $I_r(\lambda)$ can be obtained at a given delay time. To orderly block and unblock the pump and probe beams in a sequential exposition of the events are used shutters. This procedure allows to subtract the scattered light contribution from the overall signal. In practice, each transient spectrum is acquired in three steps.

- $I_p + F_p$, $I_r + F_r$; with both pump and white continuum pulses;
- I_p^0, I_r^0; with only the probe;
- F_p, F_r; with only the pump.

Where I are the intensities of the probe and reference pulses, and F are all possible sources of scattered light. When the irradiated sample shows luminescence emission, the intensity acquired by the detector system is not related only to transient phenomena. The detector system collects the light continuously and it is not able to discriminate the light pulses synchronized with the pump excitation from the delayed emissions (fluorescence and phosphorescence). Some part of static fluorescence emitted by the sample propagates collinearly with the probe pulse being acquired by the detector system, producing a transient spectrum affected by some fluorescence contribution: the stimulated emission (whose intensity is related to the amount of excited state population and hence to the delay between the pump and probe pulse) and the static fluorescence. To avoid the static fluorescence contribution we performed a third acquisition step only with the pump beam because the fluorescence has different intensities on the detection surfaces of the probe and reference beams: F_p and F_s. All of this contributions are recorded, and subtracted from the intensity obtained when both pump and probe pulses impinge on the sample. The transient transmittance at a given delay time between pump and

probe is obtained by equation 3.3:

$$T(\lambda,\tau) = \frac{[I_p(\lambda,\tau) + F_p(\lambda)] - F_p(\lambda)}{[I_r(\lambda) + F_r(\lambda)] - F_r(\lambda)} \cdot \frac{I_r^0(\lambda)}{I_p^0(\lambda)} \tag{3.3}$$

In a first step, the baseline is acquired to correct any mismatch between the two channels. Indeed, the spectral contents of probe and reference, which are the reflected and the transmitted components of the white continuum by a beam splitter, are never exactly the same. This fact makes unreliable the simple ratio for the T(λ,τ) estimation. It is striking to frequently check the stability of the baseline, the flatness and the point to point intensity fluctuations determine the sensitivity of the detection system. We generally observe that 1000 shots are sufficient to produce a baseline which is flat within a variation of absorbance (ΔA) of $\pm$ 0.002.
In general, transient absorbtion spectra arise from three different contributions: excited state absorption (ESA), stimulated emission (SE) and bleaching (B). The first contribution is due to ground-state bleach. The pump pulse has promoted a fraction of the molecules to the excited state, the number of molecules in the ground state has been decreased. Hence, the ground-state absorption in the excited sample is lower than that in the non-excited sample. Consequently, a negative signal in the ΔA spectrum is observed in the wavelength region of the ground state absorption.
The SE occurs when in a two-level system the Einstein coefficients for the absorption from the ground to the excited state (A_{12}), and the stimulated emission from the excited to the ground state (A_{21}) are identical. Thus, upon population of the excited state, stimulated emission to the ground state will occur when the probe pulse passes through the excited volume. Stimulated emission will occur only for optically allowed transitions and will have a spectral profile that follows the fluorescence spectrum of the excited chromophore, being Stokes shifted with respect to the ground-state bleach. During the physical process of stimulated emission, a photon from the probe pulse induces emission of another photon from the excited molecule, which returns to the ground state. The photon produced by stimulated emission is emitted in the exact direction as the probe photon, and hence both will be detected. It is noticeable that the intensity of the probe pulse is weak enough that the excited-state

population is not affected appreciably by this process. The SE results in an increase of light intensity on the detector, corresponding to a negative ΔA signal.
Upon excitation with the pump beam, optically allowed transitions from the excited (populated) states of a chromophore to higher excited states may occur in certain wavelength regions, resulting in absorption of the probe pulse at these wavelengths. This process is called excited-state absorption and it is characterized by a positive signal in the ΔA spectrum is observed in the wavelength region of excited-state absorption. As in the previous case, the intensity of the probe pulse is weak enough that the excited-state population is not affected appreciably by the ESA process.

3.1.3 Transient Absorption Signal in the Time Domain

The transient absorption signal is proportional to the concentration of excited states which absorbs the photons of the probe beam at wavelength λ. Within the linear response regime the signal of a pump-probe experiment in the time domain and at a wavelength λ, is given by the convolution of the molecular response function with the functions associated to the pump and probe pulses. If s(t) is the signal, R(t) is the molecular response function, p_1(t) and p_2(t) are the functions of the pump and probe pulses, then we can express

$$s(t) = R(t) \otimes p_1(t) \otimes p_2(t) \tag{3.4}$$

where $\otimes$ is the convolution operation, defined as

$$a \otimes b = \int_{-\infty}^{\infty} a(t - t')b(t')dt' \tag{3.5}$$

The equation 3.4 can be reformulated as

$$s(\tau) = \int_{-\infty}^{\infty} \int_{-\infty}^{\infty} p_2(t - \tau)p_1(t - t')R(t')dtdt' \tag{3.6}$$

Considering the associative properties for the convolution operation, we obtain:

$$g(t) = p_1(t) \otimes p_2(t) \tag{3.7}$$

$$g(t' - \tau) = \int_{-\infty}^{\infty} p_2(t - \tau) p_1(t - t') dt \tag{3.8}$$

The function g(t'-τ) is the instrumental function which, considering the convolution theorem, is given by the crosscorrelation function between the pump and probe pulse. We can reformulate the equation 3.4 as

$$s(t) = R(t) \otimes p(t) \tag{3.9}$$

hence

$$s(t) = \int_{-\infty}^{\infty} g(t' - \tau) R(t') dt \tag{3.10}$$

The molecular response function is generally associated with the response of the molecular system to an applied perturbation and, therefore, it contains the information about the temporal evolution of the system itself. Hence, R(t) defines the evolution of the molecular property under study.
Transient absorption provides information about the photophysics and the photochemistry of the sample with a temporal resolution limited by the instrumental function. When the time constants of photophysical and photochemical processes are comparable with the instrumental function, the molecular response function can be obtained by a de-convolution operation on the acquired signal. The former operation assumes the detailed knowledge of the instrumental function's profile.

3.1.4 Characterization of the Instrumental Function

In order to achieve a faithful deconvolution of the kinetic profiles, the knowledge of the instrumental function is required. The instrumental function is defined as cross-correlation between pump and probe pulses. However, in order to determine the "real" function, a suitable experiment should be designed, whilst using the same sample cell in the identical conditions (angle between pump and probe and their diameters, for example) used for the actual measurements.Due to the inherent difficulty to achieve such ideal conditions, in practice the instantaneous signals appearing in transient absorption spectra can be conveniently utilized[18]. These

signals include two-photon absorption (TPA), stimulated Raman gain (SRG) and cross-phase modulation (XPM). TPA and SRG are non-linear effects produced by the short laser pulses with very high pump power density, while the XPM arises from the temporal chirp of the continuum white probe[19]. The temporal envelope of these signals reproduces the pump-probe cross-correlation function of equation $g(t) = \int I_{pump}(t')I_{probe}(t'+t)dt'$.
In particular, in most cases we determined the instrumental function by measuring the time profile of stimulated gain of the most intense Raman bands of the solvent. For a qualitative description of this phenomenon, we can assume that two photons of appropriate frequencies, spatially overlapped and coincident in time, impinge onto the sample. When the excitation frequency is close to a specific component of the probing white continuum, the emission of a third photon can be stimulated. The stimulated gain energy corresponds to the difference between the molecular ground state and a virtual energy level through which the pump photons are scattered and it is specific for each medium. The Raman wavelength λ_{SRG} and the pump wavelength λ_{exc} can be related by means of the following expression:

$$\frac{1}{\lambda_{exc}(nm)} - \frac{1}{\lambda_{SRG}(nm)} = \nu \cdot 10^{-7}(cm^{-1}) \tag{3.11}$$

The wavelengths must be expressed in nm, while ν, that is the frequency of an active Raman transition of the molecular system, is in cm^{-1}. SRG does not contain any relevant information about the sample; nonetheless, the plot of the intensity of the Raman signal *vs* the delay time (see fig. 3.2) gives the pump-probe cross-correlation function. Figure 3.2 shows a typical cross-correlation function obtained by this method: the time profile is Gaussian, with a full width half maximum (FWHM) equal to 130 $\pm$10 fs. This method allows to measure the instrumental function, even if indirectly. The measure is accurate only if one refers to a probing wavelength near the Raman signal. As a matter of fact, the temporal resolution is primarily determined by the pulse duration; however, the latter is not the only parameter that one should consider for the instrumental function evaluation. There is another effect that possibly contributes to the broadening of the instrumental function. If the

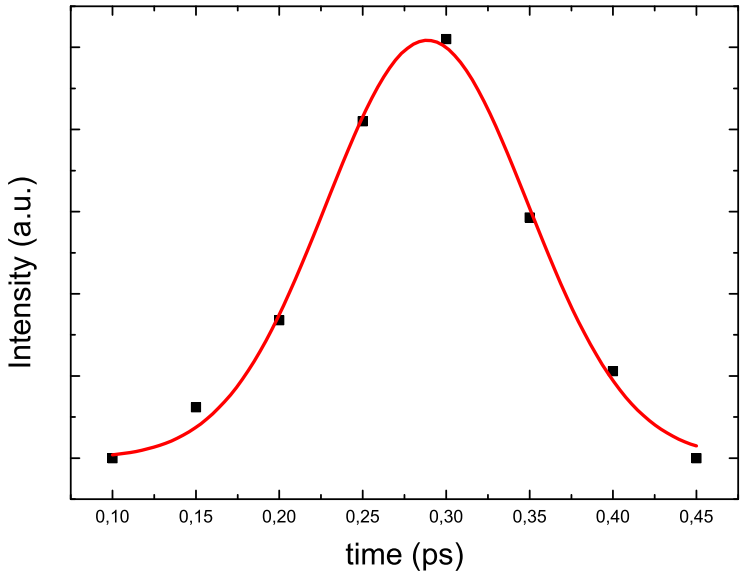

Figure 3.2: Intensity of the stimulated gain Raman signal *vs* the delay time between pump and probe pulses in water ($\lambda_{exc} = 520$ nm; $\lambda_{SRG} \approx 620$ nm). The red line is the result of a Gaussian fit that provides the instrumental function with temporal width of FWHM equal to 130 $\pm$10 fs

central wavelength of the pump and of the probe are different, the refractive index experienced by the two pulses inside the sample cell is different and hence there is a mismatch of the velocity (GVM) of the two pulses. In other words, the pump and probe pulses travel at different speeds in the medium, and the cross-correlation function broadens. In the case of Gaussian pulses, the instrumental function broadening due to GVM can be calculated from:

$$G(t) = \frac{c}{a\Delta n}\{erf[a(\tau + \frac{l}{c}\Delta n)] - erf(a\tau)\} \tag{3.12}$$

where Δn is the difference between the refractive indexes of the medium at the pump and probe wavelengths, l is the optical path

(length of the interaction volume)and the a constant is given by:

$$a = 2\sqrt{\frac{ln2}{\Delta\tau_{pump}^2 + \Delta\tau_{probe}^2}} \tag{3.13}$$

$\Delta\tau$ indicates the duration of the pulses, i.e. their full width half maximum (FWHM). The broadening effect described by Eq 3.12 is obviously dependent on the probe wavelength. This leads us to conclude that the GVM effect although present, is small and approximatively constant through the entire probe wavelength range considered, at least for the limited path length of the pulses in our samples (tipically 1 mm). As a consequence we can avoid any further correction, and assume that the measured instrumental funcion contains also some average contribution of GVM.

3.1.5 Group Velocity Dispersion (GVD)

Using white continuum pulse as probe, we are able to record in one step a broad range of wavelengths. In practice, the wavelengths composing such a pulse are affected by a significant positive chirp due to group velocity dispersion (GVD). A detailed discussion of this effect can be found in reference[20]. The GVD effect influences the recorded spectral features; a possible method to limit this undesirable effect is to reduce the total amount of optical materials introduced into the beam path. However, for the analysis of the spectra in the first picosecond, is necessary to correct the spectral artifact produced by this effect. The red components of the white continuum speed over the blue components, so that probing in the two visible regions does not occur at the same delay time.

3.1.6 Single Value Decomposition (SVD)

Transient absorption spectra can be examined by different methods. Kinetics are plotted at any given wavelength to obtain the time course of the spectral features of interest. In addition, single value decomposition SVD can be practised to extract the spectra of the kinetic components, trying benefit from the global analysis[21–23]. When a large time-wavelength data set is available, it would be

convenient to analyze all of them together. SVD is a factorization procedure that reduces the data matrix to a series of orthogonal basis components into time-independent spectra and wavelength independent kinetics[24]. If A(λ,t) is an m×n matrix then the SVD returns three matrixes, as below:

$$A(\lambda, \tau) = USV^T \tag{3.14}$$

where U is an m by m matrix, the matrix S is m by n with nonnegative numbers on the diagonal (as defined for a rectangular matrix) and zeros off the diagonal, and V denotes an n by n matrix. U contains a set of orthonormal "output" basis vectors, i.e. basis spectra as a function of U. Associated with each basis is a eigenvalue in the diagonal matrix S, so that each diagonal element can be considered as scalar "gain" by which each corresponding input is multiplied to give a corresponding output. The orthonormal "input" or "analyzing" basis vectors are enclosed in matrix V and the rows of the transpose V^T express the time course of the spectra basis. The number of components that one have to consider is determined by the weight in the S eigenvalue matrix. If the single value component, scaled according to its respective singular value, is comparable with the experimental noise, then the component will be neglected. Global analysis was performed using the GLOTARAN package (http://glotaran.org)[24,25], and employing a linear unidirectional "sequential" model, shown in figure 3.3:

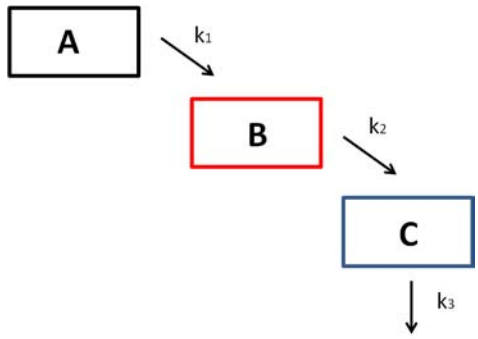

Figure 3.3: Sequential kinetic model applied for global analysis

3.2 Ns-Laser Transient Absorption Technique

The transient behavior was investigated using a flash photolysis setup previously described[26] based on an Nd:YAG Continuum laser (Surelite II, third harmonics, $\lambda_{exc} = 355$ nm, pulse width ca. 7 ns and energy ca. 1 mJ pulse). The transient spectra were obtained by monitoring the optical density changes every 5-10 nm over the 300-800 nm range and averaging at least 10 decays at each wavelength. The kinetic analysis of the signals at selected wavelengths allowed the transient decay time to be determined. The calibration of the experimental setup, for quantum yield determinations, was carried out with an optically matched solution of benzophenone in acetonitrile (triplet quantum yield, $\phi_T = 1$ and $\epsilon_T = 6500\ M^{-1}\ cm^{-1}$)[27]. The experimental errors on the transient decay time values are estimated to be about 10% while those on the quantum yields are about 15%. All the measurements were performed in air-equilibrated samples.

3.3 Single Photon Counting Technique (SPC)

The luminescence decay, τ_L (mean deviation of three independent experiments, ca. 5%), was measured by single photon counting method using an Edinburgh Instrument 199S setup. A pulsed LED was used as excitation source, and a Hamamatsu R7400U-03 detector acquired the signal.

3.4 Steady-State Spectroscopy

The absorption spectra have been recorded by a Lambda 950 Perkin Elmer model spectrophotometer. The fluorescence spectra, corrected for the instrumental response, and quantum yields were measured by means of a Perkin-Elmer spectrophotofluorimeter (mod. LS55).

Chapter 4

Electron Dynamics and Charge Transfer Process in CdTe QDs

4.1 Photophysical Properties and Recombination Dynamics in CdTe QDs with Different Thioglycolic Capping Agents

The design of hybrid nanomaterials based on colloidal semiconductor nanocrystals (or quantum dots, QDs) and organic moieties have attracted prominent attentions in the last three decades due to their physical and chemical properties. In most wet synthetic procedures, the full control of the nucleation and growth processes is achieved by use of organic capping agents which in many cases affect the growing process, the structure and the electronic properties of the colloidal nanocrystals. The deep investigation of the effects of capping agents enabled the development of a wide variety of research and different applications[28–34]. The design of hybrid nanomaterials based on colloidal semiconductor nanocrystals (or quantum dots, QDs) and organic moieties have attracted prominent attentions in the last three decades due to their physical and chemical properties. In most wet synthetic procedures, the full control of the nucleation and growth processes is achieved by use of organic capping agents which in many cases affect the growing process, the

structure and the electronic properties of the colloidal nanocrystals. The deep investigation of the effects of capping agents enabled the development of a wide variety of research and different applications such as CdTe[34–38], CdS[39–42], CdSe[38,43,44], ZnS[45], ZnSe[46,47], HgTe[48]

During the excitation with UV/Vis radiation, if the charges are not trapped or transferred but remain localized on the conduction band (CB), the excitonic species will recombine by radiative and non-radiative processes towards the valence band (VB). However, the exciton evolution strongly depends on the nature of the materials, of the defects of the lattice and of the surface, thus becoming sensitive to the capping agent and to the surroundings (solvent). Therefore, under these circumstances, the role of capping agent becomes of primary importance and it can be investigated through optical techniques.

A large number of studies were devoted to understand how the stabilizers act on the chemical and physical properties of nanocrystals[49–54]. The aim of capping agents is not only the prevention of the particles flocculation. They play a key role both by influencing the growth kinetics and thus the lattice properties especially at the surface of the nanostructures, and by affecting the chemistry of the surface[55].

In this work we have investigated cadmium telluride (CdTe) QDs synthesized in water using 1-thioglycerol (1TG) and 3-mercaptopropionic-acid (MPA) as capping agents. In order to have a wider overview on how these capping agents influence the chemical-physical properties of the nanocrystals and the dynamics of their exciton state, the QDs were synthetized following similar procedures. The photophysical properties were then investigated with stationary and time-resolved techniques. Through stationary photoluminescence studies the presence of lattice defects has been proved. The time-resolved measurements, the single photon counting (SPC) and the UV/Vis ultrafast transient absorption spectroscopy (TAS), enabled to investigate the relaxation processes of charge carriers formed upon photoexcitation.

4.1.1 Synthesis, Morphological and Steady-State Characterization

The CdTe QDs were prepared with the colloidal methods previously reported in literature[35–37]. As a firs step 0.2 mmol of $Cd(NO_3)_2 \cdot 4H_2O$ and 0.4 mmol of 1TG were added to a volume of 40 ml of milliQ water under vigourous magnetic stirring. When the solution is well mixed is added NaOH 1 M by dropwise addition until to obtain a pH value around 12. Meanwhile the tellurium precursor was prepared adding in 10 ml of milliQ water 0.4 mmol of tellurium powder and 1 mmol of $NaBH_4$; the reduction occurs maintaining the environment to 80 degrees for 30 minutes in nitrogen atmosphere.
The solutions previously obtained were mixed with a molar ratio between Cd and Te of 5:1 in order to prepare the nanocrystals. The growth and nucleation processes of the nanocrystals are then conducted at 100 °C in an inert atmosphere. The same procedure previously reported for the 1TG capped QDs was also used for the synthesis of the QDs with MPA as stabilizers, with the only difference that in this case the molar ratio between Cd and Te is 1:1.
In Figure 4.1, the absorption and photoluminescence spectra of 1TG and MPA capped QDs collected at different reaction times are shown, and in Table 4.1 the emission quantum (QY) and other spectral parameters at different reaction times are reported. Both kinds of colloids show a well-resolved absorption band corresponding to the first electronic transition, suggesting a quite narrow size distribution of the nanocrystals. Increasing the reaction time it is possible to notice that the absorption maximum of the exciton transition shifts to higher wavelengths due to the increasing size of the colloids. This phenomenon is prominent for the MPA capped QDs. These latters maintain a higher definition of the BG transition at longer reaction times than the 1TG capped particles. In general, a broadening of the luminescence spectra with increasing the reaction time corresponds to a widening of the size distributions of the aqueous QDs. In the present samples, the comparison of the full width half maximum (FWHM) of the emission band has shown similar values (few cm^{-1} difference) with increasing the reaction time, for both samples, suggesting that the dimension of the

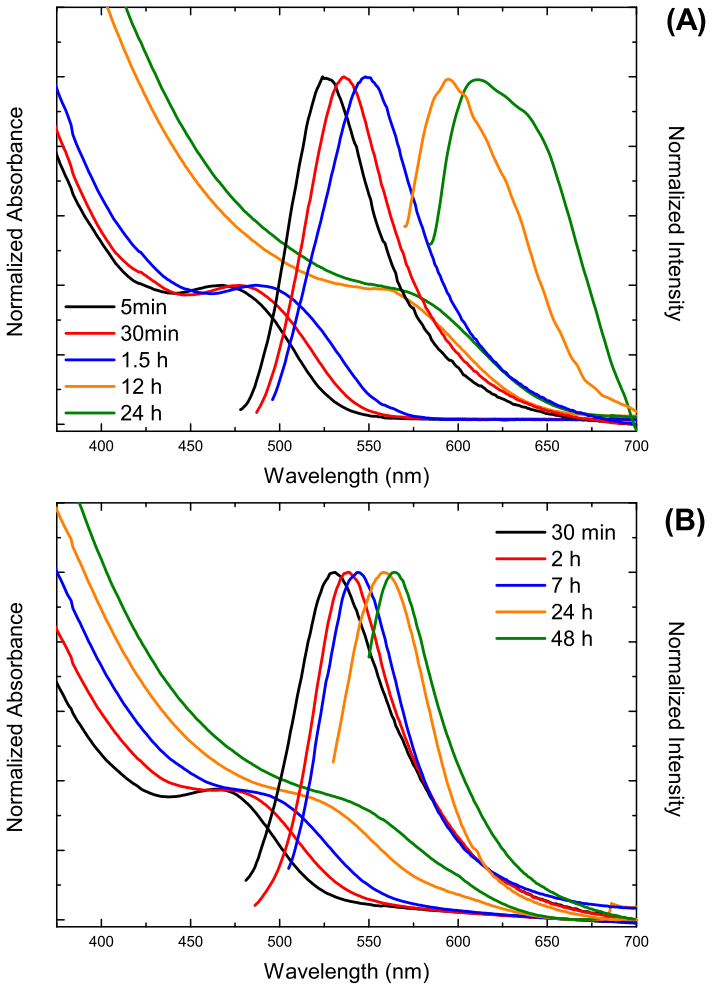

Figure 4.1: Absorption and luminescence spectrum of (A) CdTe MPA capped QDs and (B) CdTe 1TG capped QDs in water. All sample was excited at the maximum of the BG transition

colloids increases without altering the contribution of different size populations. However, significant differences can be observed for the Stokes shift values and the luminescence QY values. Generally, a higher shift of the emission band, compared to the band gap

CdTe MPA capped

time	BG(nm)	FWHM(cm^{-1})	SS(cm^{-1})	QY(%)
5 min	468	2020	2360	6.2
30 min	478	1930	2260	9.1
1.5 h	487	1890	2320	11
12 h	565	1840	890	17
24 h	574	2100	1050	18

CdTe 1TG capped

time	BG(nm)	FWHM(cm^{-1})	SS(cm^{-1})	QY(%)
30 min	465	2260	2670	1.8
2 h	476	1900	2420	1.6
7 h	490	1810	2020	4.2
24 h	518	1820	1420	10
48 h	535	1740	960	10

Table 4.1: Band gap position, FWHM of the luminescence band, Stokes shift (SS) and luminescence QY at different reaction times

absorption energies, and the quite low QY values indicate the low lying emitting states, such as defects states, and/or the occurrence of non-radiative deactivation channels able to compete with the exciton radiative recombination. However considering the evolution of these parameters for the two sample (Table 4.1), it is possible to observe that an increase of the reaction time leads to an increase of the QY and a decrease of the Stokes shift . This observation confirms that the longer the reaction time the smaller the contribution of the defects on emission behaviour. The comparison of data obtained for MPA- and 1TG-CdTe suggests that MPA enable a better control of the growth process and act as a better capping agent since higher QY values have been measured for MPA-CdTe samples. However even for these samples the occurrence of efficient non-radiative recombination processes have to be taken into account.

To better understand how these two stabilizers affect the photophysical properties of the CdTe QDs, one sample for each stabilizer was chosen to be subjected to a deeper characterization; the se-

lection was done taking into account the samples having the most similar size which are the MPA capped sample obtained after 12 hours of reflux and 1TG capped colloid after 24 hours of reaction (see below).
The size distribution in the samples was monitored by AFM measurements. In Figure 4.2A, the AFM images recorded on MPA capped QDs sample taken after a reaction time of 12 hours confirm the formation of spherical nanocrystals. Size dispersion was achieved by analysing the height distribution histograms (Figure 4.2B). Observing the size distribution, the sample presents only

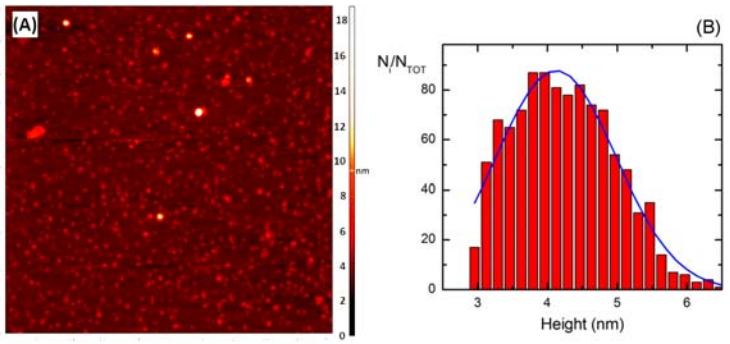

Figure 4.2: AFM image (A) and size distribution histograms (B) of CdTe-MPA nanocrystals in water

one broad population, having an average size of 4 ± 1 nm. For the 1TG capped sample obtained after 24 hours of reaction, the size distribution appear more complex and show two major populations with a total weight of 83% and a mean diameter of 3.7 ± 0.9 nm and several minor populations with higher mean diameters 4.5 ± 0.2 (9%) and 4.8 ± 0.4 (8%) nm (Figure 4.3). The 1TG capped QDs show a narrower distribution of the main population suggesting a better control of the growth process with 1TG as capping agent than MPA.
The absorption spectra of the suspensions (Figure 4.4) are characterized by a single BG feature centred around 565 and 520 nm for QDs with MPA and 1TG as stabilizer, respectively. Both systems present the characteristic absorption due to the continuum energy states at higher energies.

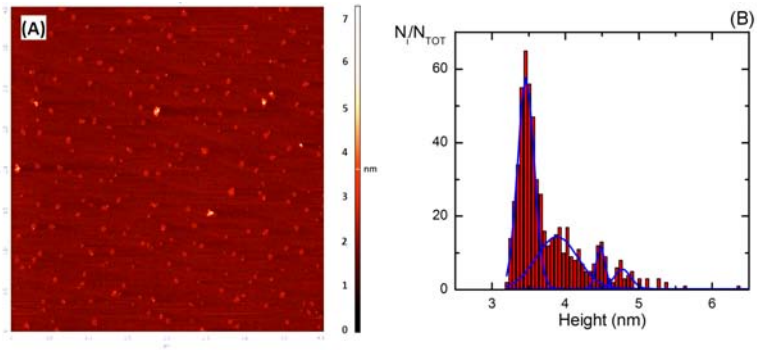

Figure 4.3: AFM image (A) and size distribution histograms (B) of CdTe-1TG nanocrystals in water

In agreement with the model proposed by Donegá and Koole[56] it is possible determine the QDs extinction coefficient at higher energy (400 nm) by the following equation

$$\epsilon_{400} = \left[\mu_{400} N_A z \frac{V_{QD}}{V_{UC}}\right] (2303)^{-1} \tag{4.1}$$

where μ_{400} is the absorption cross section per unit ion pair at 400 nm, N_A is the Avogadro's number, z is the number of unit ion pairs per unit cell, V_{QD} and V_{UC} are volumes (cm^3) of the QD and unit cell. Another method to determine the ϵ coefficient has been developed by Peng et al.[57] where the value for the CdTe nanocrystals is determined at the band gap and is given by the empirical function

$$\epsilon = 3450 \Delta E(D)^{2.4} \tag{4.2}$$

where ΔE is the energy gap and D is the diameter of the nanoparticles. The absorption coefficient values achieved with the two methods are reported in Table 4.2 together with the QDs molar concentrations, determined using the Lambert-Beer law.

Since for each suspension the concentration values are the same, within the experimental errors, at the two wavelengths, the accuracy of the methods for the absorption coefficient determination is good. The comparison of the coefficients for the MPA- and 1TG-capped samples indicates that the nature of the capping agent has

CdTe MPA capped		CdTe 1TG capped	
ϵ_{400}=748000	[QD]=4.5×10^{-6}	ϵ_{400}=545000	[QD]=5.3×10^{-6}
ϵ_{565}=198000	[QD]=4.5×10^{-6}	ϵ_{520}=215000	[QD]=5.5×10^{-6}

Table 4.2: Molar extinction coefficient at different wavelengths achieved with different methods and QDs molar concentration

a negligible effect on the cross section of the band gap transition, since similar values have been obtained; on the other hand a discrepancy of about 30% can be observed in the absorption coefficients determined at 400 nm, thus suggesting that the stabilizer affects the probabilities of the transitions above the band gap.
The photoluminescence spectrum of the CdTe-MPA QDs obtained exciting the sample at the maximum of BG (565 nm) presents a single emission band centered at 595 nm with a relevant shoulder on the red edge (Figure 4.4A). The appearance of this component it is generally ascribed to the contribution of trap states. The occurrence of dissipative or trapping processes has been confirmed by the quite low luminescence efficiency measured (17%) for the CdTe suspension[58,59]. However, in this case we need to consider that a further contribution to the spectral features on the red-edge of the QDs luminescence is given by the broad size distribution of these nanocrystals. The photoluminescence behaviour of the 1TG capped QDs (Figure 4.4B), upon excitation of the nanocrystals at 520 nm, shows a single symmetric emission band centred at 560. However, 1TG- CdTe has a higher Stokes shift and a lower luminescence QY (10%) compared to MPA-capped samples, indicating that the 1TG capped QDs are affected by a greater amount of defects.

With the aim to deeper investigate the role of the capping agent and the effects on the relaxation of the exciton state, an accurate characterization of the electronic dynamics after the exciton formation has been carried out. As it is well known from the literature[53,60–62], the radiative electron-hole recombination in QDs systems occurs within a time window of the order of nanoseconds. Therefore, SPC measurements were performed to correctly characterize the radiative electron-hole recombination.

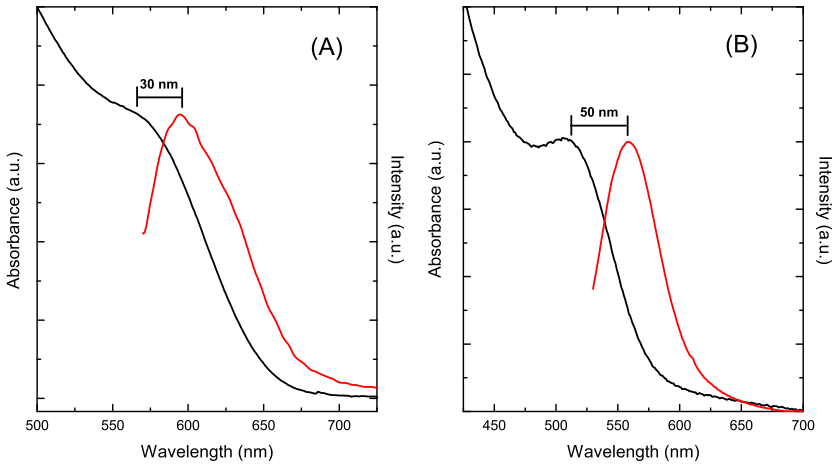

Figure 4.4: Stationary absorption spectrum (black line) and luminescence spectrum (red line) of (A) CdTe-MPA QDs in water exciting at 565 nm and (B) CdTe-1TG QDs in water exciting at 520 nm

SPC measurements, carried out exciting at 460 nm and collecting the photons at 620 nm, show a nonexponential behaviour of the luminescence decay curves, as previously observed for colloidal samples[63–66], principally ascribable to size distribution. The photoluminescence decays could be reproduced for both species by biexponential functions which likely reflect the distribution of decay times related to the distribution of excitonic populations[64,65,67]. The biexponential fit can be described by the function

$$F(t) = y_0 + \sum_{n=1}^{\infty} A_n exp(-t/\tau_n) \tag{4.3}$$

and the average time is calculated using[53,66]

$$\tau = \sum_{n=1}^{\infty} A_n \tau_n^2 / \sum_{n=1}^{\infty} A_n \tau_n \tag{4.4}$$

The decay parameters are collected in Table 4.3 along with the averaged decay time value. The photoluminescence decay times, as well as the quantum yield, are strongly influenced by the quality of

	τ_1 (ns)	A_1(%)	τ_2 (ns)	A_2(%)	$<\tau>$ (ns)
CdTe-MPA	7.1	49.0	30.1	51.0	25.8
CdTe-1TG	20.8	58.9	51.6	41.1	40.3

Table 4.3: Luminescence decay parameters for CdTe QDs in water

the lattice structure and by the presence of surface defects and how these latters are passivated by the capping agents. The two samples present quite different luminescence decay times indicating that, despite the size effects, the organic ligands alter the dynamics of the exciton recombination. In particular, longer decay times were measured for 1TG-QDs, for which higher contribution of defect states has been supposed.

4.1.2 Time Resolved Absorption Measurements

To better understand the electronic evolutions that occur below the nanosecond time scale we have used ultrafast UV-Vis TAS. The excitation energies were chosen with the aim to excite electrons in the conduction levels (CB), but in different energetic conditions. Therefore the samples have been excited near the BG and at higher energies. In these latter conditions the electrons are promoted to energy levels with a greater density than the states near the LUMO level, causing higher electron mobility. In these conditions the charges can follow other deactivation pathways towards the fundamental state and then cause modifications for charge and energy transfer processes. The MPA capped nanocrystals were pumped at 520 nm near the BG, and at 400 nm with an energy excess of 0.72 eV (5800 cm^{-1}) respect to BG. The 1TG capped QDs were excited at 476 nm near the BG and at 374 nm for the transition into higher energy states, maintaining the same energy difference of the MPA capped particles. It is important to notice that the pump power was kept small with the aim to reduce multiexciton generation processes due to the multiphoton absorption. Moreover, according to previous works[68–70], TAS measurements were carried out in a static cell (2 mm thick) under magnetic stirring to avoid the accumulation of long living transient species; to confirm the correct experimental conditions we have optimized the stirring speed

in order to reproduce results comparable with those measured in a flow cell.
The transient measurements of MPA capped QDs after the resonant excitation at 520 nm are shown in Figure 4.5. The spectrum on the left shows the correspondence between the transient absorption spectrum (red line) registered after 3 ps, and the BG transition in the steady-state absorption spectrum (blue line). The transient spectrum exhibits an intense bleaching signal, which corresponds to the BG transition in the stationary spectrum, with a maximum around 565 nm. In addition to the bleaching band, the former exhibits a positive broad signal at lower probe energy (above 600 nm). This is due to the excited state absorption (ESA) of the electrons from the lower energy levels to the continuum energy state on the CB[68].
The bleaching kinetic traces recorded at different wavelengths are

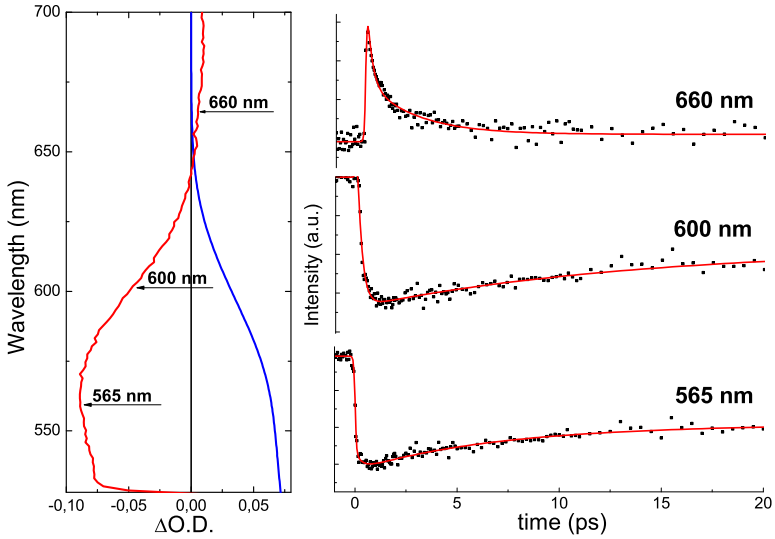

Figure 4.5: The Figure on the left shows the stationary absorption spectrum (blue line) and the transient spectrum (red line) after 3 ps than the exciter at 520 nm of the MPA capped QDs; on the right are present the kinetic traces at different wavelengths

reported and it is possible to notice a fast rise component and a decay dynamics, which can be reproduced by a triexponential func-

tion. The ESA signal can be satisfactorily represented by a single exponential function confirming the different nature of the transitions; it is worth to underline that the ESA signals do not present rise components. The values of the decay times and the normalized pre-exponential factors are reported in Table 4.4.
Since the longer decay time of the bleaching band is due to the radiative electron-hole recombination, the average decay time previously obtained with the SPC was fixed during the fitting analysis of the kinetic traces. Analyzing the kinetics associated to the bleaching, it is possible to see that the rise of the signal can be described with a time constant of about 320 fs. This process can be due to the cooling dynamics of the electrons into the VB. Although the excitation should take place from the HOMO level, a part of the electrons in the lowest energy states are promoted to the CB, causing a refilling of the holes by the cooling of the electrons at higher energies.
As observed in previous studies, the decay times τ_2 and τ_3 are too fast to be a radiative electrone-hole recombination[71] and usually in nanocrystals QDs the non-radiative electron-hole recombinations are principally dominated by surface trapping and Auger recombination[71–73]. In the present case the decay time τ_2 could be assigned to Auger recombination due to multiexciton in the CB or to non-radiative recombination processes induced by the surface traps[51,71,74,75]. In order to understand the nature of the faster time and to reduce the contribution due to the multiexciton formation by multiphoton absorption, we have changed the pump fluence for all the excitation wavelengths. Increasing the pump power the decay time τ_2 remains constant. This observation confirms that the process associated with the decay time τ_2 is not due to the presence of multiexciton in the CB but likely to the surface defects[68,71,74]. The third component τ_3 is reduced upon an increase of laser power and this suggests that this process is due to Auger recombination[76]. The ESA decay is well defined by a 1.5 ps decay time and the transition can be assigned to the absorption of the excited electron into the continuum[68].
Regarding the MPA capped nanocrystals excited with an excess of energy (400 nm), the same transient spectral features are observed than upon excitation at 520 nm. The transient and stationary spec-

tra and the kinetic traces taken at different wavelengths are shown in Figure 4.6. The kinetic traces recorded at different wavelengths

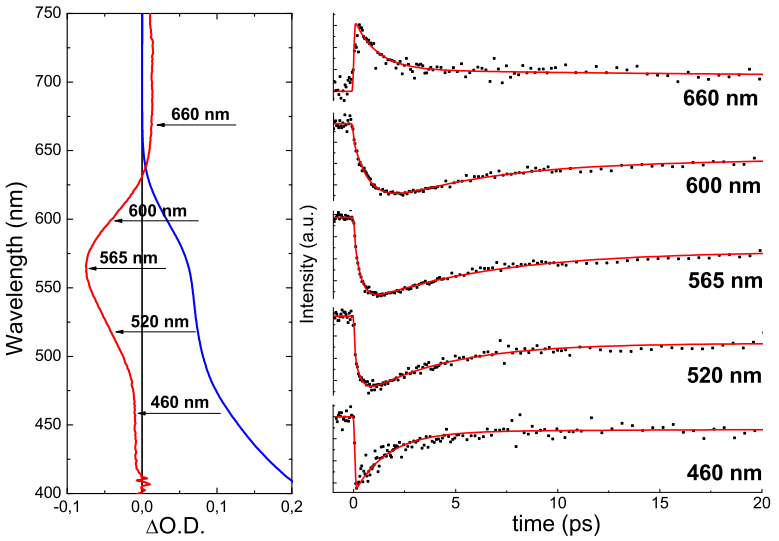

Figure 4.6: The Figure on the left shows the stationary absorption spectrum (blue line) and the transient spectrum (red line) after 3 ps than the exciter at 400 nm of the MPA capped QDs; on the right are present the kinetic traces at different wavelengths

on the bleaching band show a well-defined trend in the rise of the signal, i.e. the rising time increases from 410 to 800 fs moving towards longer wavelengths. The decay time τ_2 shortens when the excitation wavelength is set at 400 nm. This behaviour, ascribed to the effect of surface trapping sites, is due to the higher mobility of the electrons into the continuum respect to those present on discrete levels. A similar trend is observable for the τ_3 component where the decay time becomes five times smaller when the energy increases. Furthermore it is interesting to notice that independently from the capping agent, the normalized pre-exponential factor of the radiative component (A_4) is smaller by exciting at 400 nm rather than at 520 nm. This observation indicates that upon exciting the samples to higher energy states reduces the efficiency of radiative decay path and makes non-radiative process more competitive, particularly evident for the decay time τ_2, which

has a maximum relative weight (87%) at 450 nm. The ESA decay time is, within the experimental errors, indepent from the pumping energy.
In Figure 4.7 the results obtained pumping the 1TG capped QDs are shown near the BG at 476 nm and in Figure 4.8 the results obtained exciting at 374 nm. . The decay time values and the normalized pre-exponential factors are reported in Table 4.4. Also in this case the transient spectra show a bleaching band that corresponds to the BG transition and an ESA due to the absorption of the electrons into the energy continuum levels[68].

As in the CdTe MPA capped QDs, the fitting was carried out

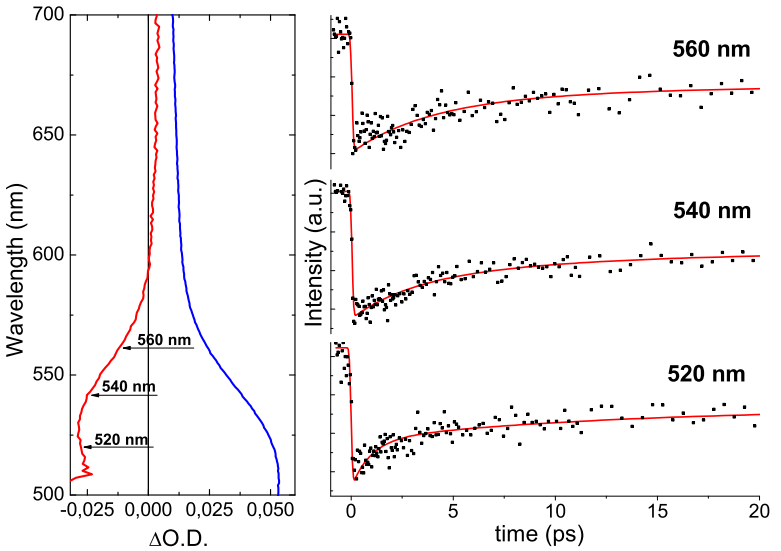

Figure 4.7: The Figure on the left shows the stationary absorption spectrum (blue line) and the transient spectrum (red line) after 3 ps than the exciter at 476 nm of the 1TG capped QDs; on the right are present the kinetic traces at different wavelengths

considering the average decay time for the longer photoluminescent electron-hole recombination obtained by the SPC technique. In this case the bleaching kinetic traces of the resonant excitation show an instantaneous rise independently of the wavelength. Instead the excitation at high energies produces a signal that grows with a time constant ranging from 500 to 700 fs due to the electron

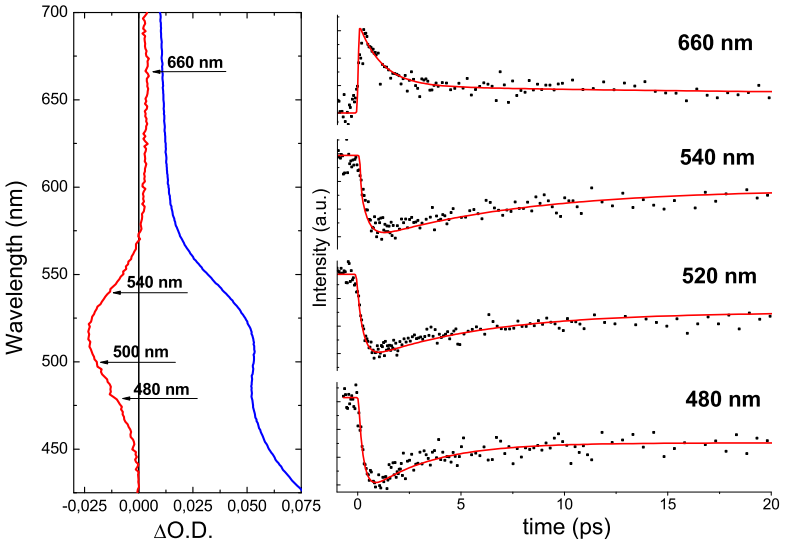

Figure 4.8: The Figure on the left shows the stationary absorption spectrum (blue line) and the transient spectrum (red line) after 3 ps than the exciter at 374 nm of the 1TG capped QDs; on the right are present the kinetic traces at different wavelengths

cooling that occurs into the VB. The assignment of the decay times is the same of that proposed for MPA QDs.

Exciting the QDs near the band gap, we have therefore observed that the decay times for 1TG capped QDs is the half than MPA capped QDs. In both systems it is possible to notice an increase of the electron mobility in the CB at high excitation energies and a reduction of the decay times of the charges in the traps. The presence of 1TG as capping agent, for which a higher contribution of defect states was supposed, significantly reduces the decay times τ_2 and τ_2, suggesting that in this sample the non-radiative recombination processes are kinetically more competitive with radiative processes.

At this point we have a general description of the excitons of CdTe QDs after excitation on the CB where the first electron can undergo deactivated processes by surface defect sites in few picoseconds or it can decay on the VB by a radiative recombination. The second process is due to charges remaining in the CB for a few tens of

nanoseconds before photoluminescent electron-hole recombination occurs.

4.1.3 Conclusions

The synthesis of CdTe QDs in water with two different stabilizers shows significative differences in both morphological and photophysical properties. AFM measurements show a different size distribution with a broader population for MPA capped QDs. In parallel, the steady-state characterization shows a higher luminescent quantum yield for the MPA capped QDs. The spectra are more affected by surface defects and size distributions. The SPC measurements enable to investigate the radiative electron-hole recombination, which strongly depends on the nature of the capping agent, despite the size distribution. The photoexcited electrons studied with ultrafast TAS show a multiexponential recombination with a rise time due to the electron cooling in the VB. The fast decay is due to the trapping state, while the intermediate decay time (τ_3) can be attributed to Auger recombination. The attribution of these processes is supported by pump fluence dependent measurements. Furthermore, increasing the excitation energy it is possible to notice for the samples a reduction of both decay times due to the greater mobility of the electrons in the higher energy states. Therefore the comparison of the results obtained with QDs with two different stabilizers shows that MPA capped QDs are more affected by the different excitation energy, leading to significant changes in the value of intermediate the decay time τ_3. The fastest lifetime in 1TG capped QDs suggests a greater influence of the surface traps, in agreement with the results obtained by photoluminescence measurements.

MPA

λ_{exc}(nm)	λ(nm)	A_1(%)	τ_1(ps)	A_2(%)	τ_2(ps)	A_3(%)	τ_3(ps)	A_4(%)	τ_4(ns)	τ_{ESA}^{660}(ps)
400	460	0	0	87	1.6	3	30	10	25.8	1.4
	520	-44	0.41	26	1.8	12	16	18		
	565	-47	0.61	34	0.9	8	20	10		
	600	-72	0.80	6	1.0	9	25	13		
520	565	-14	0.32	33	6.7	12	129	41	25.8	1.5
	600	-31	0.33	28	12	11	140	30		

1TG

λ_{exc}(nm)	λ(nm)	A_1(%)	τ_1(ps)	A_2(%)	τ_2(ps)	A_3(%)	τ_3(ps)	A_4(%)	τ_4(ns)	τ_{ESA}^{660}(ps)
374	480	-50	0.58	49	0.6	0.5	9.0	0.8	33.5	3.2
	520	-50	0.47	26	1.1	10	12	15		
	540	-51	0.70	35	1.1	7	16	8		
476	520	0	0	32	2.0	23	14	45	33.5	low signal
	540	0	0	34	3.1	21	15	45		
	560	0	0	43	4.7	14	27	43		

Table 4.4: Time constant and relative pre-exponential factors of CdTe MPA and 1TG capped QDs; A_1 and τ_1 are relative to the rise component

4.2 Electron Transfer Dynamics from CdTe QDs to MethyViologen molecules

In the previous paragraf we have carachterized the electron dynamics of CdTe QDs with different thyioglicolic capping agents. It is necessary that the nanocrystals are able to donate electric charges in order to be utilized in some devices[28–34,59]. Furthermore, in order to have an efficient charge transfer process it is necessary that the non-radiative deactivation channels are absent or at least minimized. One of the limits of semiconductor nanocrystals is the formation surface and lattice defects providing non-radiative deactivation pathways. Therefore, according to the previous characterization, we have chosen to investigate the charge-transfer processes of CdTe MPA capped QDs. These particles have shown a lower amount of defects with a higher QY and an absorption spectrum shifted to the red that allows to absorb a large portion of solar radiation. The charge transfer process was studied in presence of methylviologen (MV^{2+}), molecule known in the literature to be a good electron acceptor[58,77,78] capable to statically interact with the QDs surface.

4.2.1 Photoluminescent Characterization

With the aim to determine how the luminescence properties of the nanocrystals can be influenced by an electron acceptor as MV^{2+} in solution, luminescence quenching measurements were done (Figure 4.9).

Resonant excitation of the BG (565 nm) shows an efficient emission quenching with a non-linear trend when the quencher concentration increases. The deviation from typically Stern-Volmer trend suggests that the interaction has both a static and a dynamical nature. In addition quenching can be due to different binding sites on the QDs surface[1,63,66,79–82]. In nanocrystal systems the probability to have a static interaction depends on the properties of the quencher to be adsorbed on the particles surface and on its relative affinity in comparison to the stabilizer. In our system this interaction is confirmed by the nanocrystals flocculation when the MV^{2+} concentration is around 10^{-4} M. This is due to the presence of a

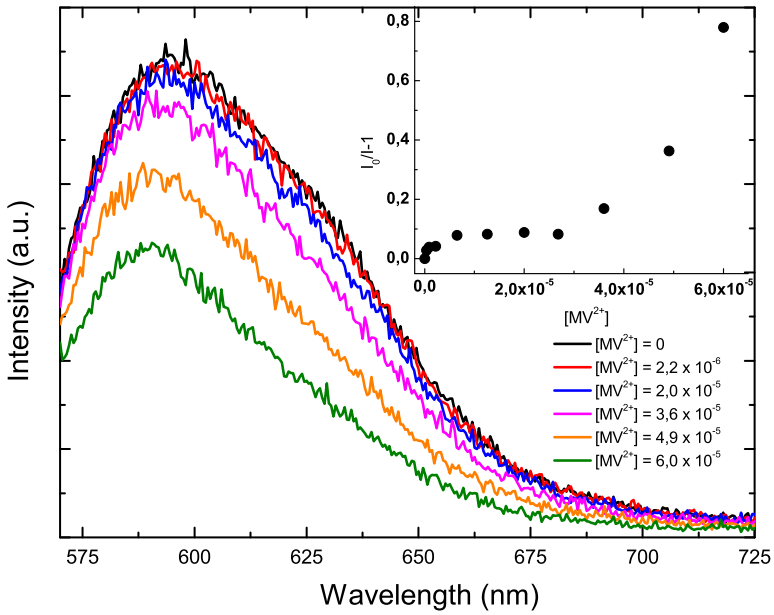

Figure 4.9: Luminescence spectra of CdTe nanocrystals in the prencence of increasing concentration of MV^{2+}; in the inset is shown the Stern-Volmer plot (λ_{max}=595 nm

highly charged molecule such as MV^{2+} on the particles surface in a strongly polar solvent such as water. Therefore the high electrostatic charge causes an instability on the particles surface leading to flocculation phenomena. Furthermore the static interaction is also confirmed by the blue-shift of the emission band with a progressive disappearance of the should on the red-edge of the luminescence spectra. This interaction induce a reorganization of the ligands on the surface due to the adsorption of the quencher molecules leading to a better passivation of the surface defects[59,64].
In order to obtain new pieces of information concerning the association equilibrium between the CdTe QDs and the MV^{2+} molecules the model proposed by Sharma et al.[59,83] has been utilized. The apparent association constant (K_{app}) can be expressed as a function

of emission intensity of the complexed (ϕ') and uncomplexed (ϕ_0) CdTe species and in terms of observed emission intensity (ϕ_{obs})

$$\frac{\phi_0}{\phi_0 - \phi_{obs}} = \frac{\phi_0}{\phi_0 - \phi'} + \frac{\phi_0}{K_{app}(\phi_0 - \phi')[MV^{2+}]} \tag{4.5}$$

The plot shows a biphasic trend at low and high quencher con-

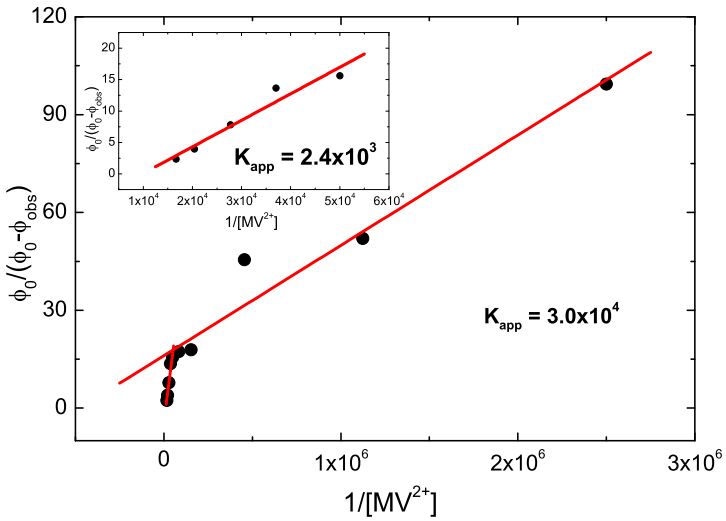

Figure 4.10: Plot of $\phi_0/(\phi_0$-$\phi_{obs})$ as a function of the reciprocal of $[MV^{2+}]$; the inset shows the trend at high concentrations

centrations. In particular at low concentrations ($K_{app} = 3.0 \times 10^4$) the constant is higher than that registered at high concentrations ($K_{app} = 2.4 \times 10^3$). This evidence is an indication that at low concentrations the static interaction is dominant and there is a strong affinity of the QDs surface to be complexed by MV^{2+}. A progressive increasing of the quencher concentration causes the dynamic interaction to prevale over the static adsorption. This trend can be explained considering that an initial progressive increase of the MV^{2+} concentration allows the adsorption of the latter on the surface sites of the particle. Subsequently the decrease of the accessible sites leads to an increase of the probability of having dynamic interactions.

Single photon counting measurements (Figure 4.11) of the QDs

with different MV^{2+} concentrations was carried out exciting at 460 nm and collecting the emitted photons at 620 nm. The kinetic traces shown a biexponential decay for all samples. The non-exponential decay is related to the distribution of excitonic populations[64,65,67]. In Table 4.5 the values of the time constants and

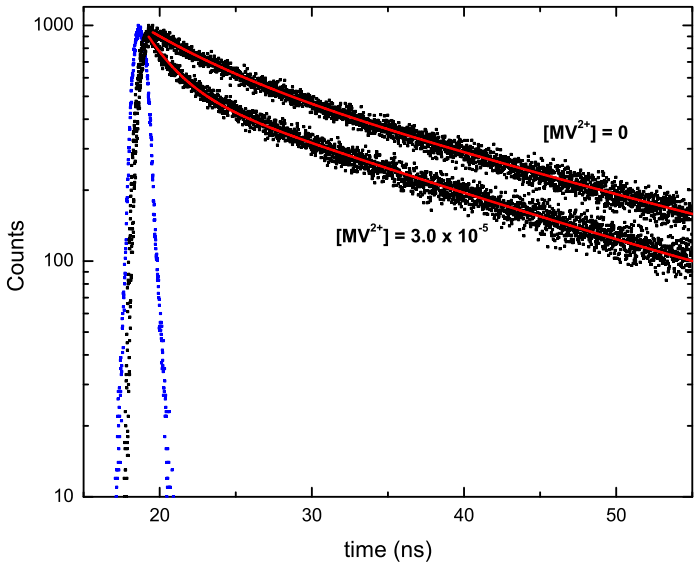

Figure 4.11: Single photon counting decay traces and instrumental function with and without MV^{2+}

normalized pre-exponential factors are reported. The values show that the two components are differently affected by the presence of MV^{2+}. The slow radiative lifetime component shows a decrease of the decay times from 30 to 25 ns and a more consistent reduction of the relative pre-exponential factor. The same trend can be observed for the fast component with a more consistent decrease of the recombination time, with an increasing of the relative pre-exponential factor. It is important to notice that these modifications become evident in both components, and consequently in the average time, when the quencher concentration exceeds the 10^{-5} M.

$[MV^{2+}]$	$A_1(\%)$	τ_1 (ns)	$A_2(\%)$	τ_2 (ns)	$\bar{\tau}$ (ns)
0	49.0	7.05	51.0	30.1	25.8
2.0×10^{-7}	49.4	7.17	50.6	30.3	25.9
4.4×10^{-7}	48.6	6.69	51.4	29.6	25.6
6.6×10^{-7}	48.8	6.67	51.2	29.7	25.6
1.1×10^{-6}	49.5	7.31	50.5	30.2	25.8
2.2×10^{-6}	49.4	7.14	50.6	30.2	25.9
4.2×10^{-6}	49.5	7.06	50.5	30.1	25.8
6.2×10^{-6}	49.5	6.78	50.5	29.8	25.6
9.8×10^{-6}	50.1	6.96	49.9	29.7	25.4
1.8×10^{-5}	52.3	4.98	47.7	27.6	23.9
2.4×10^{-5}	59.5	2.83	40.5	25.7	22.5
3.0×10^{-5}	67.7	2.02	32.3	24.7	21.4

Table 4.5: Photoluminescence decay parameters for CdTe QDs in water with different MV^{2+} concentrations

4.2.2 Nanosecond and Ultrafast Time Resolved Absorption Measurements

Ns-laser transient absorption experiments have been carried out to investigate the nature of the interactions between CdTe QDs and MV^{2+} molecules. Upon excitation of nanocrystals at 355 nm, transient signal can be detected only in presence of MV^{2+} (Figure 4.12). The transient absorption data can be rationalized considering that at least two transient species are photochemically produced. Therefore the signals centered at 400 and 600 nm can be attribuited to the excited state absorption of the methylviologen transient species. In particular the former at 600 nm is due to the radical cationic specie $MV^{\bullet+}$ absorption, while the band at 400 nm is characteristic of the combined absorption of the radical cation ($MV^{\bullet+}$) and neutral (MV^0) species[77,84,85]. With the aim to achieve a good transient signal with a low signal to noise ratio, it was necessary to work with a MV^{2+} concentration limit of $7,5 \times 10^{-5}$ M, higher than the photoluminescence measurements but well below the limit value where the flocculation occurs. The flash photolisys characterization has confirmed that the charge transfer processes occurs from the CdTe QDs to the MV^{2+} after the excitation of the nanocrys-

tals.

The analysis with ultrafast TAS technique was carried out in order

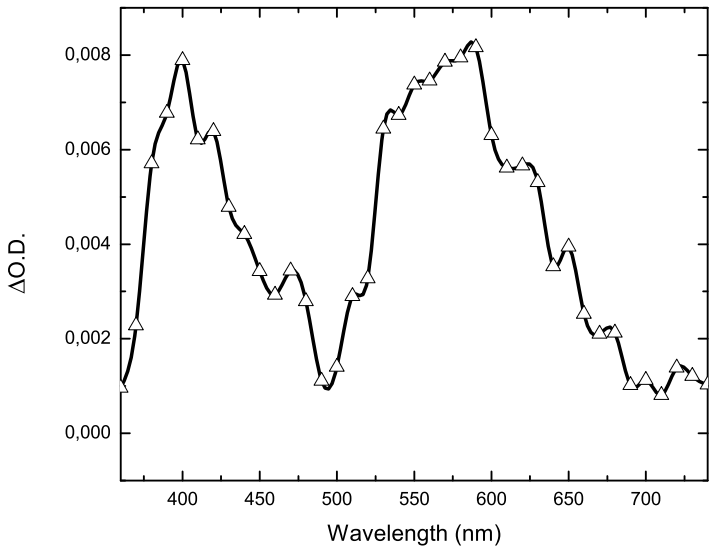

Figure 4.12: Ns-laser transient absorption spectra of CdTe QDs with a MV^{2+} of $7,5 \times 10^{-5}$ M after a delay of 2 μs

to obtain information about the evolution of the excited state of the CdTe with different concentration of MV^{2+}. In order to have a good overview of these processes, in addition to the sample without the quencher, we have chosen two concentrations corresponding to the plateau in the Stern-Volmer curve (one at the start and one at the end) and a third value on the maximum of the quenching.
Also in this case the samples were excited with two different wavelengths; near the BG transition at 520 nm and at high energy levels on the CB with a wavelength at 400 nm. For both excitation wavelengths the transient measurements show the same spectral components (Figure 4.13). The bleaching transition is centered around 565 nm and a positive signal above the 600 nm due to the ESA. The analysis of the spectra shows a broadening of the bleaching band

with increasing the quencher concentration and this leads to suppose that the MV^{2+} molecules interact differently with the excited QDs populations. This latter phenomenon is not observed in the groundstate absorption spectra probably because of the presence of the continuum absorption at lower wavelengths.
Despite of the flash photolysis measurements, the ultrafast transient signals of the MV^{2+} transient species do not appear. This is ascribable to the concentration of the methylviologen species under the detection limit. In literature the MV^{2+} transients have been characterized at concentrations orders of magnitude higher[77]. As previously mentioned it is impossible to increase the dye concentration due to the particles flocculation.

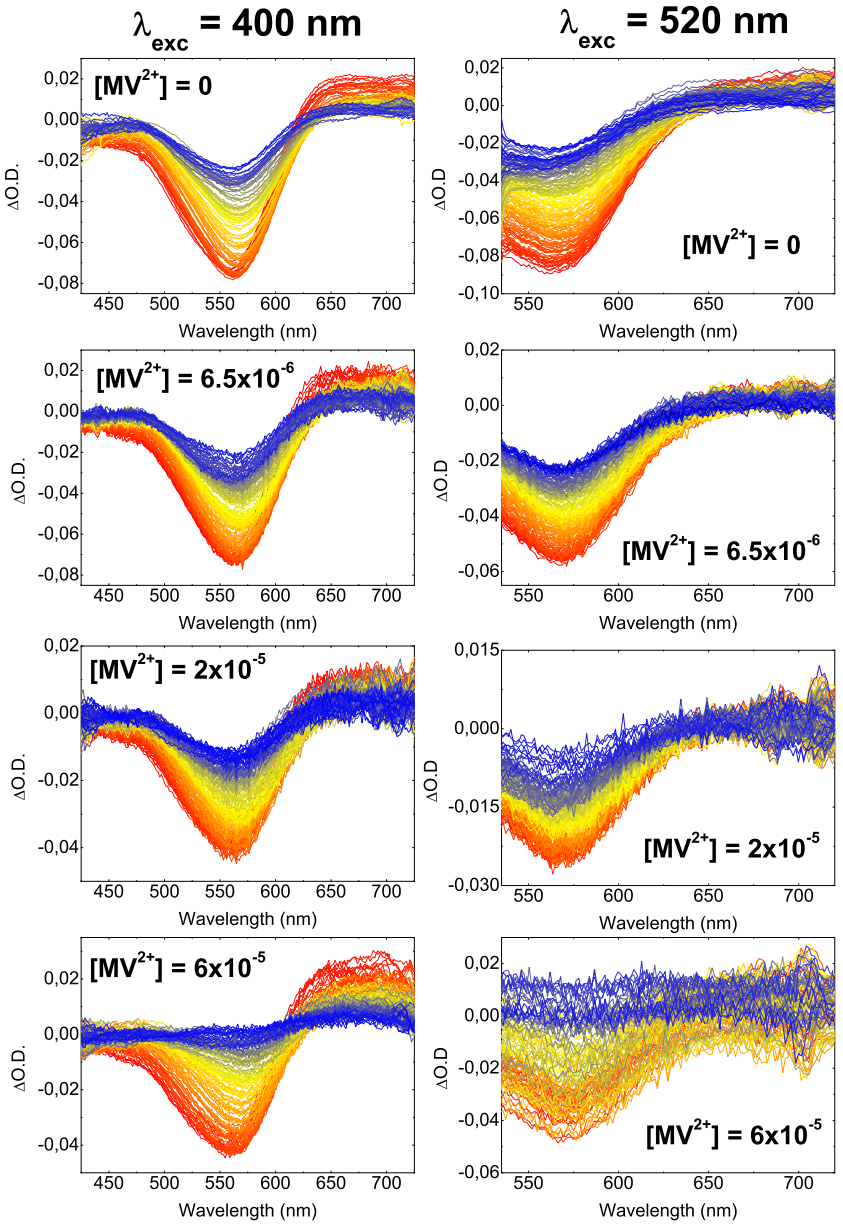

Figure 4.13: Single photon counting decay traces and instrumental function with and without MV^{2+}

Figure 4.14 shows the normalized kinetic traces extracted at the maximum of the bleaching band at different MV^{2+} concentrations for both excitation wavelengths. Since the longer time is due to the luminescence electron-hole recombination, the average decay time obatined with the SPC was fixed during the fitting analysis. The parameters obtained from the data analysis are reported in Table 4.6.

The rise component, due to the electron cooling on the VB, re-

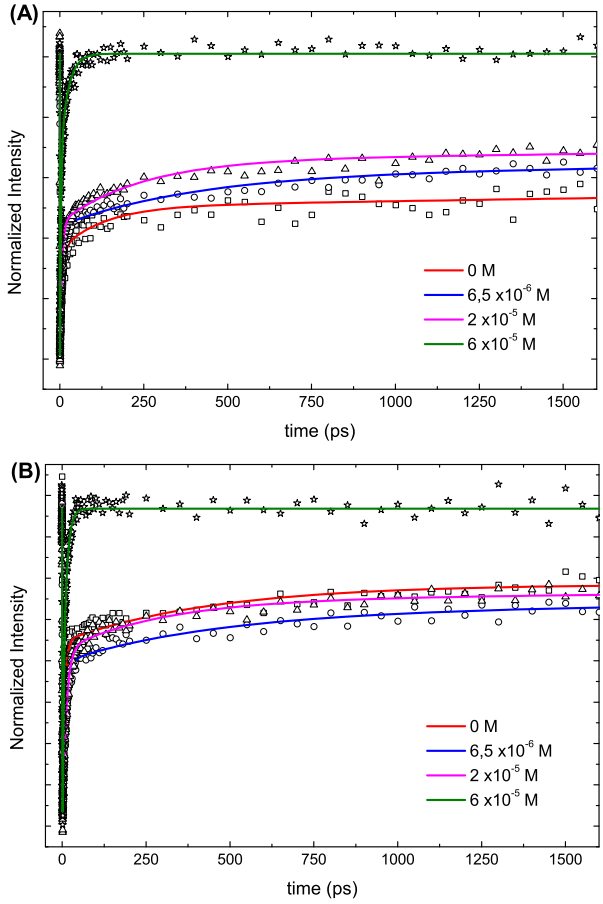

Figure 4.14: Kinetic traces recorded on the bleaching maximum at 565 nm with different MV^{2+} concentration exciting at (A) 520 nm and (B) 400 nm

main constant for both excitation wavelengths. This confirms that the electron transfer process occurs from the excited state on the CB and the presence of the MV^{2+} on the surface does not affect the energy of the ground levels.
The analysis of the recombination processes show interesting behaviours. The increment of the electron-acceptor concentration should result in a reduction of the decay times due to the capture of the electron by the MV^{2+}. However the time decay ascribable to the surface trapping and Auger recombination increases and it is drastically reduced when the quencher concentration is 6×10^{-5} M. This trend confirms that the charge transfer processes involves differet excited states. The presence of multiexcitonic species on the CB increases the electron density on the external levels, and the double positive charge of MV^{2+} stabilizes the more external levels. Therefore at lower concentration the MV^{2+} mainly interacts with the external levels, i.e. the states ascribable to the surface defects and the Auger recombination, leading to an incremnt of their lifetime. However, when the concentration exceeds a mimimum value, corrisponding to the last point on the Stern-Volmer plateau before the rise, the charge transfer process becomes dominant. At high MV^{2+} concentration (6×10^{-5} M) the bleaching is characterized by a fast decay in which the long radiative electron-hole recombination component disappears. This evidence is ascribable to the depopulation of the excited state due to the electron transfer to the acceptor molecule.

4.2.3 Conclusions

According to our measurements, the CdTe QDs have the tendency to give electrons in the presence of electron acceptor systems. The transfer process is supported by the strong affinity of the quencher molecules that statically interact with the QDs surface sites. This evidence was confirmed thanks to the photoluminescence characterization and in particular by the strong non-linearity of the Stern-Volmer plot and by the high values of K_{app}. Furthermore the SPC measurements have shown that the MV^{2+} molecules interact differently with the emitter populations of the QDs.
The presence of the electron transfer process was confirmed by the

nanoseconds transient absorption where it has been possible to obtain tansient spectra characterized by two different bands due to the absorption of the MV^{2+} transient species. Also the ultrafast TAS measurements have revealed the transfer process thanks to the disappearance of the long radiative decay component. Regarding the shortest component due to the surface trapping and Auger recombination, it was possible to characterize a strong dependence of these two states by the bicationic nature of the acceptor. Given their presence on the outer levels of the QDs, the molecules positively charged initially stabilize the outer electrons and subsequently the transfer process accelerates with a consequent reduction of the decay times.

MPA									
λ_{exc}(nm)	$[MV^{2+}]$	A_1(%)	τ_1(ps)	A_2(%)	τ_2(ps)	A_3(%)	τ_3(ps)	A_4(%)	τ_4(ps)
400	0	-47	0.61	34	0.9	8	20.2	10	25800
	6.5×10^{-6}	-42	0.37	40	9.9	9	462	9	25600
	2×10^{-5}	-40	0.49	41	11	12	297	7	23200
	6×10^{-5}	-46	0.95	38	1.6	16	10.5	0	0
520	0	-14	0.32	32	6.7	12	129	41	25800
	6.5×10^{-6}	-18	0.23	38	6.9	14	404	30	25600
	2×10^{-5}	-13	0.20	42	5.8	18	243	26	23200
	6×10^{-5}	-5	0.21	63	2.9	31	22.8	0	0

Table 4.6: Time constant and relative pre-exponential factors of CdTe MPA capped QDs with different MV^{2+} concentrations; A_1 and τ_1 are relative to the rise component

Chapter 5

Internal Charge Transfer Processes in a Push-Pull Dye and Solvatochromism Effects

In the previous chapter we have discussed the electronic properties of the CdTe nanocrystals and the charge transfer processes from the QDs to the MethylViologen molecules. Now we are going to treat a further charge transfer process that occurs with an intramolecular mechanism. A large number of studies on photoinduced intramolecular electron transfer in materials of interest for energy harvesting devices and solar concentrators, have been published during the past decades [86–89].
The molecule under investigation, called F500, is characterized by an extended conjugation and is shown in Figure 5.1. The electron acceptor group is represented by a benzothiadiazole that is connected to two electron rich thiophenic groups. In order to have an efficient solar concentrator system the simultaneous presence of a high emission quantum yield and a high Stokes shift (reduced autoquenching phenomena) is necessary. These characteristics are strongly influenced by the properties of the solvents. In solution, after the excitation of the dye, the variation of dipole moment causes a reorganization of the first solvation sphere of the solvent leading to a further stabilization of the excited state. As a result of this

process a change in the fluorescence quantum yield and a Stokes shift dynamic are expected.
In this work we have studied the optical properties of the F500 in different conditions of the chemical surrounding. In particular we have combined a steady state characterization with transient absorption technique in order to obtain information about the intramolecular charge transfer (ICT) process and how this is modified by the environment. Lastly we have compared the ICT characterization in solvents with the one made in a matrix of polymethyl methacrylate (PMMA).

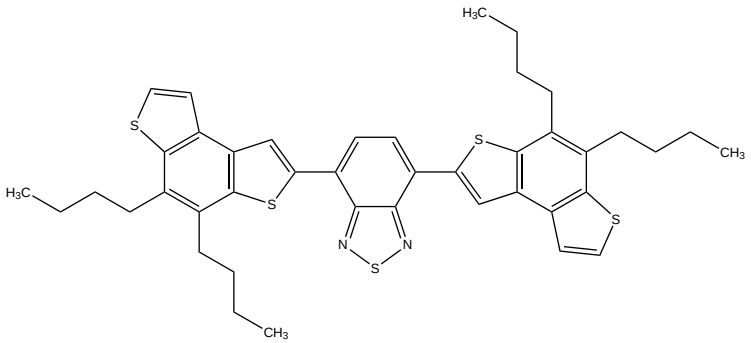

Figure 5.1: F500 molecular structure

5.1 Steady-State Characterization

In Figure 5.2 are shown the absorption and emission spectra of the F500 in different solvents while in Table 5.2 are given different spectroscopic parameters. The samples in the various solvents were excited at 485 nm and the emission spectra recorded in the range from 500 to 850 nm. The absorption spectra show two bands centered around 500 and 345 nm. Their position is not influenced by the solvent polarity. We notice that the band at 345 nm is narrower than that at 500 nm and in apolar solvents it is possible to notice a defined vibronic progression to the band on the UV region. This is clearly due to their different nature. The two signals can be assigned to two different transitions. The first peak in the UV

region can be associated to the $\pi \rightarrow \pi^*$ transition and the second one centered around 500 nm is the result of the $HOMO \rightarrow LUMO$ transition. In this system the electronic density for the ICT transition is localized on the acceptor group benzothiadiazole, while regarding the groundstate and the $\pi \rightarrow \pi^*$ transition, the electronic density is delocalized throughout the molecule.
In contrast to that observed in the absorption spectra, an important Stokes shift can be observed on the fluorescence emission measurements. In particular the Stokes shift is strongly influenced by the dielectric constant of the solvents: a red-shift of 4500 cm^{-1} is observed in DMSO and a shift of 2360 cm^{-1} in hexane. Furthermore the emission band in apolar solvents shows two different components that disappear increasing the polarity of the medium. This evidence can be ascribed to the presence in solution of different molecular conformations. Comparing the data obtained in solution with those obtained in PMMA it is possible to notice that the Stokes shift is 3860 cm^{-1}, that it is an intermediate value between those obtained in THF and DCM (Table 5.1). However while the absorption spectrum does not show significative differences, the emission spectrum shows a narrower spectral feature like that registered in THF. Therefore the emission spectrum in a solid matrix, characterized by a smaller full width half maximum (FWHM), confirms that the broadening of the emission is due to the presence of different structural conformations.

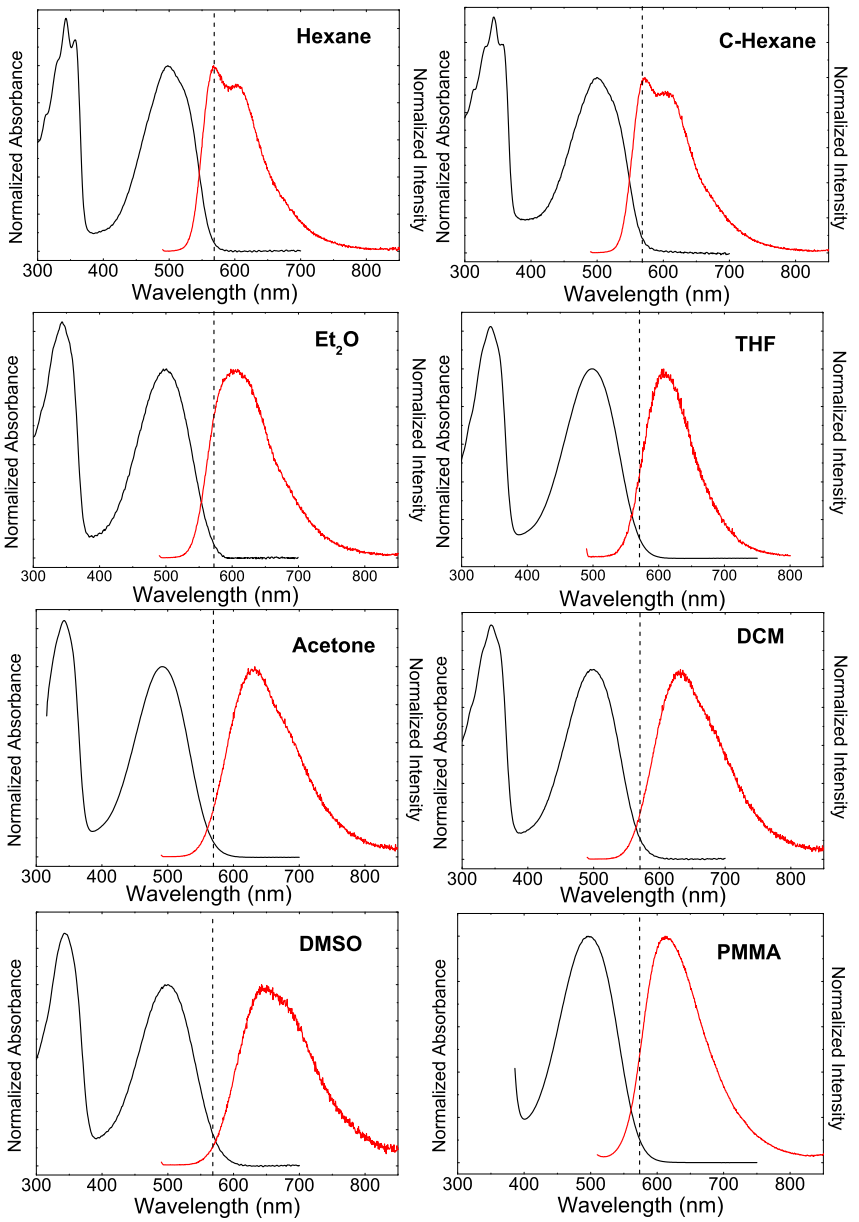

Figure 5.2: Absorption and emission spectra of F500 in different solvents (λ_{exc} = 485 nm), the dotted line is centered at the maximum of the emission in hexane

The emission quantum yields (QY) values are reported in table 5.1. As can be seen from Figure 5.2, the F500 molecule is characterized by a very broad emission spectrum, undergoing a considerable shift in function of the polarity of the solvent used. It was not possible to find a fluorescence standard able to provide an accurate estimate of the relative emission quantum yields. In order to obtain the same response of the phototube it is necessary that the emission spectral region of the reference compound is the same or at least comparable to that of the sample. Therefore according to these observations, the quantum yields were determined using both Rhodamina 6G and Cresyl Violet. For the samples in apolar solvents Rhodamina 6G in ethanol were used having a QY of 0.95 exciting at 480 nm[90], while for the polar solutions the Cresyl Violet were used in ethanol, having a QY of 0.54 exciting at 540 nm[91].
The photochemistry of the molecules is strongly influenced by the

Solvent	Polarity	FWHM(cm^{-1})	$\tilde{\nu_a}$-$\tilde{\nu_f}$(cm^{-1})	QY(%)
Hexane	1.89	2720	2360	67
Ciclohexane	2.02	2720	2760	70
Et_2O	4.33	2780	3550	64
THF	7.5	2250	3590	66
DCM	8.93	2860	4340	90
Acetone	20.7	2800	4200	78
DMSO	46.68	2920	4500	86
PMMA	-	2620	3860	-

Table 5.1: FWHM of the emission spectra, Stokes shift and emission quantum yield of F500 in solvents at differen polarity

chemical and physical properties of the medium. Since the dipole moment of the excited state (μ_g) is bigger than that of the ground-state (μ_e), the dielectric constant and the refractive index of the solvent lead to changes on emission spectra of the dyes. Therefore when the system is perturbed towards an excited state, the solvent molecules respond to the charge distribution changes on the fluorophore reorganizing their coordination sphere around the dye. As a result of this process, the excited state of the chromophore is stabilized towards lower energies (solvatation energy) and therefore

leading to a further shift of the emission band. This phenomenon is called solvatochromism and can be treated by the model developed by Onsager. In this theory the solute is a punctiform dipole, with a polarizability, placed at the center of a spherical cavity, of radius a. The solute is considered immersed in a continuous dielectric characterized by a dielectric constant (ϵ) and a refractive index (n). By employing of this model and the quantum mechanical second order perturbation theory, Kawski et. al[92–94] have related the Stokes shift and the sum of the wavenumbers at the maximum of absorption and emission spectra with the solvent polarity parameters $f(\epsilon, n)$ and $f(\epsilon, n) + 2g(n)$

$$\tilde{\nu_A} - \tilde{\nu_F} = m_1 f(\epsilon, n) + const \tag{5.1}$$

$$\tilde{\nu_A} + \tilde{\nu_F} = m_1 \left[f(\epsilon, n) + 2g(n)\right] + const \tag{5.2}$$

where

$$m_1 = \frac{2(\mu_e - \mu_g)^2}{hca^3} \tag{5.3}$$

$$m_2 = \frac{2(\mu_e^2 - \mu_g^2)}{hca^3} \tag{5.4}$$

a is the Onsager radius, equal to 6.1 Å obtained by applying the method of the increments of Edwards[95]. In this case the Onsager cavity for this molecule is given by an ellipsoid and the solvent polarity parameters $f(\epsilon, n)$ and $f(\epsilon, n) + 2g(n)$ can be determined from the equations 5.5 and 5.6

$$f(\epsilon, n) = \frac{\phi - \phi'}{(1 - \phi)(1 - \phi')^2} \tag{5.5}$$

$$g(n) = \frac{\phi'(1 - \frac{1}{2}\phi'}{(1 - \phi')^2} \tag{5.6}$$

where

$$\phi' = \frac{3A(1 - A)(\epsilon - 1)}{2[\epsilon - (\epsilon - 1)A]} \tag{5.7}$$

$$\phi' = \frac{3A(1 - A)(n^2 - 1)}{2[n^2 - (n^2 - 1)A]} \tag{5.8}$$

A defines the shape of the solute molecule. The F500 molecule can be describe by an ellipsoidal prolate where the value of the constant A is considered equal to 0.174[92,93]. At this point it is possible to determine the dipole moments of the ground and excited state. In table 5.2 the calculated solvent polarity parameters are reported, while in figures 5.3A and 5.3B the trend of the $\tilde{\nu_a}$-$\tilde{\nu_f}$ and $\tilde{\nu_a}$+$\tilde{\nu_f}$ in relation of the $f(\epsilon, n)$ and $f(\epsilon, n) + 2g(n)$ are reported respectively.

The values of m_1 and m_2 are obtained by the linear equations

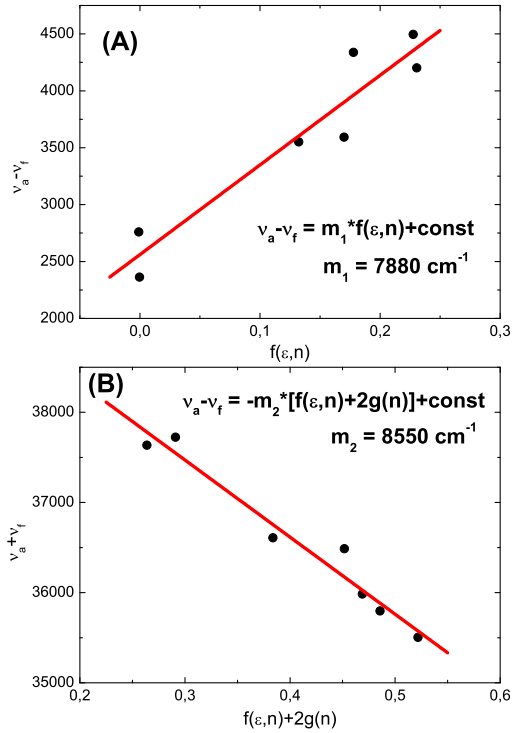

Figure 5.3: (A) Plot of $\nu_A - \nu_B$ versus $f(\epsilon, n)$ and (B) plot of $\nu_A + \nu_B$ versus $f(\epsilon, n) + 2g(n)$ in different solvents

5.3 and 5.4. It is possible to determine the dipole moments of the grond and excited states

$$\mu_g = \frac{m_2 - m_1}{2} \left(\frac{hca^3}{2m_1} \right)^{\frac{1}{2}} = 0.57D \tag{5.9}$$

$$\mu_e = \frac{m_1 + m_2}{2} \left(\frac{hca^3}{2m_1} \right)^{\frac{1}{2}} = 13.87D \tag{5.10}$$

The high dipole moment variation ($\Delta\mu = 13.30D$) confirms the larger observed Stokes shift. Solvents with higher polarizability tend to reorganize the coordination sphere as a function of the dipole moment changes and therefore stabilizing the excited state. However comparing these results with those obtained in DTBT by Basagni[94], it is possible to notice that in our case we have a monophasic behaviour due to the hindered movements of the thiophenic groups around the axis bond.

5.2 Ultrafast Transient Absorption Characterization

Transient absorption measurements were done under magnetic stirring and pumping the sample solutions with a wavelength tuned at 485 nm with an energy of 150 nJ and a repetition frequency of 100 Hz, near the maximum of the ICT transition. By comparing the obtained results we want to know how the dielectric properties of the solvents can influence the spectral properties of the excited states and the recombination dynamics of the transient species, in particular as concerning the F500 in PMMA.
The recorded spectra (figure 5.4) have shown the same spectral features for all solvents. The bleaching band is ascribed to the HOMO-LUMO transition (ICT transition) and shows a well defined minimum at the same energy to that observed in the steady-state absorption spectrum. However the bleaching is partially masked by the scattered excitation light, and the signal on the red edge of the band is partially covered by the overlapping with the stimulated emission (SE) signal. The F500 molecule is characterized by a broader excited state absorption (ESA) that partially covers the SE band. This overlapping becomes more and more significant increasing the solvent polarity. Although it is difficult to discriminate the temporal evolution of the individual transitions due to their proximity, in all samples it is possible to observe an evolution of the SE signal towards higher wavelengths due to a dynamical

Solvent	$f(\epsilon, n)$	$f(\epsilon, n) + 2g(n)$	$\tilde{\nu_a}$-$\tilde{\nu_f}(cm^{-1})$	$\tilde{\nu_a}$+$\tilde{\nu_f}(cm^{-1})$
Hexane	-9.6×10^{-4}	0.51	2360	37640
Ciclohexane	-2.6×10^{-3}	0.58	2760	37730
Et_2O	0.38	0.86	3550	36610
THF	0.55	1.10	3590	36490
DCM	0.59	1.17	4340	35980
Acetone	0.79	1.28	4200	35800
DMSO	0.84	1.42	4500	35500

Table 5.2: Solvent polarity parameters $f(\epsilon, n)$ and $f(\epsilon, n) + g(n)$, Sokes shift $\tilde{\nu_a}$-$\tilde{\nu_f}(cm^{-1})$ and sum of the wavenumebers at the maximum of absorption and emission spectra $\tilde{\nu_a}$+$\tilde{\nu_f}(cm^{-1})$

Stokes shift, i.e. related to the solvent reorganization around the excited molecules. The ESA is characterized by a positive signal on the red edge of the spectra.

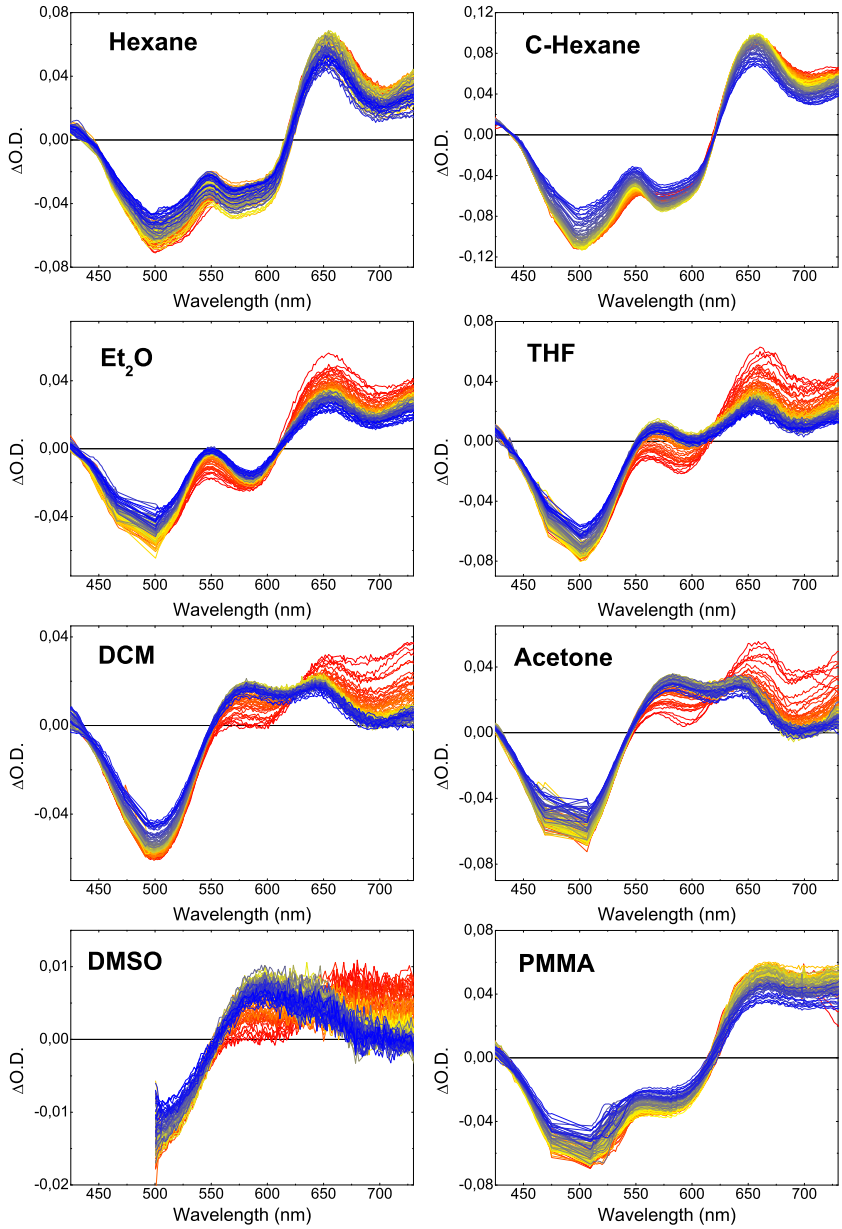

Figure 5.4: Transient absorption spectra obtained exciting the sample at 485 nm (spectral evolution from red to blue)

Therefore in order to analyze the temporal evolution and extract the dynamics from the various components of the transient spectra we have applied the global analysis through the GLOTARAN package (http://glotaran.org)[24,25]. This method consists of a combined approach of singular values decomposition (SVD)[21–23] and of the simultaneous fitting of all the collected kinetic traces. In figure 5.5 the evolution associated decay spectra (EADS) of the F500 in different solvents are shown, while in table 5.3 the decay time and the normalized weigth extracted from the global analysis are reported.

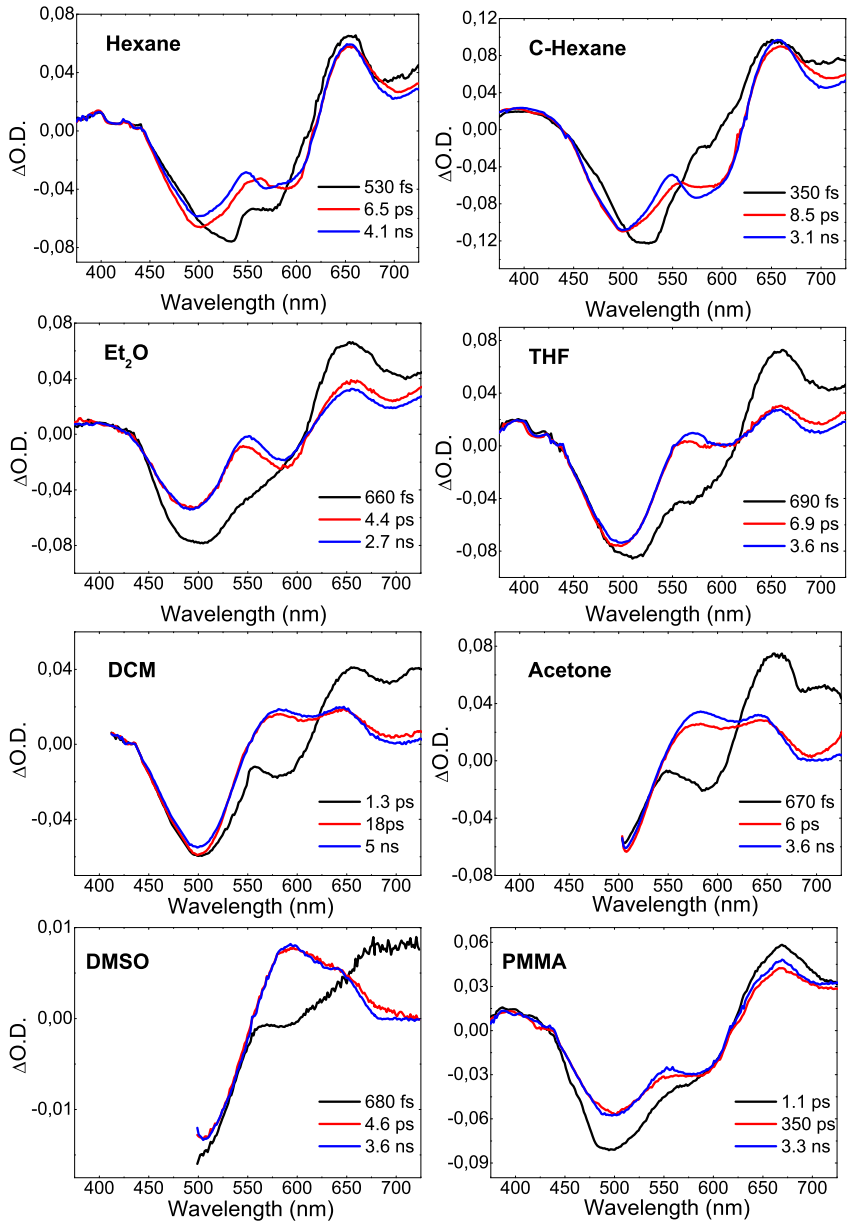

Figure 5.5: Evolution associated decay spectra (EADS) obtained by the simultaneous fit of all the kinetic traces recorded for the F500 in different solvents

Solvent	t_1(ps)	A_1(%)	t_2(ps)	A_2(%)	t_3(ns)	A_3(%)
Hexane	0.53	0.05	6.5	0.63	4.1	99.3
Ciclohexane	0.35	0.04	8.5	0.86	3.1	99.1
Et_2O	0.66	0.07	4.4	0.45	2.7	99.4
THF	0.69	0.07	6.9	0.68	3.6	99.25
DCM	1.30	0.12	18	1.72	5.0	98.16
Acetone	0.67	0.06	6.0	0.60	3.6	99.34
DMSO	0.68	0.07	4.6	0.45	3.6	99.48
PMMA	1.10	0.1	348	31.2	3.3	68.7

Table 5.3: Decay times and normalized weights extracted from the global analysis

The global analysis has shown three different components for each sample with similar kinetic constants associated to the system relaxation for all the different solvents. From the EADS it is possible to notice how the formation of the bleaching and the SE signals is instantaneous and after a delay time of few picoseconds, the signal of the SE is compensed by the ESA transition.
The first component is ascribed to the signal of the molecule before the solvent reorganize the coordination sphere. Therefore the kinetic constant below the picosecond is correlated to the dynamical Stokes shift. The presence in solution of various molecular conformations leads to a nonexponential behaviour with similar EADS features for the other two components. However the blue-shift and the decay on the red edge of the ESA signal and the partial narrowing of the bleaching band of the third component, suggests that the second decay time, of the order of a few picoseconds, is ascribable to structural rearrangements and/or vibrational coolings. Lastly the nanosecond decay constant is due to the recombination of the ICT states, i.e. to the HOMO-LUMO orbitals. The nature of this transition is confirmed by the high value of normalized weight reported in table 5.3. However it is necessary to consider that the longer time is affected by a large error due to the shorter length of the delay line.
Comparing the data obtained in PMMA with that recorded in solvents with different optical properties, it is possible to notice how the transient spectra and the EADS obtained with the global anal-

ysis are more similar to that recorded in apolar solvents. This trend can be explained in terms of polarizability; in solvents with higher polarizability occurs a faster reorganization of the solvent molecules around the solute when excited and the dipole moment increases. Therefore the high rigidity of a PMMA matrix is comparable to a system with solvents of low polarizability. Furthermore the second component in a PMMA matrix show a decay time of 350 ps, two order of magnitude slower than the molecule in solvents, confirming that this component is due to a structural rearrangements of the F500 molecules.

5.3 Conclusions

Therefore it is possible to conclude that the F500 molecule is strongly affected by the polarizability of the solvent with a greater stabilization of the ICT state in polar solvents, and it is confirmed by the high dipole moment of the excited state. Emission measurements have shown that the sample in PMMA has an intermediate behaviour between the dye in THF and DCM, with a narrower FWHM that confirms a lower amount of conformers. The study of the evolution of the excited state with the transient absorption technique associated with the global analysis has shown a trend similar to that obtained in apolar solvent. This phenomena can be explained associating the rigidity of the PMMA matrix to the lower polarizability of the apolar solvents.

Chapter 6

Energy Transfer Processes in Supramolecular Complexes: Models for the Photosynthetic Antenna-Reaction Center

The photosynthesis is a very complex process which many organisms in nature use to produce energy. In spite of their complexity due to the wide organization of a multitude of chromophores with distinct photochemical and photophysical properties, these natural systems have an extremely high energy production efficiency. In order to disentangle the various contributes to the overall energy conversion it is important to develope simple systems capable to reproduce partial mechanisms present in natural systems.
In this chapter we are going to investigate the energy transfer processes in systems with potential applicability as antenna systems. The two systems under investigation are calix[4]arenes assemblies and a BODIPY donor-acceptor system. Therefore, after an initial characterization of the photophysical properties by steady-state technique, the energy transfer processe is studied through ultrafast transient absorption spectroscopy.

6.1 Excited Energy Transfer in a Supramolecular BODIPY-Styryl Pyridinium Complex

The energy transfer from an aminostyryl pyridinium molecule (SF117), which acts as acceptor, to a donor that consist in a BODIPY system (SF106) is characterized. The molecular structure of the two separate moieties are reported in Figure 6.1.

The borondipyrromethene (BODIPY) dyes constitute one of the

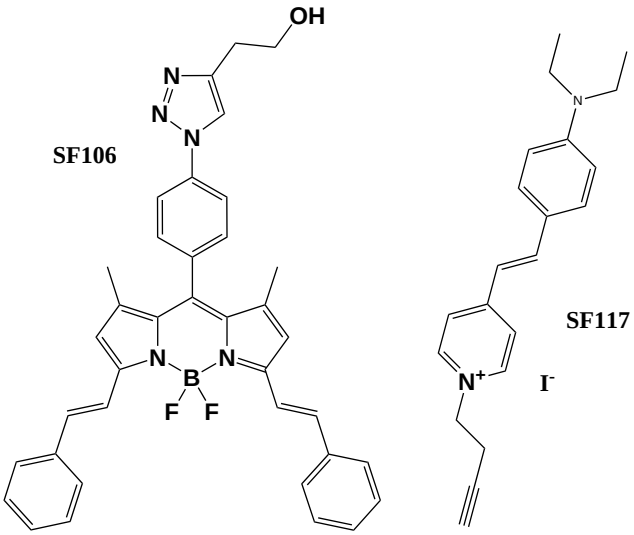

Figure 6.1: Donor (SF117) and acceptor (SF106) molecular structures

most efficient class of fluorescent chromophores. The BODIPY molecules have attracted attention in the recent years thanks to their stability, absorption coefficient and emission quantum yields. These properties have allowed to use this family of compounds in many systems such as light harvesting for solar energy conversion[96–99], biological sensor[100,101] and laser dyes[102]. Therefore we have chosen this componds as acceptors in order to exploit their unique optical properties.

Aminostyryl pyridinium dyes are known as heterocyclic organic molecules and they have been widely used in several areas. In par-

ticular this molecular system has found applications especially as a laser material[103,104] and as a biological sensor[105,106]. The excited state of this molecule is characterized by an intramolecular charge transfer (ICT) where the electron moves from the styryl group to the pyridinium group[105,107–109]. In our system the SF117 is linked to a BODIPY by a covalent bridge that does not allow delocalization of the charges. The structure of the bichromophore (SF119) is show in Figure 6.2.

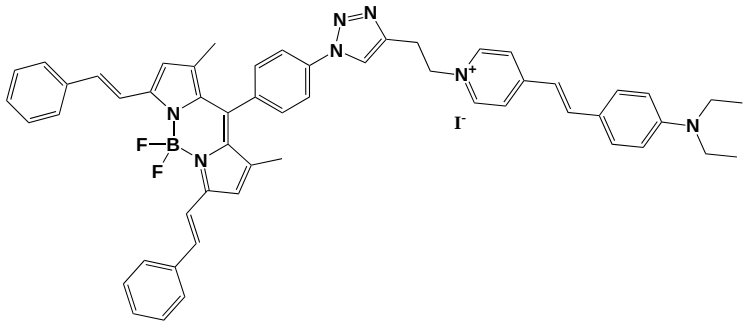

Figure 6.2: Bichromophore (SF119) molecular structures

6.1.1 Steady-State Measurements

The necessary condition to achieve an excitation energy transfer (EET) is the overlapping between the absorption spectrum of the acceptor and the emission spectrum of the donor, the distance and the relative orientation of the two dipoles. In figure 6.3 it is possible to notice the good overlap between the spectra of the two molecules. Furthermore the high Stokes shift between the absorption and emission spectra of the donor reduces potential phenomena of autoabsorption.
In Table 6.1 are reported the values of the quantum yields (QY) obtained for the molecules under investigation. The quantum yields were determined using Rhodamina 6G as standard[90]. The donor show a very low QY with a value of 0.1% in chloroform and 0.005% in acetonitrile suggesting the presence of efficient nonradiative deactivation pathways. Regarding the acceptor we have obtained val-

ues of the order of 70% with higher values in chloroform than in acetonitrile. The maximum values of QY are achieved when the sample is excited at 570 nm in both solvents.

The absorption spectrum of the bichromophore in Figure 6.4 is

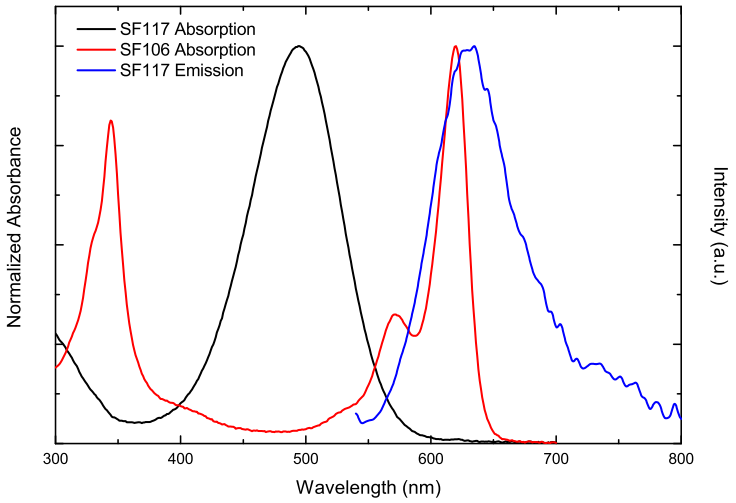

Figure 6.3: Absorption spectrum of the donor (black line) and overlap between the absorption spectrum of the acceptor (red line) and the emission spectrum of the donor (blue line)

perfectly reproduced by the sum of the two independent moieties. This is the finger print of a small coupling between the orbitals of the donor and acceptor molecules. The band on the UV region at 350 nm is ascribable to the transition $\pi \rightarrow \pi^*$ of the acceptor. The other two signals centered at 500 and 620 nm are ascribable to the $HOMO \rightarrow LUMO$ transition of the donor and acceptor respectively. In particular the transition in the aminostyryl pyridinium group correspond to the ICT process. The emission spectrum (red line) shows a narrower band centered at 630 nm with a shoulder on the red-edge of the spectrum. The Stokes shift of 10 nm is the same of the isolated acceptor. Analysing the QY in Table 6.1 it is possible to notice an almost unitary EET in chloroform indipendently from the excitation wavelength. Therefore despite the low QY registered for the donor the EET process proves to be very

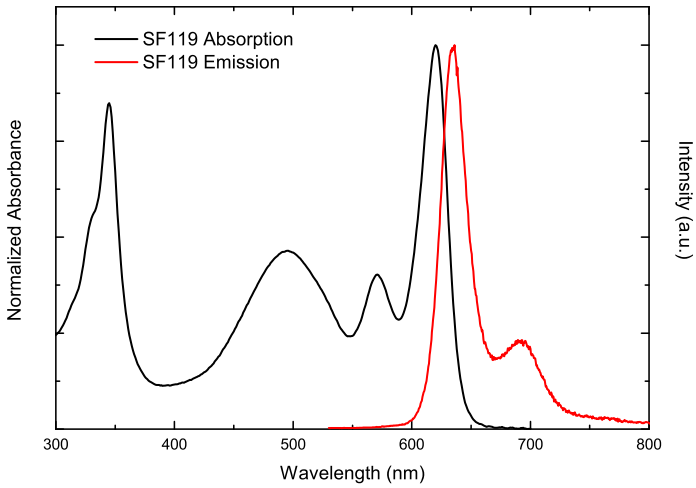

Figure 6.4: Absorption (black line) and emission (red line) spectra of the bicromophore SF119

efficiet in particular in a low polar solvent such as chloroform.

Donor - SF117

Solvent	λ^{exc} (nm)	ϕ^{em}
Chloroform	530	0.1
Acetonitrile	530	5×10^{-3}

Acceptor - SF106

Solvent	λ^{exc} (nm)	ϕ^{em}
Chloroform	620	0.77
	570	0.99
	350	0.79
Acetonitrile	620	0.68
	570	0.72

SF119

Solvent	λ^{exc} (nm)	ϕ^{em}
Chloroform	620	0.85
	570	0.97
	500	0.98
Acetonitrile	620	0.35
	570	0.37
	470	0.36

Table 6.1: Emission quantum yields of SF117 (donor), SF106 (acceptor) and SF119 (bichromophor) at different excitation wavelengths in chloroform and acetonitrile

6.1.2 Ultrafast Transient Absorption Measurements

In order to obtain new pieces of information about the excited states evolution and how these contribute to the EET process we have performed TAS measurements. Before the analysis of the bichromophore system, we have studied the donor and acceptor systems separately in order to analyze how the photophysical properties change when they are linked together. As a first step we have collected the transient spectra of the donor in chloroform and acetonitrile. The transient spectra were recorded pumping at 520 nm with an energy of 150 nJ for both samples. Since the excitation light is tuned with a wavelength near the absorption maximum of the donor, the bleaching signal is not well resolved due to the scattered light of the pump. In order to extract the dynamics from the various components of the transient spectra and obtain their temporal evolution we have used global analysis provided by the GLOTARAN package (http://glotaran.org)[24,25].
The transient spectra of the donor recorded in chloroform (Figure 6.5A) have shown an excited state absorption (ESA) centered at 450 nm and a stimulated emission (SE) evoleving toward longer wavelengths. This evolution is ascribable to the dynamical Stokes shift where the solvent molecules reorganize around the excited state. This process is most prominent in the acceptor system due to the ICT from the styryl to the pyridinium group that leads to an important dipole moment variation[105,107–109]. This latter is made more evident by the evolution associated spectra (EADS) in Figure 6.5B and is characterized by a slower dynamics. The global analysis shows two faster component of 300 fs and 1.6 ps. The population decay has a time constant of 254 ps.
The transient spectra of the sample in acetonitrile (Figure 6.5C) show the same spectral features with slight differences than those obtained in chloroform. The ESA signals is centered at 450 nm and it is characterized by a larg band. Regarding the bleaching it is possible to notice a narrow band that it is not well separated from the SE band. A narrower structure is also showed by the SE signals with a red shift of the maximum. In this case the dynamical Stokes shift is characterized by a faster dynamics. The global analysis (Figure 6.5D) shows a fast solvent rearrangement around

the donor molecules with a time constant of 1.5 ps. In acetonitrile the system relax with a time decay of 25 ps confirming the presence of larger amount of nonradiative deactivation pathways.

The BODIPY acceptor molecules have been studied in the same

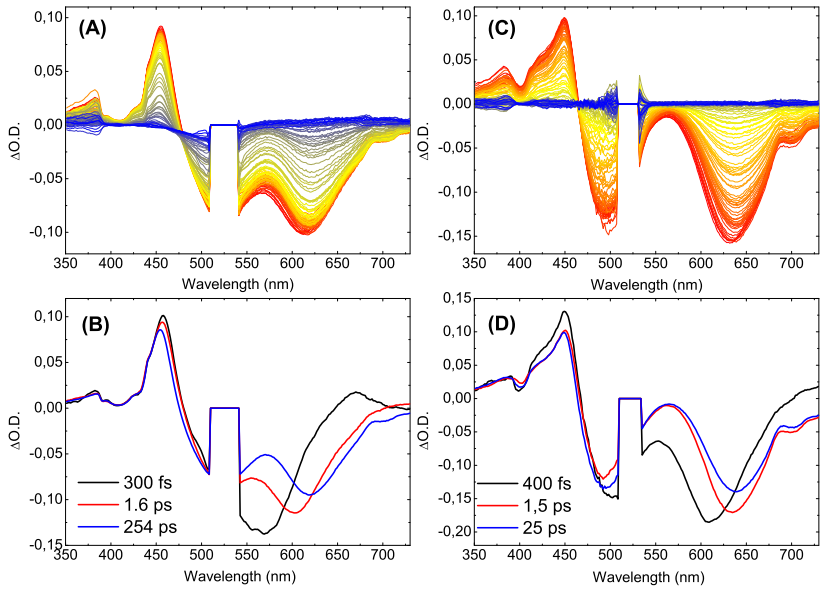

Figure 6.5: Transient absorption spectra at different delay time (signal evolution from red to blue) in (A) chloroform and (C) acetonitrile; Evolution associated decay spectra (EADS) obtained by the simultaneous fit of all the kinetic traces recorded in (B) chloroform and acetonitrile (D) for the donor (SF117)

solvents of the donor with an excitation wavelength of 570 nm and an energy pump of 150 nJ. The TAS measurements in chloroform are show in Figure 6.6A while the TAS measurements in acetonitrile are in Figure 6.6C . The transient spectra exhibit the same spectral features with an ESA around the 450 nm and a negative signal centered at 630 nm in both solvents. The latter component is characterized by a convolution of the bleaching and SE signals due to the little Stokes shift. Contrary to that observed in the donor, in this case it is not detected a dynamical Stokes shift process. In all cases three kinetic components are necessary to satisfactorily fit the data. The first EADS (black line) is defined by a decay time

of 300 and 400 fs respectively and the negative signal contains a shoulder on the blue edge of the band due to the bleaching signal. Increasing the delay time the bleaching becomes less defined leading to the formation of a broader band. The other EADS show differences in the decay time and in the spectral features suggesting a low dependence of the BODIPY excited states from the polarity of the solvent.

Subsequently to the analysis of the excited states evolution of the

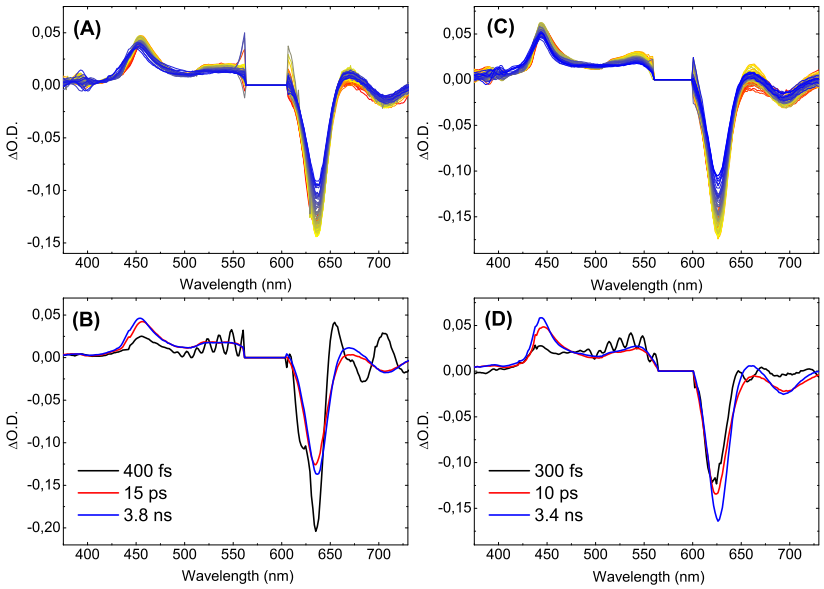

Figure 6.6: Transient absorption spectra at different delay time (signal evolution from red to blue) in (A) chloroform and (C) acetonitrile; Evolution associated decay spectra (EADS) obtained by the simultaneous fit of all the kinetic traces recorded in (B) chloroform and acetonitrile (D) for the acceptor (SF106)

donor and acceptor molecules, we have studied the EET process in the bichromophore system. As in the previous measurements, we have analyzed the process in both acetonitrile and chloroform solvents. The ultrafast transient spectra and the EADS obtained by the global analysis are reported for the sample in chloroform in Figure 6.7 and for the sample in acetonitrile in Figure 6.8. All the spectra were recorded exciting the samples at 520 nm on the donor

absorption band; at this wavelength the absorption of the acceptor is negligible.
The transient spectra recorded in chloroform show the formation of three different components; two negative signals and a positive signal due to the ESA transition. The bleaching signal of the donor cannot be observed because it is covered by the scattered light of the pump. The first SE component centered around 575 nm is ascribable to the donor and disappears in a few hundreds of femtoseconds. The second signal is due to a combination of the bleaching and SE signal of the acceptor moiety and show a well define band centered at 630 nm and decay with a time consatnt of 2.9 ns. Regarding the ESA band, it is necessary to consider that the absorption on the excited state for the reference compounds previously studied have shown a similar signal in the same position. Therefore in this case the ESA features under observation represent a convolution of the two signals relative to the acceptor and donor.
The global analysis of the system shows four different EADS components. The shorter component has a decay time of 600 fs and describe the SE features of the donor moiety with a shoulder around 620 nm due to the initial formation of the acceptor bleaching-SE signal. The second component is associated to a decay constant of 6 ps. The signal of the donor almost disappear and the acceptor signal is fully formed in tens of femtoseconds. Therefore the biphasic nature of the EET, i.e. the presence of two transfer times, implies the presence in solution of two main conformations in solution capable to give energy transfer. In the last two components, the donor signal is completely decayed and the spectral features of the acceptor remain the same. The third component has a time constant of 166 ps and the fourth decay is 2.9 ns. Such behaviour can be ascribed to different conformations probably interconverting during the emission process.
From the TAS measurements in acetonitrile (Figure 6.8A) it is possible to achieve transient spectra with the same components than those obtained in chloroform. The most important difference is the faster decay of the donor SE component. The correct interpretation of this evidence is obtainable after the global analysis from the EADS (Figure 6.8B). The shortest component show a weak signal relative to the SE of the donor moiety and an instantaneous for-

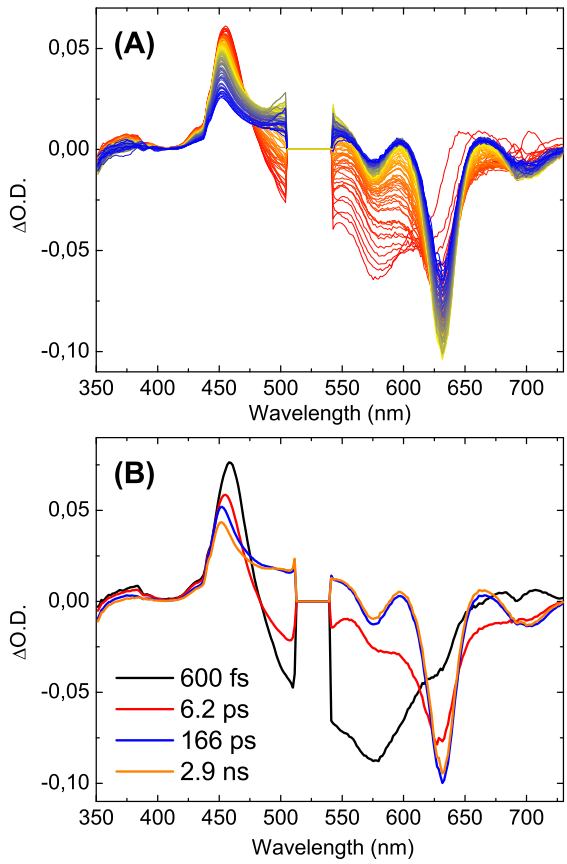

Figure 6.7: (A) Transient absorption spectra at different delay time (signal evolution from red to blue); (B) Evolution associated decay spectra (EADS) obtained by the simultaneous fit of all the kinetic traces recorded for the bichromophor (SF119) in chloroform

mation of the signal relative to the acceptor moiety. The decay constant of this process is 260 fs. Also in acetonitrile is present a second component with a decay time of 5.5 ps that shows a residual presence of the donor bleaching on the blue-edge of the acceptor band. Therefore, as well as in chloroform, the two EET times confirm the presence of a more than one conformation able to give EET. The interpretation of the slower decay constants is the same of that proposed for the sample in chloroform, but in this case we

have obtained faster decay times of 33 ps and 2.1 ns respectively. The faster recombination time associated to a lower QY mean that there is greater interaction between the donor and acceptor moieties. Consequently this phenomenon leads to a more efficient recombination or retrodonation process. It is important to notice that in both systems the long recombination time of the acceptor moiety is smaller than a third when it is linked with the donor in the bichromophoric system. This evidence confirm the presence of a further deactivation pathway ascribable to a retrodonation process or a more efficient recombination due to the interaction with the donor.

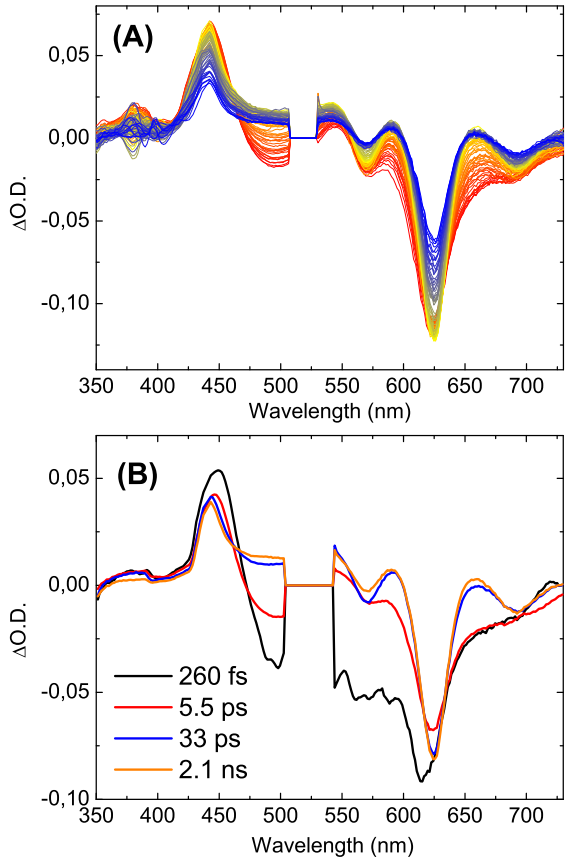

Figure 6.8: (A) Transient absorption spectra at different delay time (signal evolution from red to blue); (B) Evolution associated decay spectra (EADS) obtained by the simultaneous fit of all the kinetic traces recorded for the bichromophor (SF119) in acetonitrile

6.1.3 Energy Transfer Rates

After the acquisition of the experimental data we have determined the EET constant (k_{EET}) and copared to that obtained by *Förster* theory[110]. The rate of EET is given by the following equation

$$k_{EET} = \frac{\phi_D \kappa^2}{\tau_D R^6} \left(\frac{9000(ln10)}{128\pi^5 N_A n^4} \right) \int_0^\infty F_D(\lambda)\epsilon_A(\lambda)\lambda^4 d\lambda \qquad (6.1)$$

The equation 6.1 can be also expressed by

$$k_{EET} = \frac{\phi_D}{\tau_D} \left(\frac{R_0}{R} \right)^6 = \frac{\phi_D}{\tau_D} \left(\frac{8.785 \times 10^{-25} J(\epsilon)}{n^4 R^6} \right) \qquad (6.2)$$

where ϕ_D and τ_D are the quantum yield and the lifetime of the donor respectively, N_A is the Avogadro's number, n is the refraction index of the medium, R is the center-to-center separation in cm and κ^2 describes the orientation factor associated with the dipole-dipole interaction between donor and acceptor. The parameters into the overlap integral (J(ϵ)) represent $F_D(\lambda)$ the normalized emission spectrum of the excited donor in the wavelength range λ to $\lambda + \Delta\lambda$, ϵ_A is the extintion coefficient of the acceptor at the wavelength λ. J(ϵ) is expressed in units of $cm^3 M^{-1}$.
From DFT calculations of structural optimization we have obtained two limit values of R: 10Å is the distance of maximum coupling and 18.8Å is ascribable to the conformation with minimum coupling. The potential couplings at different dihedral angle are reported in Figure 6.9, while the EET times obtained by the equation 6.2 and by the analysis of the transient spectra are reported in Table 6.2.
The EET constant can be calculated using the coupling at different values of R by applying the following equation

$$k_{EET} = \frac{2\pi}{\hbar} V^2 J \qquad (6.3)$$

where V is the coupling expressed in cm^{-1} and J is the overlapping integral normalized for the overlapping areas of the emission spectrum of the donor and the absorption spectrum of the acceptor. From the minimum geometry (R=18.8Å) we have obtained a

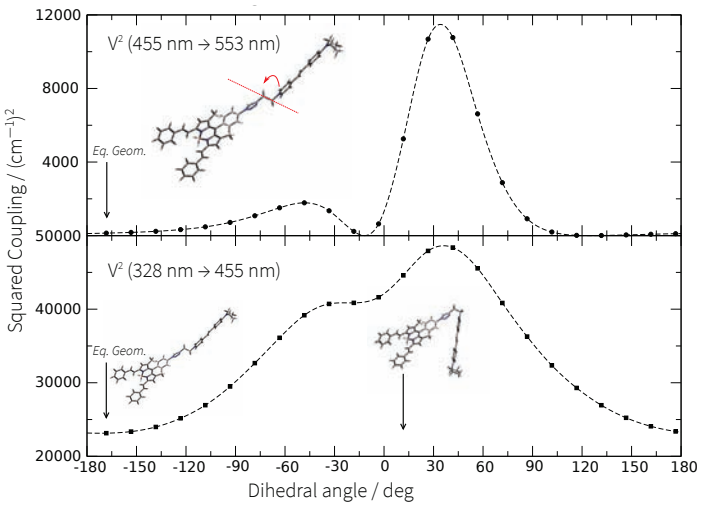

Figure 6.9: Variation of the square of the coupling V^2 to vary the dihedral angle between the acceptor and donor in chloroform

	Förster **R=10Å**		*Förster* **R=18.8Å**		**TAS**	
Solvent	$k(s^{-1})$	τ(fs)	$k(s^{-1})$	τ(ps)	$k(s^{-1})$	τ(fs)
Chloroform	2.13×10^{12}	470	1.43×10^{11}	7	1.66×10^{12}	600
Acetonitrile	4.44×10^{12}	225	5×10^{10}	20	3.84×10^{12}	260

Table 6.2: Excited energy transfer constant (k_{EET}) and time (τ_{EET}) of the bichromophore in chloroform and acetonitrile calculated by *Förster* theory and by TAS

EET time of 22 ps, while considering a distance of 10Å where the coupling is maximum we have achieved a time of 300 fs. The values calculated with the two equations are in good agreement with the experimental data when R assumes the limit value of 10Å.

6.1.4 Conclusions

The steady-state characterization of the bichromophoric system has shown well separated bands for the donor and the acceptor suggesting a small coupling between the orbitals of the two molecules. Furthermore the emission QY measurements have shown an effi-

cient EET process.
TAS measurements of the donor have shown an important dynamical Stokes shift on the SE band due to the ICT process. This process is not observed for the acceptor where the Stokes shift is smaller. The bichromophore is characterized by a fast EET process with a time constant of 600 fs in chloroform and 260 fs in acetonitrile, while the residual signal after a few ps is due to a different molecular conformation able to give energy transfer. An interesting results is the shorter lifetime of the species in acetonitrile (2.1 ns) than in chloroform (2.9 ns). This trend suggest the presence of a further deactivation pathways principally ascribable to the back energy transfer. Lastly the application of the *Förster* theory using the two limit values of R has lead to comparable results with those obtained experimentally by the TAS technique only in the case when R is equal to 10Å. Therefore it is possible to affirm that the *Förster* model is able to describe the EET process that occurs in the our BODIPY system.

6.2 Energy Transfer in Supramolecular Calix[4]arenes Assemblies

An important limiting factor for the development of antenna systems is the building of artificial structures which contain multiple chromophores providing sequential energy transfer. With this aim, here we report an example where the calix[4]arenes are used as building blocks for the construction of multichromophore systems. The excited energy transfer has been studied as a function of the position of the chromophores linked to the calix[4]arene ring and of the different system conformations.
The calix[4]arene skeleton is almost blocked in a cone conformation. However the tetraalkylated[111] derivatives retain some conformational flexibility and in solution it's possible to observe a dynamic equilibrium between two flattened cone conformations of C_{2v} symmetry (Figure 6.10)[112].

The presence of two substituents on the 1,3-distal positions of

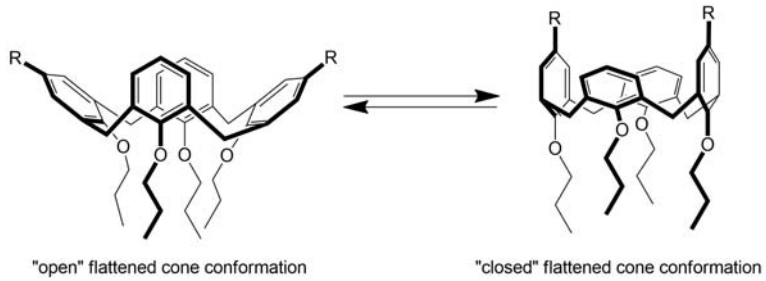

Figure 6.10: Conformational motion of cone calix[4]arenes. If R corrispond to an hydrogen atom the two conformers have equal stability

the calix[4]arene upper rim differentiates the relative stabilities of the two C_{2v} conformers. Usually, the conformation with the two substituted aromatic rings outward oriented and the phenol rings parallel to each other ("open" flattened cone conformation) is the most stable, since it minimizes the steric repulsions between the substituents[113]. However, in presence of intramolecular attractive interactions between the upper rim substituents, the opposite conformation ("closed" flattened cone conformation) can be favoured[114,115].

The two complementary fluorescent dyes were chosen with the aim to have a good overlap between the emission spectrum of the donor and the absorption of the acceptor (see Figure 6.11). In this case the NBD donor and Nilered acceptor have been chosen. They were covalently linked to the calix-scaffold structure. Since both the conditions are thoroughly fulfilled in our systems, a very efficient energy transfer is expected.

The spectroscopic measurements were done firstly on the calix[4]a-

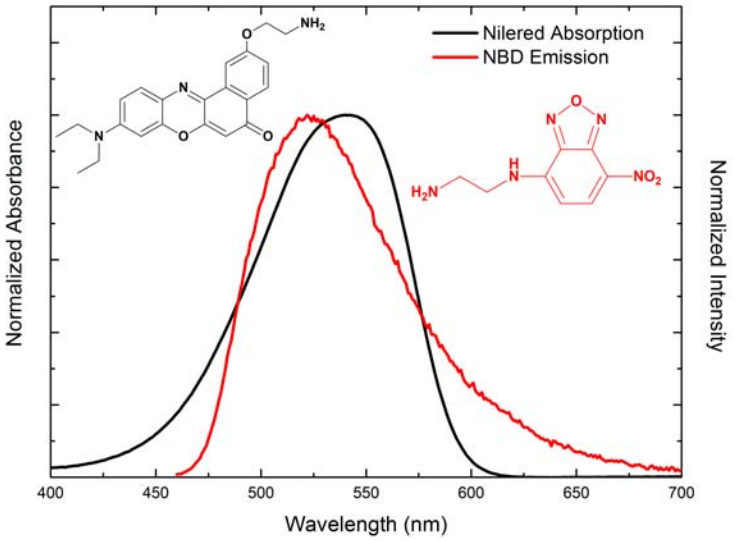

Figure 6.11: Overlap between the absorption spectrum of Nilered and emission spectrum of NBD in chloroform

renes with only the donor and the acceptor unit in order to verify the photochemical and photophysical properties of the single chromophores (see Figure 6.12) and subsequently on the conformers with both donor and acceptor species (see Figure 6.13).

6.2.1 Steady-State Measurements

In order to obtain information about the electronic evolution and energy transfer efficiency with different structure conforma-

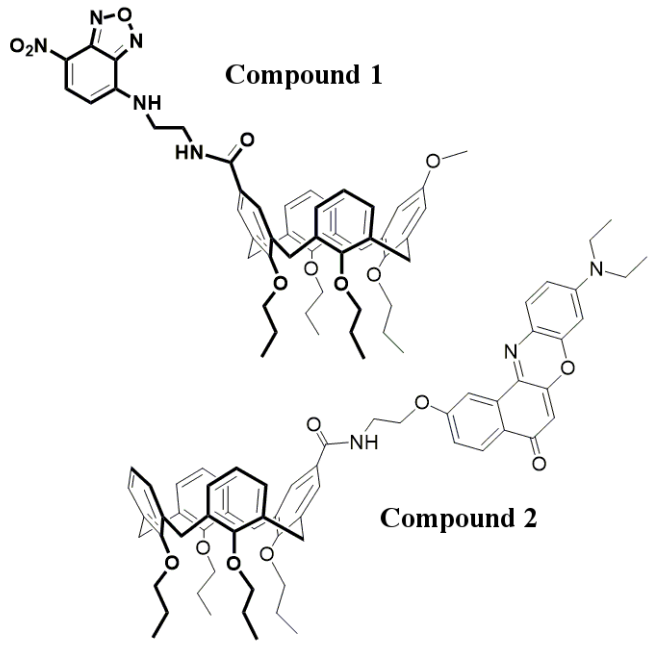

Figure 6.12: calix[4]arene structures with the donor NDM (Compound 1) and acceptor Nilered (Compound 2) dyes

tion of calix[4]arene, steady-state and transient spectroscopic characterization have been performed in solution of organic solvents with different polarity. In particular acetonitrile, dimethyl sulfoxide (DMSO) and chloroform were chosen. The relative absorption and emission spectra are reported in Figure 6.14 and Table 6.3.
In all solvents the absorption spectra of heterodimers 4 and 5 can be obtained as the sum of the spectra of the reference compounds, while for heterodimer 3 this is true only in the polar solvents, acetonitrile and DMSO, while in chloroform the shape of the absorption spectrum is different.
The emission spectra are independent from the excitation wavelength and show a very efficient EET from the donor NBD to the acceptor Nilered. Considering the donor emission quenching of the heterodimer with respect to the reference donor compound, it's possible to estimate a 98% energy transfer efficiency in the com-

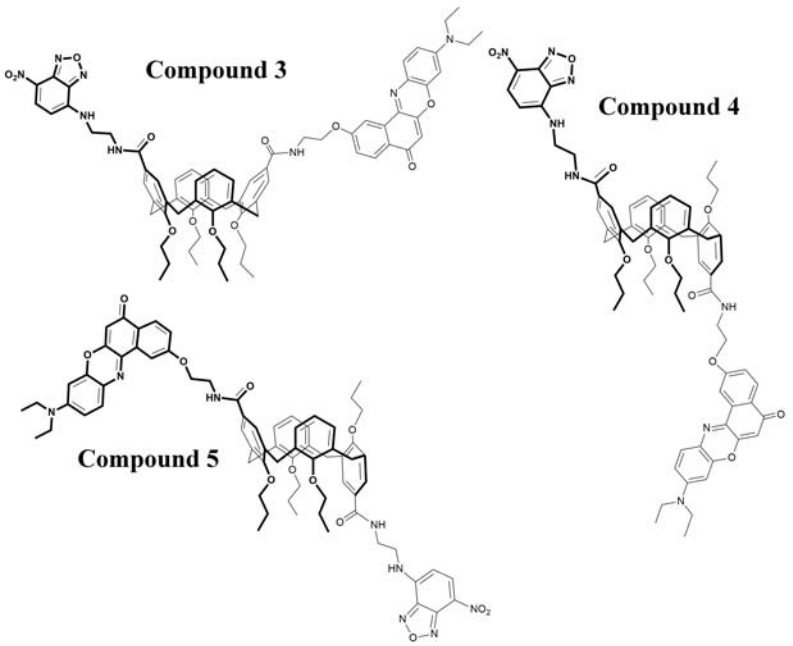

Figure 6.13: Different calix[4]arene structures with both donor NDM and acceptor Nilered dyes

pound 3, and a nominally quantitative transfer in compounds 4 and 5. These results are confirmed by the fluorescence excitation profiles of the heterodimers when detecting the acceptor fluorescence: the excitation profiles almost perfectly match the absorption spectra of the heterodimers, pointing to an almost quantitative energy transfer from the donor to the acceptor chromophore.

6.2.2 Ultrafast Transient Absorption Measurements

Reference Compounds 1 and 2

Transient absorption data analysis were carried out applying a combined approach, through the GLOTARAN package (http://glotaran.org)[24,25], consisting of singular values decomposition[21–23,116] and the simultaneous fitting of all the collected kinetic traces (global analysis). The transient spectra of the reference compounds 1 and

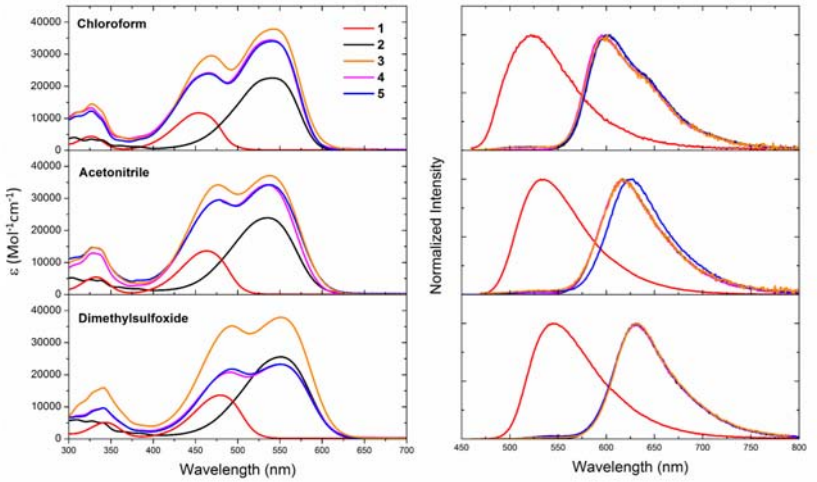

Figure 6.14: Absorption and emission spectra of the investigated compounds in chloroform, acetonitrile and dimethylsulfoxide

2 have been measured by setting the excitation wavelength at 470 nm, while the compound 2 was been excited also at 530 nm. As it is shown in the following, the covalent linkage of the laser dyes NDB and Nilered to the calix scaffold does not significantly affect the dynamics of their relaxation upon visible excitation, thus the molecules behave similarly to what previously reported for the isolated dyes[117–119].

Figure 6.15 shows a collection of transient spectra of compound 1, recorded at selected delay times in acetonitrile, DMSO and chloroform. Spectra in chloroform have been recorded only in the region 500-750 nm. It is possible to recognize a bleaching band centred respectively at 460 nm in acetonitrile and 470 nm in DMSO. The SE band, which in DMSO is red-shifted with respect to the acetonitrile and chloroform solutions, is in agreement with the steady state fluorescence spectra measured in these solvents. The time traces recorded in the three selected solvents have been globally analyzed in order to extract the kinetic constants describing the evolution of the system. In all cases three kinetic components were necessary to

Solvent	Compound	λ_{abs}^{max} (nm)	λ_{em}^{max} (nm)	ϕ^{em}
Chloroform	1	454	522	0.60
	2	540	601	0.96
	3	469; 543	600	0.38
	4	465, 540	601	0.74
	5	466; 538	596	0.72
Acetonitrile	1	463	535	0.72
	2	534	617	0.59
	3	477; 538	617	0.86
	4	479, 538	626	0.27
	5	478; 535	616	0.57
DMSO	1	479	546	0.58
	2	550	631	0.85
	3	492; 551	631	0.60
	4	493, 551	630	0.71
	5	490; 550	630	0.76

Table 6.3: Absorption and emission properties of the investigated compounds in chloroform, acetonitrile and DMSO. The reported quantum yield of binary compounds 4, 5, 6 are referred to Nilered fluorescence obtained by direct excitation of NBD. The NBD quantum yield is less than 1%

satisfactorily fit the data. The EADS (Evolution Associated Decay Spectra) obtained by global analysis are reported in Figure 6.16.

In all solvents the SE band shift towards higher wavelengths on a few picoseconds time scale. This is most probably due to a dynamic Stoke-shift, i.e. related to the solvent reorganization around the excited molecules. In chloroform the SE band also gains in intensity on a 2.7 ps time scale. Although only a minimal spectral evolution is observed on a 50-170 ps time scale in the examined solvent (in all cases there is a small red-shift of the SE band), it was necessary to include an intermediate kinetic component in the analysis in order to correctly fit the long time component. The excited state lifetimes estimated by the transient absorption measurements are in reasonable agreement with the fluorescence lifetimes previously reported[117].

Compound 2 was excited both at 530 nm, which is close to the maximum of its absorption band in all the examined solvents and at 470 nm, in order to evaluate its relaxation dynamics when excited at a wavelength close to the maximum absorption of the NBD

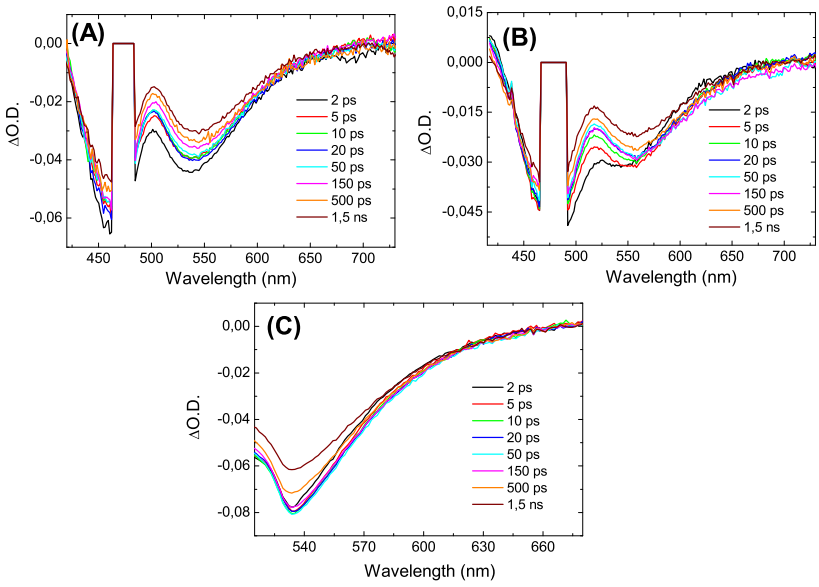

Figure 6.15: Selected transient absorption spectra of compound 1 measured in (A) acetonitrile (B) DMSO and (C) chloroform, upon excitation at 470 nm

dye. The relaxation dynamics of the system, as well as the shape of the transient absorption profiles, was independent from the excitation wavelength. The comparison of selected time traces obtained upon excitation at different wavelengths is reported in Figure 6.17. Figure 6.18 reports a collection of time resolved spectra for compound 2, recorded at different time delays in acetonitrile and DMSO e chloroform. Both in acetonitrile and DMSO the ground state bleaching band, which should be centered around 530nm, is very weak, while it is more pronounced in chloroform. The bleaching is partially masked by scattered excitation light, moreover an ESA bands develops at very early times in the same spectral region where it should appear, compensating the bleaching contribution. The SE band is on the contrary evident in all solvents and is centered around 620-630 nm depending on the solvent. The SE shifts towards higher wavelengths on a few ps timescale. This is particularly pronounced in DMSO, where a band shift of about 20 nm is

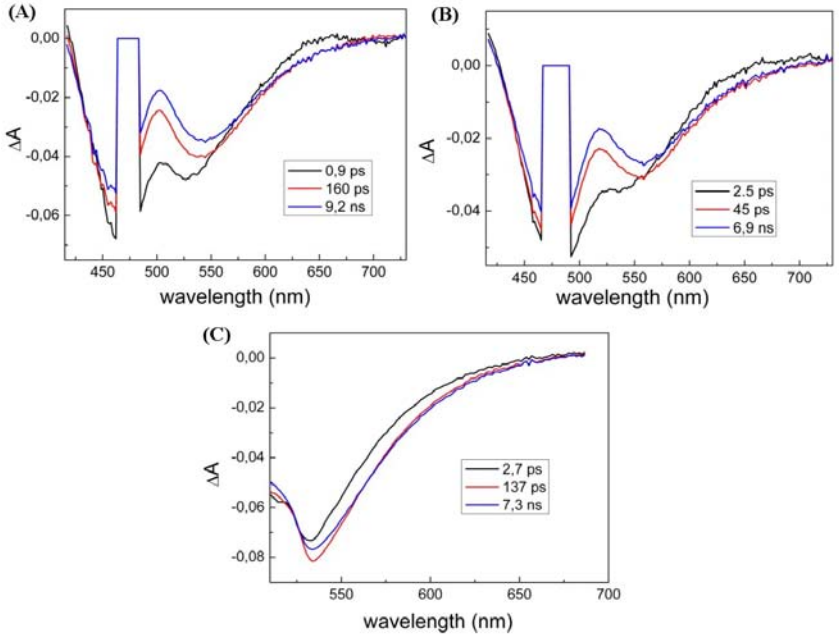

Figure 6.16: Evolution associated decay spectra (EADS) obtained by the simultaneous fit of all the kinetic traces recorded for the compound 1 in: (A) acetonitrile, (B) DMSO, (C) chloroform

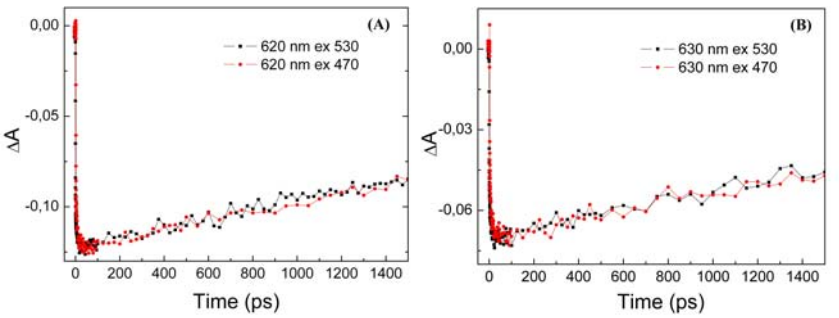

Figure 6.17: Kinetic trace measured at the maximum of the SE band for compound 2 upon excitation at 530 nm (black line) and 470 nm (red line) in (A) Acetonitrile and (B) Chloroform.

observed between 2 and 10 ps delay. Besides solvent reorganiza-

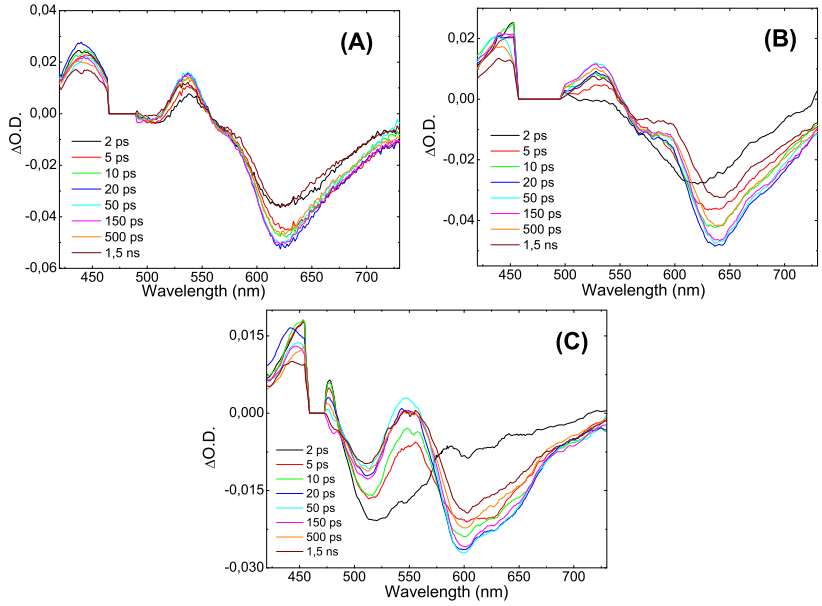

Figure 6.18: Selected transient absorption spectra of compound 2 measured in (A) acetonitrile (B) DMSO and (C) chloroform, upon excitation at 470 nm

tion, such a large shift can be attributed to the formation of an ICT, whose occurrence has been previously discussed for Nilered dissolved in polar solvents[118,119].
Also in this case we have analyzed the collected kinetic traces by mean of a global analysis procedure, obtaining the EADS reported in Figure 6.19. The kinetic constants associated to the system relaxation are similar in acetonitrile and DMSO, being of the order of 1 ps, 8 ps and ≈3.5 ns and slightly different in chloroform. As previously anticipated by visually inspecting the transient spectra, the SE band substantially red-shifts on a timescale of about 1 ps (black → red line in Figure 6.18). With the second spectral component (red line) an intensity increase of both the SE and the ESA bands is observed. Again, the SE band exhibit a slight red-shift, possibly associated with vibrational relaxation processes. Finally the last spectral component (blue line) appears. In chloroform the

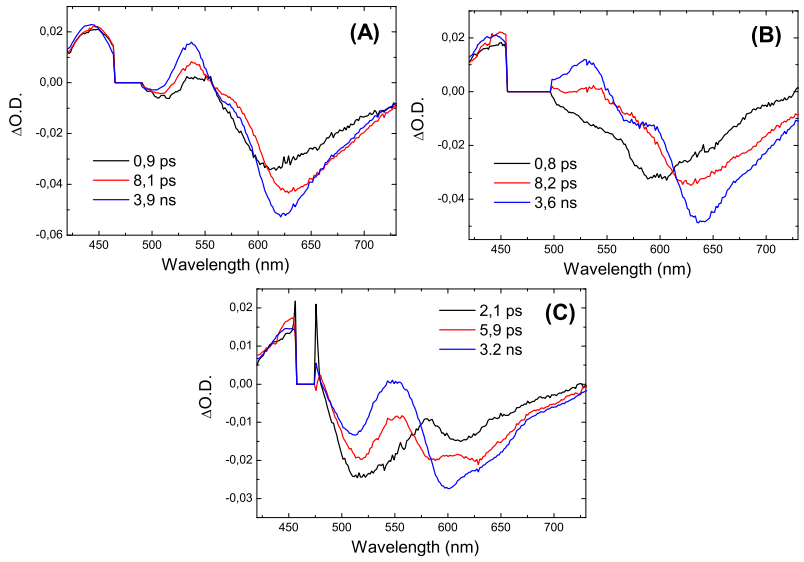

Figure 6.19: Evolution associated decay spectra (EADS) obtained by the simultaneous fit of all the kinetic traces recorded for the compound 2 in: (A) acetonitrile, (B) DMSO, (C) chloroform

bleaching band is much more pronounced compared with the other two solvents, possibly because the ESA band partial overlap with it is less intense and/or blue shifted in comparison with the other cases. Furthermore, the SE band has a different structure as compared with the other two solvents, showing two peaks (600 nm and 625 nm) which decays with different times (note the change in the relative intensity of the two bands between the red and blue line in Figure 6.18 C). Previous studies suggested that the two bands can be associated with two different excited states (an ICT state and a covalent state)[118].
The lifetimes estimated by global analysis for compound 1 and 2 are summarized in Table 6.4.

Binary Compounds 3,4,5

Transient absorption spectra of compounds 3,4,5 have been recorded by exciting the sample in the donor absorption region,

Compound 1			
Solvent	τ_1 (ps)	τ_2 (ps)	τ_3 (ns)
Acetonitrile	0.9	160	9.2
Chloroform	2.7	137	7.3
DMSO	2.5	45	6.9

Compound 2			
Solvent	τ_1 (ps)	τ_2 (ps)	τ_3 (ns)
Acetonitrile	0.9	8.1	3.9
Chloroform	2.1	5.9	3.2
DMSO	0.8	8.2	3.9

Table 6.4: Kinetic parameters extracted from global analysis for compounds 1 and 2

at 470 nm. From the steady state spectra of compound 1 and 2 it can be estimated that in all solvents at this excitation wavelength there is at least 25-30% of direct excitation of the acceptor moiety. Figure 6.20 reports the transient spectra registered for compound 3 in the three analyzed solvents. The transient spectra of compounds 5 and 6 are very similar to those of compound 3, although the relaxation dynamics is affected by the fact that the donor and acceptor molecules are maintained at a longer distance, being linked on the opposite side of the calyxarene scaffold. In the transient spectra at early times it is possible to recognize spectral features of the donor moiety, in particular in its bleaching region around 470 nm, less evident in chloroform. In the 450-550 nm region multiple contributions from both the donor and acceptor molecules appear, since in this region both the SE of the donor and an ESA band of the acceptor are located. The SE of the acceptor moiety is already visible at early time delays, and it is partially due to direct excitation of the Nilered chromophore which has a not negligible absorption at 470 nm. By comparing the kinetic trace measured at the maximum of the SE of the Nilered chromophore in compound 2 and 3 a notably different rise time is observed when the chromophore is directly excited (in compound 2) with respect to the situation in which its

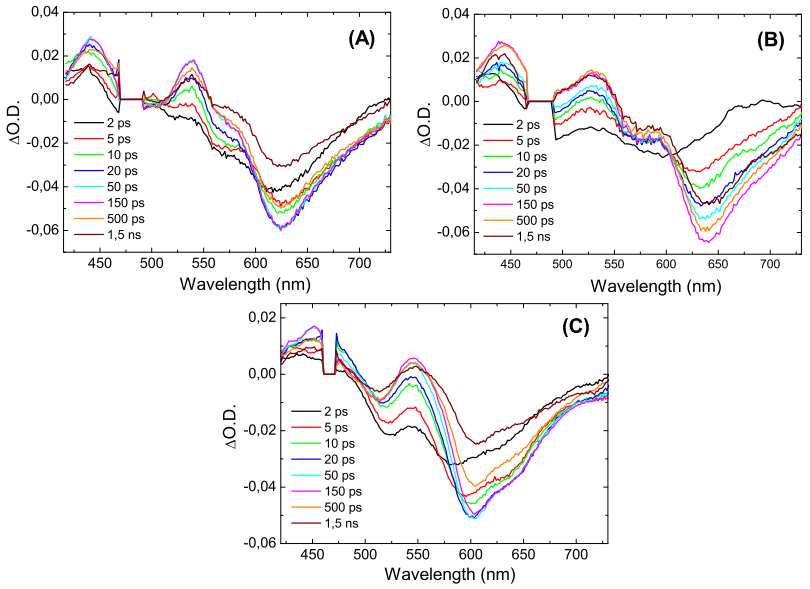

Figure 6.20: Selected transient absorption spectra of compound 3 measured in (A) acetonitrile (B) DMSO and (C) chloroform, upon excitation at 470 nm

excited state is populated as the result of energy transfer from the donor (in compound 3) in DMSO. In the other two solvents traces are similar on the short time scale (up to 10 ps), but differ on the long time scale, where in compound 3 we observe a slower rise component, due to energy transfer, but a faster decay, see Figure 6.21. In compound 3 the acceptor SE, as well the acceptor ESA band, located at lower wavelengths, increase in time as result of energy transfer. The evolution of the system is different depending on the solvent, as evidenced by the time constants extracted by global analysis. Nevertheless in all cases energy transfer appears to be nearly quantitative, as demonstrated by the fact that at long time delays the transient spectra of compound 2 and 3 are essentially equal. The EADS obtained by global analysis are reported in Figure 6.22. In all cases three kinetic components are necessary to satisfactorily fit the data. The first EADS (black line) contains features pertaining both to the donor (negative band $< 530nm$)

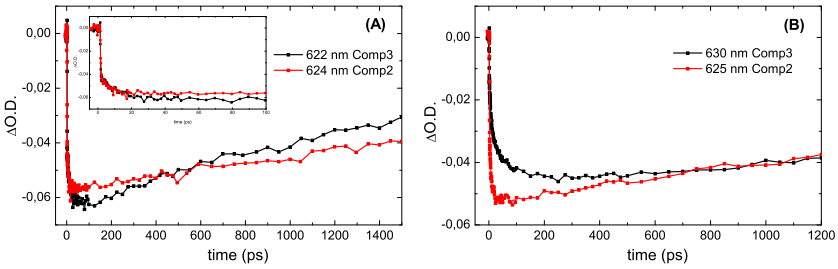

Figure 6.21: Kinetic trace measured at the maximum of SE for compound 2 (red line) and compound 3 (black line) obtained by exciting the sample at 470 nm in (A) Acetonitrile and (B) DMSO

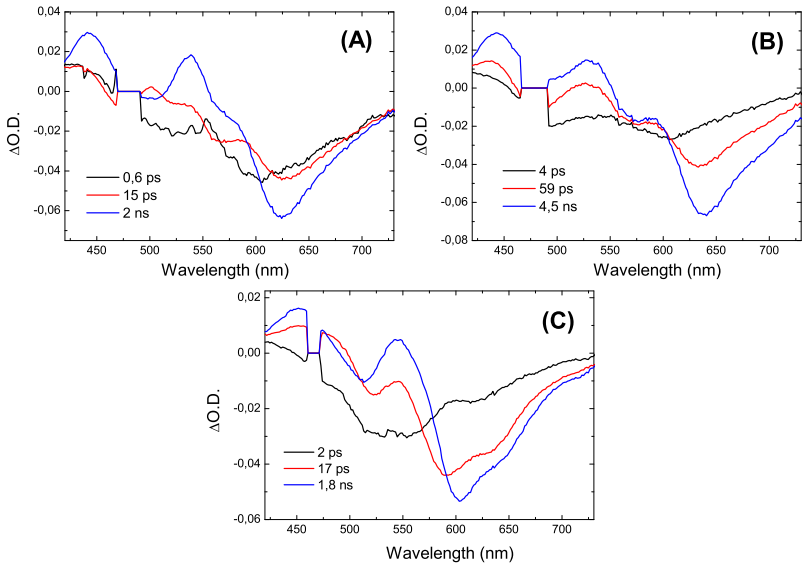

Figure 6.22: Evolution associated decay spectra (EADS) obtained by the simultaneous fit of all the kinetic traces recorded for the compound 2 in: (A) Acetonitrile, (B) DMSO, (C) Chloroform

and the acceptor chromophores. The fastest kinetics is observed in acetonitrile, where already at less than 1 ps delay there is a substantial signal due to the acceptor SE/ESA, indicating fast energy transfer (besides direct excitation). In all cases the dynamics of en-

ergy transfer appears to be bi-exponential, with a fast component on the 1-2 ps time scale and a slower (≈15 ps) component in acetonitrile and chloroform. In DMSO both components are slower, being about 4 and 60 ps. These findings confirm that in DMSO the chromophores are more far apart than in the other solvents, which makes the energy transfer slower. In Figure 6.23 the kinetic traces measured at the maximum of the acceptor SE in the three analyzed solvents are compared, in order to illustrate the dependence of the relaxation dynamics of the system on the solvent. The last lifetime

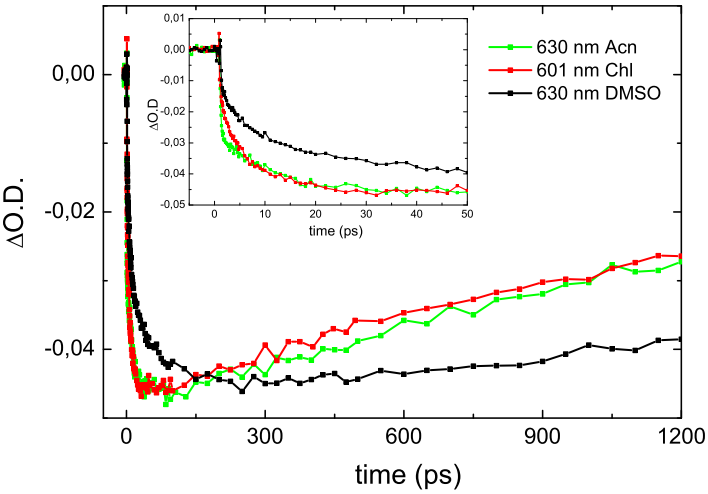

Figure 6.23: Kinetic trace measured at the maximum of the acceptor SE band in Acetonitrile (green line), Chloroform (red line) and DMSO (black line) for compound 3 excited at 470 nm. Early time delays are reported in the inset.

component should correspond to the lifetime of the isolated acceptor molecule. This is true in DMSO, where the two molecules are only weakly interacting, but not in the other two examined solvents. In both acetonitrile and chloroform we observe a shortening of the lifetime, which results of ca 2 ns. This finding, together with the results of fluorescence quantum yields (see Table 6.3) and the fact that the absorption spectrum of the dimer in chloroform can not be obtained as the sum of the spectra of the donor and acceptor moi-

eties indicates a stronger interaction between the chromophores. In order to investigate how the presence of the donor could modify the relaxation dynamics of the acceptor molecule we measured the transient spectra of compound 3 excited by a 580 nm pulse in chloroform and acetonitrile solutions. According to the spectra reported in Figure 6.14 the NDB chromophore does not absorb at this wavelength so that, if the donor and acceptor chromophores are only weakly interacting one would expect to obtain transient spectra very similar to those measured for compound 2. The obtained results show however some differences. In acetonitrile the Nilered SE immediately appears after excitation, rising faster than in compound 2 (see Figure 6.24A and 6.24B). The negative band is initially much broader than what observed both for compound 2 and 3 excited at 470 nm. On a few picoseconds timescale however the SE loses some intensity and becomes similar in shape to that observed with blue excitation. At lower wavelength three positive bands respectively peaked at 440, 500 and 560 nm are observed. The positive feature at 500 nm is not observed in both compounds 3 and 2 when excited at 470 nm (and in compound 2 if excited at 560nm), while the other two bands are attributable to ESA features of the Nilerd chromophore since are present both in compounds 2 and 3 upon 470 nm excitation. On the long timescale the transient spectra become similar to those measured by exciting both compound 2 and 3 at 470 nm.

By applying global analysis to these transient data three components are obtained: a fast 0.8 ps component, an intermediate 18 ps component and a much longer 2.0 ns component. As already observed, at short timescales the dynamics of the system shows a fast decay phase for the initially detected SE. The SE band, initially peaked at ca 600 nm, substantially decreases in intensity on the blue side in less than 1 ps, resulting in a sharper band peaked at 620 nm (black to red evolution in Figure 6.25). On the same timescale a positive feature at 500 nm grows. The final spectral component, living 2 ns coincides with that obtained by exciting Compound 3 at 470 nm, which is itself very similar to that obtained by exciting the acceptor molecule (compound 2) at the same wavelength. In chloroform the situation is similar. Also in this case we observe an instantaneous rise of the Nilered SE band and absorption features

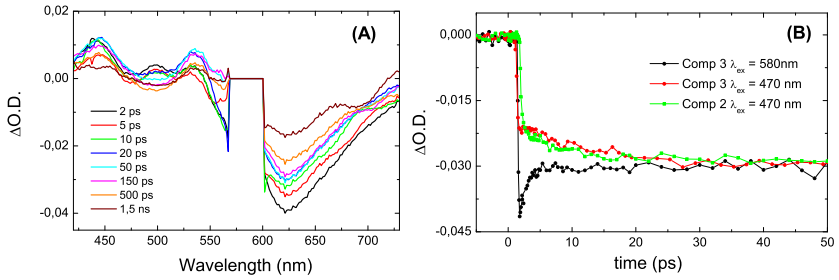

Figure 6.24: (A) Transient spectra recorded at selected time delay obtained by exciting compound 3 with a 580 nm pulse in acetonitrile; (B) Comparison of the kinetic trace at 620 nm measured for Compound 3 excited at 580 nm (black line); Compound 3 excited at 470 nm (red line); Compound 2 excited at 470 nm (green line)

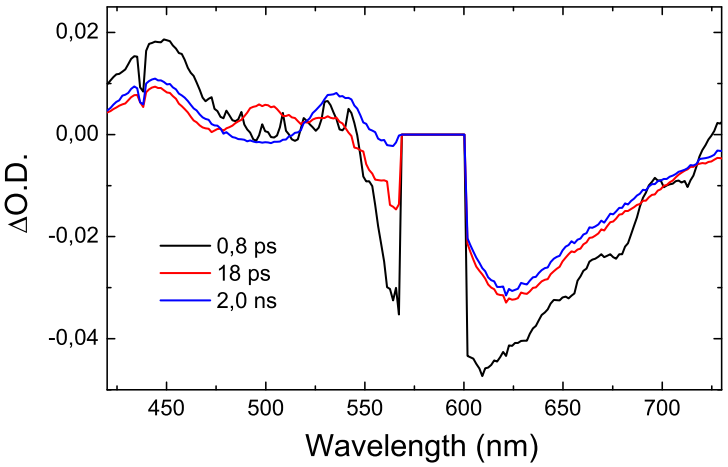

Figure 6.25: EADS obtained by global analysis of the kinetic traces recorded by exciting compound 3 at 580 nm

on the 450-500 nm spectral range rising on a few picoseconds time scale (see figures of spectral profile, EADS and time traces in Figure 6.26).

The spectral features observed upon excitation at 580 nm sug-

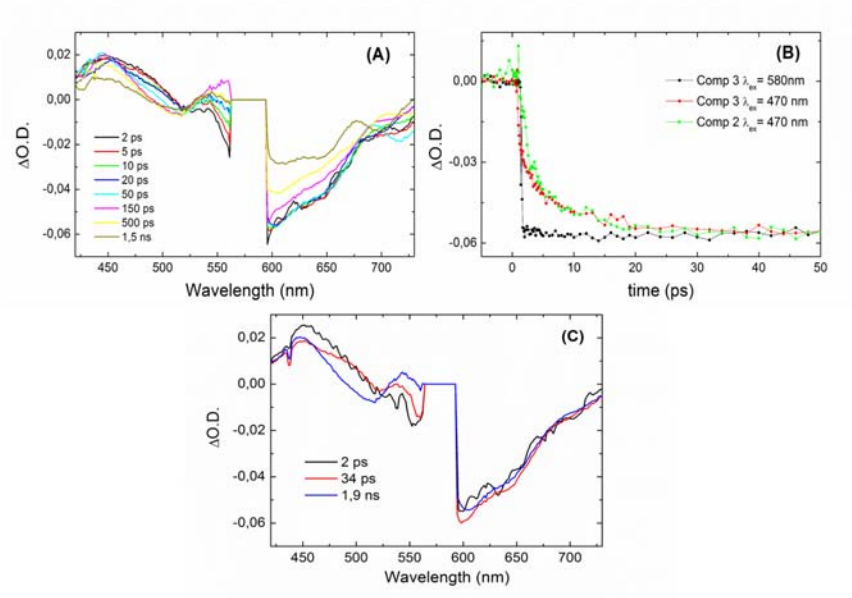

Figure 6.26: (A) Transient spectra recorded at selected time delay obtained by exciting compound 3 with a 580 nm pulse in chloroform; (B) EADS obtained by global analysis of the kinetic traces recorded by exciting compound 3 at 580 nm; (C) Comparison of the kinetic trace at 620 nm measured for Compound 3 excited at 580 nm (black line); Compound 3 excited at 470 nm (red line); Compound 2 excited at 470 nm (green line).

gest that in compound 3, dissolved in chloroform or acetonitrile, there is some electronic interaction between the donor and acceptor molecules so that the spectra obtained by exciting the acceptor moiety in the complex are different with respect to those obtained by exciting the isolated acceptor. The absorption features appearing at about 500 nm could possibly reflect a certain amount of back energy transfer from the excited acceptor towards the donor. In acetonitrile, the transient spectra of compound 1 show a feature around 500 nm which could correspond to that observed when compound 3 is excited at 580 nm. In the isolated donor spectra the transient signal is negative at 500 nm due to the presence of bleaching and SE but, considering that in case of energy transfer

from the acceptor to the donor molecule the bleaching signal of the acceptor would not appear, such a feature could well account for the positive band rising on a few ps timescale in compound 3 upon red excitation (Figure 6.27).

It has to be pointed that even if there is some energy transfer from

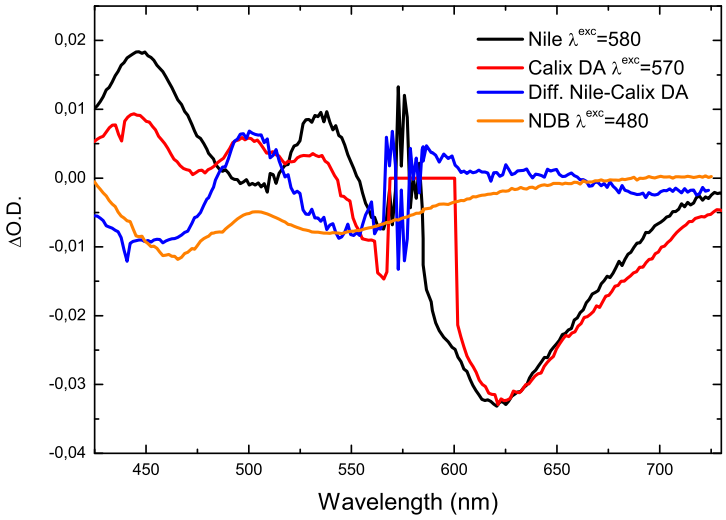

Figure 6.27: Back energy transfer process

the acceptor towards the donor, at longer time delays the energy goes back to the acceptor, since the signal measured on the long time scale for compound 3 is the same independently on the excitation wavelength.

Concerning compounds 4 and 5, the analysis of their transient absorption spectra and kinetic traces demonstrated a very small solvent dependence. In both cases, in fact, the chromophores are kept at substantial distance, being linked on the two opposite sides of the calix scaffold. The comparison between the kinetic traces measured at the maximum of the acceptor SE band in compound 4 and 5 in the three analyzed solvents is reported in Figure 6.28. As it can be noticed there is not a great variation and all the systems behave similarly to what observed for compound 3 in DMSO. The kinetic parameters obtained for compound 3, 4 and 5 by global analysis

are summarized in Table 6.5.

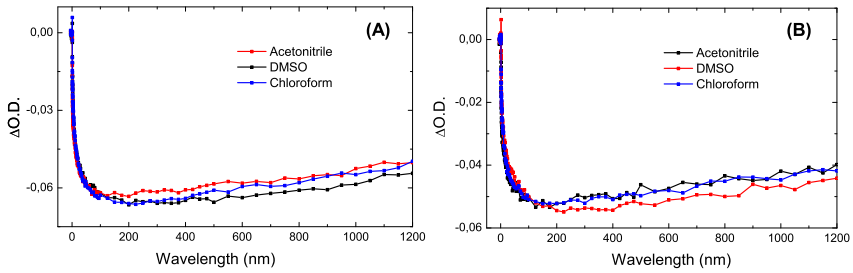

Figure 6.28: Kinetic traces measured at the maximum of the acceptor SE band in the three solvents for (A) compound 4 and (B) compound 5

Compound 3			
Solvent	τ_1 (ps)	τ_2 (ps)	τ_3 (ns)
Acetonitrile	0.6	15	2.0
Chloroform	2.0	17	1.8
DMSO	4.0	59	4.5

Compound 4			
Solvent	τ_1 (ps)	τ_2 (ps)	τ_3 (ns)
Acetonitrile	1.5	29	4.5
Chloroform	2.3	27	4.5
DMSO	2.9	57	4.6

Compound 5			
Solvent	τ_1 (ps)	τ_2 (ps)	τ_3 (ns)
Acetonitrile	1.4	29	4.2
Chloroform	2.3	35	4.1
DMSO	2.6	52	4.8

Table 6.5: Kinetic parameters extracted from global analysis for compounds 3, 4 and 5

6.2.3 Conclusions

These measurements confirm the presence of an efficient EET process. In particular steady state measurements have shown a small coupling between the two chromophores systems but the high values of emission QY have confirmed the efficiency of the process. Furthermore from the emission quenching of the heterodimer with respect to the reference donor compound, it has been possible to obtain an estimate of 98% in the compound 3 and nominally in the compounds 4 and 5 of the EET efficiency. These results are strongly influenced by the conformation of the assemblies and consequently by the nature of the solvents.
The transient absorption analysis has shown three different decay components in both references and binary compounds. The EET transfer times achieved from the global analysis show a strongly dependence by the nature of the solvent with a shorter time of few hundred of femtoseconds in acetonitrile and longer times of few picoseconds in chloroform and DMSO. Furthermore by passing from the free to the assembled system it is possible to observe the decreasing of the decay time of the acceptor due to the presence of further deactivation pathways and by retrodonation processes. Further information about the EET process will be developed in the future by molecular simulation calculations.

Bibliography

[1] J. R. Lakowicz, *Principles of Fluorescence Spectroscopy.* Springer, 2006.

[2] M. Quaranta, S. M. Borisov, and I. Klimant, "Indicators for optical oxygen sensors," *Bioanal. Rev.*, vol. 4, pp. 115–157, 2012.

[3] R. Marcus, "On the theory of oxidation-reduction reactions involving electron transfer," *J. Chem. Phys.*, vol. 24, pp. 966–978, 1956.

[4] R. Marcus, "Theoretical relations among rate constants, barriers, and bronsted slopes of chemical reactions," *J. Phys. Chem.*, vol. 72, pp. 891–899, 1968.

[5] R. Marcus and N. Sutin, "Electron transfers in chemistry and biology," *Biochim. Biophys. Acta*, vol. 811, pp. 265–322, 1985.

[6] N. Hush, "Adiabatic rate processes at electrodes. i. energy-charge relationships," *J. Chem. Phys.*, vol. 28, pp. 962–972, 1958.

[7] J. Jortner and M. Bixson, *Electron transfer: from isolated molecules to biomolecules, in Advances in Chemical Physics.* John Wiley & Sons, Inc., NY., 1999.

[8] D. L. Dexter, "A theory of sensitized luminescence in solids," *J. Chem. Phys.*, vol. 21, pp. 836–50, 1953.

[9] P. Ceroni, *The Exploration of Supramolecular Systems and Nanostructures by Photochemical Techniques.* Springer Science+Business Media B.V, 2012.

[10] T. Förster, "Zwischenmolekulare energiewanderung und fluoreszenz," *Annalen. Phys.*, vol. 2, pp. 55–75, 1948.

[11] S. A. Latt, H. T. Cheung, and E. R. Blout, "Energy transfer: a system with relatively fixed donor-acceptor separation," *J. Am. Chem. Soc.*, vol. 87, pp. 995–1003, 1965.

[12] R. M. Clegg, *Fluorescence resonance energy transfer. In Fluorescence imaging spectroscopy and microscopy.* John Wiley & Sons, New York, 1996.

[13] F. V. R. Neuwhal, L. Bussotti, and P. Foggi, "Transient absorption spectroscopy with uv-visible sub-picosecond pulses," *Res. Adv. in Photochem & Photobiol.*, vol. 1, pp. 77–94, 2000.

[14] F. V. R. Neuwahl, L. Bussotti, and P. Foggi, "Photophysical and photochemical applications of femtosecond time-resolved transient absorption spectroscopy," *Iternational Journal of Photoenergy*, vol. 3, pp. 103–109, 2001.

[15] L. Bussotti, B. Danieli, M. D'Auria, P. Foggi, G. Lesma, and R. Righini, "The photochemical behavior of colchicone and thiocolchicone," *Photochem. Photobiol.*, vol. 71, pp. 29–34, 2000.

[16] I. M. Bayanov, R. Danielius, P. Heinz, and A. Seilmeier, "Intense subpicosecond pulses tunable between 4 μm and 20 μm generated by an all-solid-state laser system," *Opt. Commun.*, vol. 113, pp. 99–104, 1994.

[17] R. Danielius, A. Piskarskas, P. Di Trapani, A. Andreoni, C. Solcia, and P. Foggi, "Visible pulses of 100 fs and 100 *mu*j from an upconverted parametric generator," *Appl. Opt.*, vol. 35, pp. 5336–5339, 1996.

[18] M. Ziółek, M. Lorenc, and R. Naskrecki, "Determination of the temporal response function in femtosecond pump-probe systems," *Appl. Phys. B*, vol. 72, pp. 843–847, 2001.

[19] M. Lorenc, M. Ziólek, M. Lorenc, R. Naskrecki, J. Karolczak, J. Kubicki, and A. Maciejewski, "Artifacts in femtosecond transient absorption spectroscopy," *Appl. Phys. B*, vol. 74, pp. 19–27, 2002.

[20] C. Rulliere, *Femtosecond Laser Pulses. Principles and Experiments.* 2004.

[21] E. R. Henry, "The use of uatrix methods in the modeling of spectroscopic data sets," *Biophys. J.*, vol. 72, pp. 652–673, 1997.

[22] E. R. Henry and J. Hofrichter, "[8] singular value decomposition: Application to analysis of experimental data. in methods in enzymology, ludwig brand, m. l. j.," *Ed. Academic Press*, vol. 210, pp. 129–192, 1992.

[23] I. H. M. van Stokkum, D. S. Larsen, and R. van Grondelle, "Global and target analysis of time-resolved spectra," *Biochimica et Biophysica Acta (BBA) - Bioenergetics*, vol. 1657, pp. 82–104, 2004.

[24] J. J. Snellenburg, S. P. Laptenok, R. Seger, K. M. Mullen, and I. H. M. van Stokkum, "Glotaran : A java -based graphical user interface for the r package timp," *Journal Of Statistical Software*, vol. 49, pp. 1–22, 2012.

[25] K. M. Mullen and I. H. M. van Stokkum, "An introduction to the special volume "spectroscopy and chemometrics in r"," *J. Stat. Soft.*, vol. 18, pp. 1–5, 2007.

[26] M. Amelia, L. Tarpani, L. Latterini, G. G. Aloisi, A. Guiotto, A. Chilin, G. Pastorini, and F. Elisei, "Photophysical properties of haloderivatives of angelicins," *J. Photochem. Photobiol. A*, vol. 198, pp. 98–105, 2008.

[27] I. Carmichael and G. L. Hug, "Triplet?triplet absorption spectra of organic molecules in condensed phases," *J. Chem. Phys. Ref. Data*, vol. 15, pp. 1–204, 1986.

[28] A. J. Nozik, "Nanoscience and nanostructures for photovoltaics and solar fuels," *Nano Lett.*, vol. 10, pp. 2735–2741, 2010.

[29] S. Rhle, M. Shalom, and A. Zaban, "Quantum-dot-sensitized solar cells," *ChemPhysChem*, vol. 11, pp. 2290–2304, 2010.

[30] K. Jeong, R. Pensack, and J. Asbury, "Vibrational spectroscopy of electronic processes in emerging photovoltaic materials," *Acc. Chem. Res.*, vol. 46, pp. 1538–47, 2013.

[31] K. Knowles, M. Peterson, M. McPhail, and E. Weiss, "Exciton dissociation within quantum dot-organic complexes: Mechanisms, use as a probe of interfacial structure, and applications," *J. Phys. Chem. C*, vol. 117, pp. 10229–10243, 2013.

[32] K. Hyeon-Deuk and O. Prezhdo, "Photoexcited electron and hole dynamics in semiconductor quantum dots: Phonon-induced relaxation, dephasing, multiple exciton generation and recombination," *J. Phys. Condens. Matter*, vol. 24, p. 363201, 2012.

[33] K. Tvrdy and P. Kamat, "Substrate driven photochemistry of cdse quantum dot films: Charge injection and irreversible transformations on oxide surfaces," *J. Phys. Chem. A*, vol. 113, pp. 3765–3772, 2009.

[34] A. L. Rogach, "Nanocrystalline cdte and cdte(s) particles: Wet chemical preparation, size-dependent optical properties and perspectives of optoelectronic applications," *Mater. Scien. and Eng. B*, vol. 69-70, pp. 435–440, 2000.

[35] N. Gaponik, D. V. Talapin, A. L. Rogach, K. Hoppe, E. V. Shevchenko, A. Kornowski, A. Eychmüller, and H. Weller, "Thiol-capping of cdte nanocrystals: An alternative to organometallic synthetic routes," *J. Phys. Chem. B*, vol. 106, pp. 7177–7185, 2002.

[36] S. K. Poznyak, N. P. Osipovich, A. Shavel, D. V. Talapin, M. Gao, A. Eychmüller, and N. Gaponik, "Size-dependent electrochemical behavior of thiol-capped cdte nanocrystals in

aqueous solution," *J. Phys. Chem. B*, vol. 109, pp. 1094–1100, 2005.

[37] K. K. Haldar, T. Sen, S. Mandal, and A. Patra, "Photophysical properties of au-cdte hybrid nanostructures of varying sizes and shapes," *ChemPhysChem*, vol. 13, pp. 3989–3996, 2012.

[38] F. Aldeek, L. Balan, J. Lambert, and R. Schneider, "The influence of capping thioalkyl acid on the growth and photoluminescence efficiency of cdte and cdse quantum dots," *Nanotechnology*, vol. 19, p. 475401, 2008.

[39] T. Vossmeyer, L. Katsikas, M. Gienig, I. G. Popovic, K. Diesner, A. Chemseddine, A. Eychmiiller, and H. Weller, "Cds nanoclusters: Synthesis, characterization, size dependent oscillator strength, temperature shift of the excitonic transition energy, and reversible absorbance shift," *J. Phys. Chem. 1994,98, 7665-7673*, vol. 98, pp. 7665–7673, 1994.

[40] Z. Sedaghat, N. Taghavinia, and M. Marandi, "Thermal control of the size and crystalline phase of cds nanoparticles," *2006 Nanotechnology 17 3812*, vol. 17, p. 3812, 2006.

[41] L. Huang and H. Han, "One-step synthesis of water-soluble znse quantum dots via microwave irradiation," *Mater. Lett.*, vol. 64, pp. 1099–1101, 2010.

[42] Z. Zhuang, X. Lu, Q. Peng, and Y. Li, "Direct synthesis of water-soluble ultrathin cds nanorods and reversible tuning of the solubility by alkalinity," *J. Am. Chem. Soc.*, vol. 132, pp. 1819–1821, 2010.

[43] A. L. Rogach, A. Kornowski, M. Gao, A. Eychmüller, and H. Weller, "Synthesis and characterization of a size series of extremely small thiol-stabilized cdse nanocrystals," *J. Phys. Chem. B*, vol. 103, pp. 3065–3069, 1999.

[44] P. Zhong, Y. Yua, J. Wu, Y. Lai, B. Chen, Z. Long, and C. Liang, "Preparation and application of functionalized nanoparticles of cdse capped with 11-mercaptoundecanoic

acid as a fluorescence probe," *Talanta*, vol. 70, pp. 902–906, 2006.

[45] H. Li, W. Y. Shih, and W.-H. Shih, "Stable aqueous zns quantum dots obtained using (3-mercaptopropyl)trimethoxysilane as a capping molecule," *Nanotechnology*, vol. 18, p. 495605, 2007.

[46] H. Qian, X. Qiu, L. Li, and J. Ren, "Microwave-assisted aqueous synthesis: A rapid approach to prepare highly luminescent znse(s) alloyed quantum dots," *J. Phys. Chem. B*, vol. 110, pp. 9034–9040, 2006.

[47] Y. Zheng, Z. Yang, and J. Y. Ying, "Aqueous synthesis of glutathione-capped znse and $zn_{1-x}cd_xse$ alloyed quantum dots," *Adv. Mater.*, vol. 19, pp. 1475–1479, 2007.

[48] A. Rogach, S. Kershaw, M. Burt, M. Harrison, A. Kornowski, A. Eychmüler, and H. Weller, "Colloidally prepared hgte nanocrystals with strong room-temperature infrared luminescence," *Adv. Mater.*, vol. 11, pp. 552–555, 1999.

[49] A. M. Smith, H. Duan, M. N. Rhyner, G. Ruana, and S. Nie, "A systematic examination of surface coatings on the optical and chemical properties of semiconductor quantum dots," *Phys. Chem. Chem. Phys.*, vol. 8, pp. 3895–3903, 2006.

[50] Y. Li and M. A. El-Sayed, "The effect of stabilizers on the catalytic activity and stability of pd colloidal nanoparticles in the suzuki reactions in aqueous solution," *J. Phys. Chem. B*, vol. 105, pp. 8938–8943, 2001.

[51] S. Kaniyankandy, S. rawalekar, S. Verma, D. K. Palit, and G. H. N., "Charge carrier dynamics in thiol capped cdte quantum dots," *Phys. Chem. Chem. Phys.*, vol. 12, pp. 4210–4216, 2010.

[52] Y. Kobayashi, L. Pan, and N. Tamai, "Effect of size and capping reagents on biexciton auger recombination dynamics of cdte quantum dots," *J. Phys. Chem. C*, vol. 113, pp. 11783–11783, 2009.

[53] Z. Yuan, A. Zhang, Y. Cao, J. Yang, Y. Zhu, and P. Yang, "Effect of mercaptocarboxylic acids on luminescent properties of cdte quantum dots," *J. Fluoresc.*, vol. 22, pp. 121–127, 2012.

[54] H. Zhang, Z. Zhou, B. Yang, and M. Gao, "The influence of carboxyl groups on the photoluminescence of mercaptocarboxylic acid-stabilized cdte nanoparticles," *J. Phys. Chem. B*, vol. 107, pp. 8–13, 2003.

[55] D. A. Hines and P. V. Kamat, "Quantum dot surface chemistry: Ligand effects and electron transfer reactions," *J. Phys. Chem. C*, vol. 117, pp. 14418–14426, 2013.

[56] C. d. M. Donegá and R. Koole, "Size dependence of the spontaneous emission rate and absorption cross section of cdse and cdte quantum dots," *J. Phys. Chem. C*, vol. 113, pp. 6511–6520, 2009.

[57] W. W. Yu, L. Qu, W. Guo, and X. Peng, "Experimental determination of the extinction coefficient of cdte, cdse, and cds nanocrystals," *Chem. Mater.*, vol. 15, pp. 2854–2860, 2003.

[58] Z. J. Jiang and D. F. Kelley, "Hot and relaxes electron transfer from the cdse core and core/shell nanorods," *J. Phys. Chem. C*, vol. 115, pp. 4594–4602, 2011.

[59] A. Iagatti, R. Flamini, M. Nocchetti, and L. Latterini, "Photoinduced formation of bithiophene radical cation via a hole-transfer process from cds nanocrystals," *J. Phys. Chem. C*, vol. 117, pp. 23996–24002, 2013.

[60] B. R. Fisher, H. J. Eisler, N. E. Stott, and M. G. Bawendi, "Emission intensity dependence and single-exponential behavior in single colloidal quantum dot fluorescence lifetimes," *J. Phys. Chem. B*, vol. 108, pp. 143–148, 2004.

[61] O. Labeau, P. Tamarat, and B. Lounis, "Temperature dependence of the luminescence lifetime of single cdse-zns quantum dots," *Phys. Rev. Lett.*, vol. 90, p. 257404, 2003.

[62] C. d. M. Donegá, M. Bode, and A. Meijerink, "Size- and temperature-dependence of exciton lifetimes in cdse quantum qots," *Phys. Rev. B*, vol. 74, p. 085320, 2006.

[63] M. Laferriére, R. E. Galian, V. Maurel, and J. C. Scaiano, "Non-linear effects in the quenching of fluorescent quantum dots by nitroxyl free radicals," *Chem. Commun.*, pp. 257–259, 2006.

[64] M. Amelia, R. Flamini, and L. Latterini, "Recovery of cds nanocrystal defects through conjugation with proteins," *Langmuir*, vol. 26, pp. 10129–10134, 2010.

[65] S. Bhattacharyya, B. Paramanik, S. Kundu, and A. Patra, "Energy/hole transfer phenomena in hybrid α-sexithiophene (α-sth) nanoparticle-cdte quantum-dot nanocomposites," *ChemPhysChem*, vol. 13, pp. 4155–4162, 2012.

[66] W. Chen, X. Wang, X. Tu, D. Pei, Y. Zhao, and X. Guo, "Water-soluble protein-on spin-labeled quantum-dots conjugate," *Small*, vol. 4, pp. 759–764, 2008.

[67] M. Berr, A. Vaneski, C. Mauser, S. Fischbach, A. Susha, A. Rogach, F. Jackel, and J. Feldmann, "Delayed photoelectron transfer in pt-decorated cds nanorods under hydrogen generation conditions," *Small*, vol. 8, pp. 291–297, 2012.

[68] P. Tyagi and P. Kambhampati, "False multiple exciton recombination and multiple exciton generation signals in semiconductor quantum dots arise from surface charge trappiing," *J. Chem. Phys.*, vol. 134, p. 094706, 2011.

[69] J. A. McGuire, J. Joo, J. M. Pietryga, R. D. Schaller, and V. I. Klimov, "New aspects of carrier multiplication in semiconductor nanocrystals," *Acc. Chem. Res.*, vol. 41, pp. 1810–1819, 2008.

[70] H. W. Midgett, H. W. Hillhouse, B. K. Hughes, A. J. Nozik, and M. C. Beard, "Flowing versus static conditions for measuring multiple exciton generation in pbse quandotsdots," *J. Phys. Chem. C*, vol. 114, pp. 17486–17500, 2010.

[71] V. I. Klimov, D. W. McBranch, C. Leatherdale, and M. G. Bawendi, "Electron and hole relaxation pathways in semiconductor quantum dots," *Phys. Rev. B*, vol. 60, pp. 13740–13749, 1999.

[72] V. I. Klimov, A. A. Mikhailovsky, S. Xu, A. Malko, J. A. Hollingsworth, C. A. Leatherdale, H.-J. Eisler, and M. G. Bawendi, "Optical gain and stimulated emission in nanocrystal quantum dots," *Science*, vol. 390, pp. 314–317, 2000.

[73] V. I. Klimov, "Optical nonlinearities and ultrafast carrier dynamics in semiconductor nanocrystals," *J. Phys. Chem. B*, vol. 104, pp. 6112–6123, 2000.

[74] M. Sanz, M. A. Correa-Duarte, L. M. Liz-Marzan, and A. Douhal, "Femtosecond dynamics of cdte quantum dots in water," *J. Photochem. and Photobiol.*, vol. 196, pp. 51–58, 2008.

[75] M. T. Trinh, A. J. Houtepen, J. M. Schins, T. Hanrath, J. Piris, W. Knulst, A. P. L. M. Goossens, and L. D. A. Siebbeles, "In spite of recent doubts carrier multiplication does occur in pbse anocrystals," *Nano Lett.*, vol. 8, pp. 1713–1718, 2008.

[76] L. Padilha, A. Neves, C. Cesar, and L. Barbosa, "Recombination processes in cdte quantum-dot-doped glasses," *Appl. Phys. Lett.*, vol. 85, pp. 3256–3258, 2004.

[77] T. Häupl, R. Lomoth, and L. Hammarström, "Femtosecond dynamics of the photoexcited methyl viologen radical cation," *J. Phys. Chem. A*, vol. 107, pp. 435–438, 2002.

[78] A. J. Morris-Cohen, M. T. Frederick, L. C. Cass, and E. A. Weiss, "Simultaneous determination of the adsorption constant and the photoinduced electron transfer rate for a cds quantum dot-viologen complex," *J. Am. Chem. Soc.*, vol. 133, pp. 10146–10154, 2011.

[79] B. Nikoobakht, C. Burda, M. Braun, M. Hun, and M. A. El-Sayed, "The quenching of cdse quantum dots photoluminescence by gold nanoparticles in solution," *Photochem. Photobiol.*, vol. 75, pp. 591–597, 2002.

[80] G. H. Shi, Z. B. Shang, Y. Wang, W. J. Jin, and T. C. Zhang, "Fluorescence quenching of cdse quantum dots by nitroaromatic explosives and their relative compounds," *Spectrochimica Acta Part A*, vol. 70, pp. 247–252, 2008.

[81] C. Tansakul, E. Lilie, E. D. Walter, F. Rivera III, A. Wolcott, J. Z. Zhang, G. L. Millhauser, and R. Braslau, "Distance-dependent fluorescence quenching and binding of cdse quantum dots by functionalized nitroxide radicals," *J. Phys. Chem. C*, vol. 114, pp. 7793–7805, 2010.

[82] Y. J. Chen and X. P. Yan, "Chemical redox modulation of the surface chemistry of cdte quantum dots for probing ascorbic acid in biological fluids," *Small*, vol. 5, pp. 2012–2018, 2009.

[83] S. N. Sharma, Z. S. Pillai, and P. V. Kamat, "Photoinduced charge transfer between cdse quantum dots and p-phenylenediamine," *J. Phys. Chem. B*, vol. 107, pp. 10088–10093, 2003.

[84] T. Watanabe and K. Honda, "Measurement of the extinction coefficient of the methyl viologen cation radical and the efficiency of its formatlon by semiconductor photocatalysis," *J. Phys. Chem.*, vol. 86, pp. 2617–2619, 1982.

[85] T. W. Ebbesen, L. E. Manring, and K. S. Peters, "Picosecond photochemistry of methyl viologen," *J. Am. Chem. Soc.*, vol. 106, pp. 7400–7404, 1984.

[86] M. G. Debije and P. P. C. Verbunt, "Thirty years of luminescent solar concentrator research: Solar energy for the built environment," *Adv. Energy Mater.*, vol. 2, pp. 12–35, 2012.

[87] B. Kippelen and J.-L. Brédasb, "Organic photovoltaics," *Energy & Environmental Science*, vol. 2, pp. 241–332, 2009.

[88] T. Edvinsson, C. Li, N. Pschirer, J. Schöneboom, F. Eickemeyer, R. Sens, G. Boschloo, A. Herrmann, K. Müllen, and A. Hagfeldt, "Intramolecular charge-transfer tuning of perylenes: Spectroscopic features and performance in dye-sensitized solar cells," *J. Phys. Chem. C Lett.*, vol. 111, pp. 15137–15140, 2007.

[89] S. Ardo and G. J. Meyer, "Photodriven heterogeneous charge transfer witn transitional-metal compounds anchored to tio_2 semiconductor surfaces," *Chem. Soc. Rew.*, vol. 38, pp. 115–164, 2009.

[90] R. F. Kubin and A. N. Fletcher, "Fluorescence quantum yields of some rhodamine dyes," *J. Luminescence*, vol. 27, pp. 455–462, 1982.

[91] D. Magde, J. H. Brannon, T. L. Cremers, and J. Olmsted III, "Absolute luminescence yield of cresyl violet. a standard for the red," *J. Phys. Chem.*, vol. 83, pp. 696–699, 1979.

[92] A. Kawski, B. Kukliński, and P. Bojarski, "Thermochromic absorption, fluorescence band shifts and dipole moments of badan and acrylodan," *Z. Naturforsch.*, vol. 57a, pp. 716–722, 2002.

[93] A. Kawski, "On the estimation of excited-state dipole moments from solvatochromic shifts of absorption and fluorescence spectra," *Z. Naturforsch.*, vol. 57a, pp. 255–262, 2002.

[94] A. Basagni. PhD thesis, LENS-European Laboratory for Non-Linear Spectroscopy, 2011.

[95] J. T. Edward, "Molecular volumes and the stokes-einstein equation," *J. Chem. Educ.*, vol. 47, pp. 261–270, 1970.

[96] R. P. Sabatini, T. M. McCormick, T. Lazarides, K. C. Wilson, R. Eisenberg, and D. W. McCamant, "Intersystem crossing in halogenated bodipy chromophores used for solar hydrogen production," *J. Phys. Chem. Lett.*, vol. 2, pp. 223–227, 2011.

[97] T. Rousseau, A. Cravino, T. Bura, G. Ulrich, R. Ziessel, and J. . Roncali, "Bodipy derivatives as donor materials for bulk heterojunction solar cells," *Chem. Commun.*, pp. 1673–1675, 2009.

[98] F. D'Souza, P. M. Smith, M. E. Zandler, A. L. McCarty, M. Itou, Y. Araki, and O. Ito, "Energy transfer followed by electron transfer in a supramolecular triad composed of boron dipyrrin, zinc porphyrin, and fullerene: A model for the photosynthetic antenna-reaction center complex," *J. Am. Chem. Soc.*, vol. 126, pp. 7898–7907, 2004.

[99] W.-J. Shi, M. E. El-Khouly, K. Ohkubo, S. Fukuzumi, and D. K. P. Ng, "Photosynthetic antenna-reaction center mimicry with a covalently linked monostyryl boron-dipyrromethene-aza-boron-dipyrromethene-c_{60} triad," *Chem. Eur. J.*, vol. 19, pp. 11332–11341, 2013.

[100] Y. Wang, D. Zhang, H. Zhou, J. Ding, Q. Chen, Y. Xiao, and S. Qian, "Nonlinear optical properties and ultrafast dynamics of three novel boradiazaindacene derivatives.," *J. Appl. Phys.*, vol. 108, p. 033520, 2010.

[101] X. Peng, J. Du, J. Fan, J. Wang, Y. Wu, J. Zhao, S. Sun, and T. Xu, "A selective fluorescent sensor for imaging cd^{2+} in living cells," *J. Am. Chem. Soc*, vol. 129, pp. 1500–1501, 2007.

[102] A. Costela, I. Garcíia-Moreno, J. Barroso, and R. Sastre, "Laser performance of pyrromethene 567 dye in solid matrices of methyl methacrylate with different comonomers.," *Appl. Phys. B: Lasers and Optics*, vol. 70, pp. 367–373, 2000.

[103] U. Narang, C. F. Zhao, J. D. Bhawalkar, F. V. Bright, and P. N. Prasad, "Characterization of a new solvent-sensitive two-photon-induced fluorescent (aminostyryl)pyridinium salt dye," *J. Phys. Chem. 1996, 100, 4521-452*, vol. 100, pp. 4521–4525, 1996.

[104] C. F. Zhao, R. Gvishi, U. Narang, G. Ruland, and P. N. Prasad, "Structures, spectra, and lasing properties of

new (aminostyryl)pyridinium laser dyes," *J. Phys. Chem.*, vol. 100, pp. 4526–4532, 1996.

[105] A. Mishra, P. Behera, R. Behera, B. Mishra, and G. Behera, "Interaction of n-alkyl styryl pyridinium dyes with tx-100 in aqueous medium: Role of the alkyl chain during solubilisation," *J. Photochem. Photobiol. A: Chem.*, vol. 116, pp. 79–84, 1998.

[106] P. Fromherz, K. H. Dambacher, H. Ephardt, A. Lambacher, C. Müller, R. Neigle, H. Schaden, O. Schenk, and T. Vetter, "Fluorescent dyes as probes of voltage transients in neuron membranes progress report," *Ber. Bunsenges. Phys. Chem.*, vol. 95, pp. 1333–1345, 1991.

[107] M. van der Meer, Z. H., R. W., and M. Glasbeek, "Femto- and picosecond fluorescence studies of solvation and non-radiative deactivation of ionic styryl dyes in liquid solution," *Chem. Phys. Lett.*, vol. 320, pp. 673–680, 2000.

[108] A. Mishra, G. Behera, M. Krishna, and N. Periasamy, "Time-resolved fluorescence studies of aminostyryl pyridinium dyes in organic solvents and surfactant solutions," *J. Lumin.*, vol. 92, pp. 175–188, 2001.

[109] S. T. Abdel-Halim and M. K. Awad, "Solvatochromism, molecular and electronic structures of trans and cis isomers of a typical styryl pyridinium cyanine dye," *J. Mol. Struct.*, vol. 920, pp. 332–341, 2009.

[110] G. D. Scholes, "Long-range resonance energy transfer in molecular systems," *Annu. Rev. Phys. Chem.*, vol. 54, pp. 57–87, 2003.

[111] K. Iwamoto, K. Araki, and S. Shinkai, "Conformations and structures of tetra-o-alkyl-p-tert-butylcalix[4]arenes. how is the conformation of calix[4]arenes immobilized?," *J. Org. Chem.*, vol. 56, pp. 4955–4962, 1991.

[112] A. Arduini, M. Fabbi, M. Mantovani, L. Mirone, A. Pochini, A. Secchi, and R. Ungaro, "Calix[4larenes blocked in a rigid

cone conformation by selective functionalization at the lower rim," *J. Org. Chem.*, vol. 60, pp. 1454–1457, 1995.

[113] Z. Asfari, V. Böhmer, J. M. Harrowfield, and J. Vicens, *Calixarenes 2001*. Kluwer Academic Publishers, 2001.

[114] J. Scheerder, R. H. Vreekamp, J. F. J. Engbersen, W. Verboom, J. P. M. van Duynhoven, and D. N. Reinhoudt, "The pinched cone conformation of calix[4]arenes: Noncovalent rigidification of the calix[4]arene skeleton," *J. Org. Chem.*, vol. 61, pp. 3476–3481, 1996.

[115] M. Lazzarotto, F. Sansone, L. Baldini, A. Casnati, P. Cozzini, and R. Ungaro, "Synthesis and properties of upper rim c-linked peptidocalix[4]arenes," *Eur. J. Org. Chem.*, vol. 3, pp. 595–602, 2001.

[116] R. W. Hendler and R. I. Shrager, "Deconvolutions based on singular value decomposition and the pseudoinverse: a guide for beginners," *Journal of Biochemical and Biophysical Methods*, vol. 28, pp. 1–33, 1994.

[117] S. Lin and W. S. Struve, "Time-resolved fluorescence of nitrobenzoxadiazole-aminohexanoic acid: effect of intramolecular hydrogen-bonding on non-radiative decay," *Photochem. Photobiol.*, vol. 54, pp. 361–365, 1991.

[118] A. K. Dutta, K. Kamada, and K. Ohta, "Spectroscopic studies of nile red in organic solvents and polymers," *Journal of Photochemistry and Photobiology A: Chemistry*, vol. 93, pp. 57–64, 1996.

[119] A. Cser, K. Nagy, and Biczók, "Fluorescence lifetime of nile red as a probe for the hydrogen bonding strength with its microenvironment," *Chem. Phys. Lett.*, vol. 360, pp. 473–478, 2002.

Acknowledgements

I would like to thank the people which I was tied in the last three years and have significantly contributed to the research presented in this thesis. First of all, I would like to thank my supervisor Prof. Paolo Foggi for giving me the possibility to work in his reseach group. A special thanks goes to my external supervisor Prof. Loredana Latterini and Dr. Luigi Tarpani of the University of Perugia for the collaboration and the time spent in their laboratories. Thanks also goes to the people of the "Femto Group" Prof. Roberto Righini, Dr. Laura Bussotti, Dr. Agnese Marcelli, Dr. Mariangela Di Donato, Dr. Andrea Lapini, Dr. Barbara Patrizi, Dr. Manuela Lima, Elena Ragnoni, Nicolò Azzaroli and Sandra Doria.
An acknowledgement to all the people I had the opportunity to meet here in florence. Lastly, my grateful goes to family for supporting me during this years.